

Synthesis of putative peroxisome proliferator-activated receptor δ antagonists

Dissertation for the degree of Master of Pharmacy

Cecilie Xuan Trang Vo



School of Pharmacy

Faculty of Mathematics and Natural Sciences

UNIVERSITY OF OSLO

2012

Synthesis of putative peroxisome proliferator-activated receptor δ antagonists

Dissertation for the degree of Master of Pharmacy

Cecilie Xuan Trang Vo

School of Pharmacy
Department of Pharmaceutical Chemistry
Faculty of Mathematics and Natural Sciences

UNIVERSITY OF OSLO

2012



Supervisors

Trond Vidar Hansen, Professor

Anders Vik, Associate Professor

© Cecilie Xuan Trang Vo, 2012

Synthesis of putative peroxisome proliferator-activated receptor δ antagonists.

<http://www.duo.uio.no/>

Trykk: Reprosentralen, Universitetet i Oslo

Acknowledgements

Most importantly, I would like to thank my supervisor Professor Trond Vidar Hansen, for the academic guidance during this work and for the opportunity to take part in this project.

I would like to express my greatest gratitude to co-supervisor Associate Professor Anders Vik for all assistance and good advice in both theoretical and practical chemistry.

My gratitude is also sent to Åsmund for the interesting discussions, help and support and to Alexander for help in the laboratory.

I would also like to express my thanks to all employees at the department for all constructive feedback and the pleasant working environment.

Last, but not least, I would also like to thank Georg for proofreading my thesis.

Cecilie Xuan Trang Vo

Blindern, May 2012

Abstract

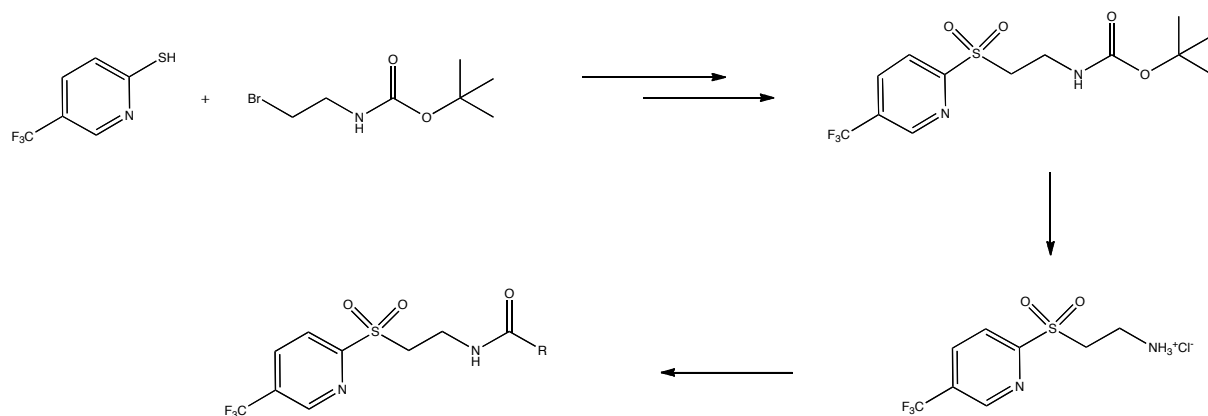
During the last decade, peroxisome proliferator-activated receptor δ (PPAR δ) has received great attention as a potential drug target for the prevention of the metabolic syndrome and type 2 diabetes. The beneficial biological effects of PPAR δ activation are well established, and increases in the amount of high-density lipoprotein (HDL) and reverse cholesterol transport, as well as a decrease in plasma glucose. However, much remains to be discovered, and to date, there are no drugs on the market targeting this receptor.

Due to the beneficial effects of PPAR δ activation, it is also of interest to investigate the effects of PPAR δ antagonism, in order to further elucidate the biological role of PPAR δ . This thesis therefore focused on the development of new high-affinity PPAR δ antagonists.

In total, eleven compounds were prepared using GSK3787, a selective PPAR δ antagonist, as the lead compound. The first-generation analogues, **7-16**, were synthesized partly by a published route. An efficient approach was developed for the synthesis of the second-generation analogue **23**. Molecular modelling studies indicate that **23** is the most potent of the synthesized compounds. Biological studies are currently ongoing.

Graphical abstract

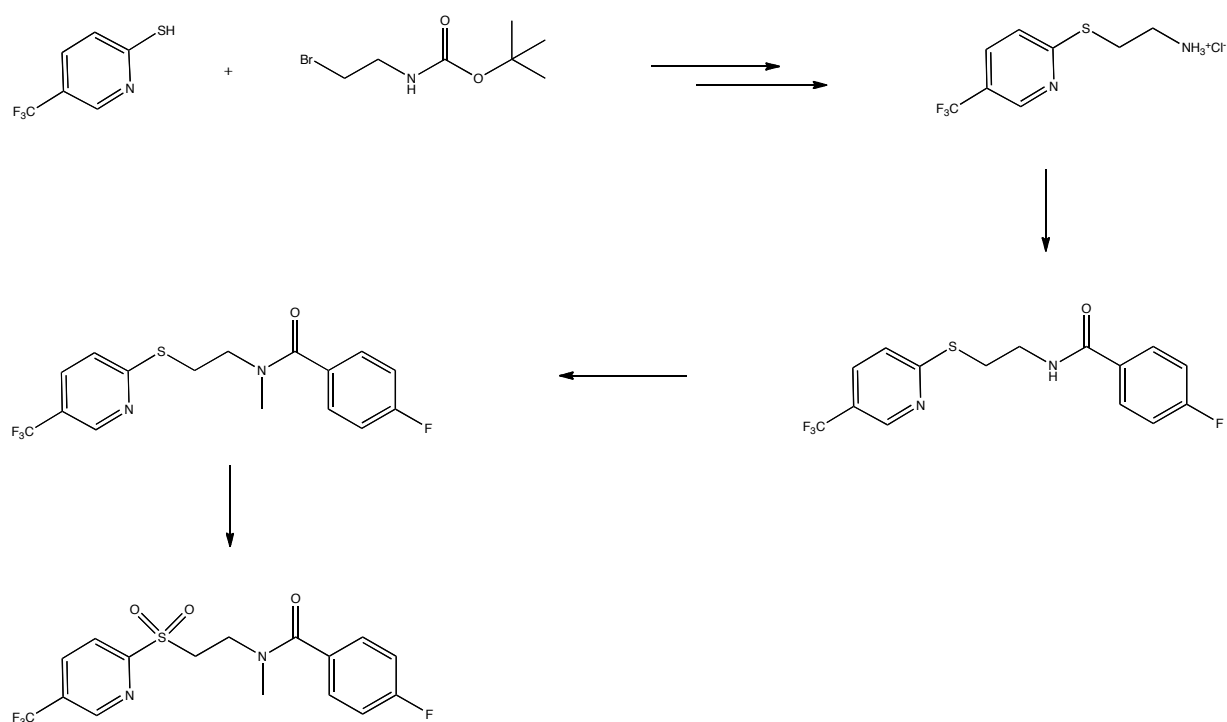
First-generation analogues



R = phenyl
R = 4-fluorophenyl
R = *iso*-propyl
R = *tert*-butyl
R = 2-naphthyl

R = 1-adamantyl
R = 2-furyl
R = 4-methoxyphenyl
R = 3-pyridyl
R = phenoxyethyl

The second-generation analogue



List of abbreviations

AF-1	activation function 1
AF-2	activation function 2
AIBN	azobisisobutyronitrile
ATP	adenosine-5'-triphosphate
Boc	<i>t</i> -butoxycarbonyl
bs	broad singlet
CoA	coenzyme A
COSY	correlation spectroscopy
<i>db/db</i>	leptin-resistant
DMF	<i>N,N</i> -dimethylformamide
DMP	1,1,1-tris(acetyloxy)-1,1-dihydro-1,2-benziodoxol-3-(1 <i>H</i>)-one
EC ₅₀	concentration that induces 50% activation of a given biological process
EtOAc	ethyl acetate
HDL	high density lipoprotein
IC ₅₀	concentration that inhibits 50% of a given biological process
<i>J</i>	coupling constant measured in Hz
K _i	the binding affinity of an inhibitor
LDL	low density lipoprotein
mp	melting point
NaHMDS	sodium <i>bis</i> (trimethylsilyl)amide
NMR	nuclear magnetic resonance (spectroscopy)
Oxone TM	potassium peroxymonosulfate
PPAR	peroxisome proliferator-activated receptor
PPRE	peroxisome proliferator response element
PrOH	propanol
PrONa	sodium propanolate
PTSA	<i>p</i> -toluenesulfonic acid
SAR	structure-activity relationship
THF	tetrahydrofuran
TMS	trimethylsilyl
VLDL	very low density lipoprotein

Table of contents

Acknowledgements.....	V
Abstract.....	VII
Graphical abstract.....	IX
List of abbreviations.....	XI
Table of contents.....	XIII
1 Introduction.....	1
1.1 Obesity, type 2 diabetes and the metabolic syndrome.....	1
1.2 Nuclear receptors	2
1.2.1 Peroxisome proliferator-activated receptors.....	2
1.2.2 Structural features.....	2
1.2.3 PPAR tissue distribution and biological effects	4
1.3 Endogenous ligands.....	5
1.4 Synthetic ligands in clinical use	5
1.5 PPARδ as a therapeutic target.....	7
1.5.1 PPAR δ and its effects in skeletal muscle.....	7
1.5.2 PPAR δ and its effects in adipose tissue.....	9
1.5.3 PPAR δ and its effects in the liver	9
1.5.4 The toxicological effects of PPAR δ	9
1.5.5 Current PPAR δ agonists	10
1.5.6 PPAR δ antagonism.....	10
1.6 Identification of GSK3787.....	14
1.7 Aim of thesis	15
2 Results and discussions.....	17
2.1 Background for the first-generation analogues of GSK3787.....	17
2.2 Synthesis of first-generation analogues 7-16	17
2.3 Attempted synthesis of first-generation analogues	20
2.4 A second-generation analogue of GSK3787.....	21
2.5 Attempted syntheses of <i>N</i>-methyl analogue 23.....	23

2.5.1	The first approach	23
2.5.2	The second approach	23
2.5.3	The third approach.....	25
2.5.4	The fourth approach.....	26
2.5.5	The fifth approach: a direct <i>N</i> -alkylation.....	27
2.5.6	The sixth approach.....	27
2.6	Successful synthesis of the <i>N</i>-methyl analogue 23.....	29
2.7	Alternative synthesis of compound 23.....	30
2.8	Molecular modelling	31
3	Conclusion and future work	33
4	Spectroscopic elucidation and characterization of compounds.....	35
4.1	General characterization of intermediates and analogues.....	35
4.2	Spectroscopic characterization of first-generation analogues 7-16 and their intermediates 4-6	36
4.2.1	Characterization of compound 4.....	36
4.2.2	Characterization of compound 5.....	37
4.2.3	Characterization of compound 6.....	38
4.2.4	Characterization of compound 7.....	39
4.2.5	Characterization of compound 8.....	40
4.2.6	Characterization of compound 9.....	41
4.2.7	Characterization of compound 10.....	42
4.2.8	Characterization of compound 11.....	43
4.2.9	Characterization of compound 12.....	44
4.2.10	Characterization of compound 13.....	45
4.2.11	Characterization of compound 14.....	46
4.2.12	Characterization of compound 15.....	47
4.2.13	Characterization of compound 16.....	48
4.3	Spectroscopic characterization of the second-generation analogue 23 and its intermediates 48-49	49
4.3.1	Characterization of compound 48.....	49
4.3.2	Characterization of compound 49.....	50
4.3.3	Characterization of compound 23.....	51
4.4	Spectroscopic characterization of compounds from attempted approaches.....	52

4.4.1	Characterization of intermediates from the sixth approach.....	52
5	Experimental section	55
5.1	General.....	55
5.2	First-generation analogues	55
5.2.1	Synthesis of intermediates	55
5.2.2	General procedure for the synthesis of first-generation analogues	56
5.3	Second-generation analogue.....	60
5.3.1	Synthesis of intermediates	60
5.3.2	Synthesis of the second-generation analogue	61
5.4	Synthesis of intermediates from the sixth approach.....	62
References		65
6	Appendix.....	67
6.1	Spectra of prepared analogues and their intermediates.....	67
6.2	Spectra of intermediates from attempted approaches.....	97

1 Introduction

1.1 Obesity, type 2 diabetes and the metabolic syndrome

Obesity is a health condition in which the proportion of body fat is abnormal or in great excess. It is a major risk factor for other conditions such as hypertension, dyslipidemia, insulin resistance and glucose intolerance [1]. These disorders, when occurring together, are known as the metabolic syndrome [2]. Furthermore, this cluster of metabolic disorders will increase the risk of cardiovascular diseases and type 2 diabetes [1].

Insulin is an important peptide hormone involved in the complex pathophysiology of the metabolic syndrome, as it stimulates the cellular uptake and storage of glucose, thus decreasing blood glucose. It is secreted from β -cells in the islets of Langerhans in the pancreas, in response to elevated blood glucose concentration. Insulin exercises its metabolic effects in the liver, adipose tissue and muscle, where its overall function is to regulate the uptake of glucose, fatty acids and fat, which subsequently become stored as the fundamental fuel for all cell activity [3]. If insulin resistance exists, the liver, adipose tissue and muscle cells will fail to respond correctly to insulin. As a result, more insulin needs to be secreted by the pancreas in order to ensure glucose uptake by cells. Eventually, if this compensatory increase of insulin fails to occur, blood glucose concentrations will elevate, increasing the risk of developing type 2 diabetes [4].

Furthermore, insulin resistance can lead to an unfavourable lipid profile, with high levels of very low-density lipoprotein (VLDL) and low levels of high-density lipoprotein (HDL) [4]. VLDL are particles containing cholesterol and newly synthesized triglycerides, and are responsible for transporting triglycerides from the liver to muscle and adipose tissue. During this process, the particles with the remaining cholesterol are converted to the low-density lipoprotein (LDL), which transports cholesterol into the cell membrane and are highly associated with the progression of atherosclerosis. Unlike LDL, HDL adsorbs cholesterol derived from cell breakdown in tissues, such as the arteries, and aids it back to the liver for excretion. Therefore, HDL is a key factor in reverse cholesterol transport and commonly referred to as the “good cholesterol” [5].

Since 1980, worldwide obesity has more than doubled. Figures from 2008 classify approximately 1.5 billion adults as overweight. Today, obesity and overweight are the fifth

leading causes of death worldwide, resulting in 2.8 million deaths every year. According to the World Health Organization (WHO), more than 311 million people worldwide suffer from type 2 diabetes. This number is expected to more than double by 2030, due to increased obesity and sedentary lifestyle [6].

With this increasing health problem in mind, new and improved ways to prevent obesity and also type 2 diabetes, are in urgent need. More knowledge and understanding of the metabolic syndrome, and the biological functions, as well as new drugs are needed. Peroxisome proliferator-activated receptors (PPARs), and in particular the δ -subtype, have gained attention due to their role in ameliorating the metabolic disorders mentioned above [2].

1.2 Nuclear receptors

1.2.1 Peroxisome proliferator-activated receptors

Peroxisome proliferator-activated receptors (PPARs) are a group of three ligand-activated transcription factors belonging to a superfamily of nuclear hormone receptors related to the retinoid, steroid and thyroid hormone receptors [7]. The PPARs were originally identified as orphan receptors owing to the lack of known endogenous ligands. Later, it was shown that these receptors are activated by endogenous fatty acids and eicosanoids, and that they regulate the transcriptions of various genes affecting the lipid and glucose homeostasis [7-9].

To date, there are three identified subtypes in humans; PPAR α (NR1C1), PPAR δ (NR1C2) and PPAR γ (NR1C3). They are expressed to a various degree in different tissues and exert distinct biological effects and ligand specificity [7, 10].

1.2.2 Structural features

All nuclear receptors show similar structural features and are composed of four distinct domains (Figure 1) [8, 11].

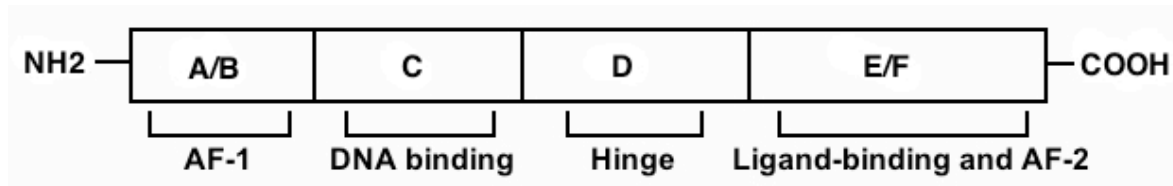


Figure 1. Functional domains of PPARs. The figure is not representative for the actual size of the various domains.

The identified domains are A/B, C, D and E/F. The ligand-*independent* activation function 1 (AF-1), located at the A/B domain, is the site of phosphorylation in the PPARs, common to all nuclear receptors. Next to A/B is the DNA binding domain (DBD) C, which interacts with peroxisome proliferator response elements (PPREs). These elements are constructed of hexanucleotides with the distinct sequence “AGGTCA_nAGGTCA”, where the “n” is a single nucleotide spacer. Domain D contains a hinge region where the cofactors are docked [8, 11]. Cofactors control the gene transcription, and the recruitment of these cofactors can either induce transcription (coactivators) or actively repress it (corepressors) (Figure 2) [12].

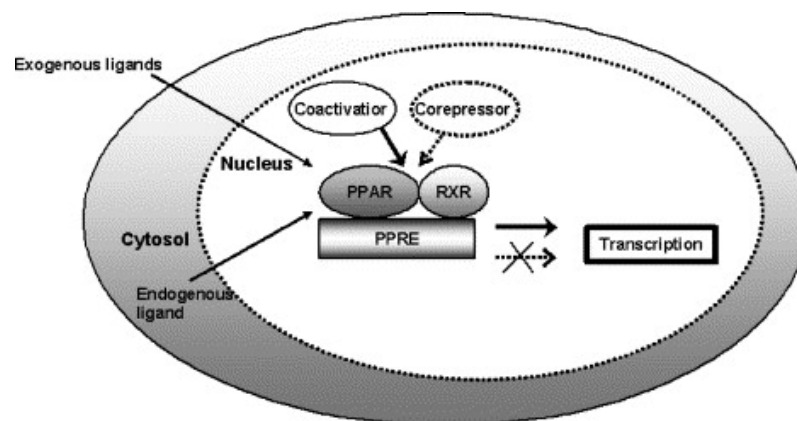


Figure 2. Gene transcription induced by PPARs [8].

The final domain at the C-terminal is the E/F domain consisting of a ligand-binding domain (LBD), including the ligand-*dependent* activation function 2 (AF-2). The LBD is involved in the heterodimerization with the retinoid X receptor (RXR), while AF-2 is responsible for the recruitment of cofactors, which are crucial for regulating gene transcription [8, 11].

1.2.3 PPAR tissue distribution and biological effects

The first receptor to be identified, named PPAR α , was found to be expressed mainly in the heart, liver, skeletal muscle, kidney and intestine, but also in vascular cells, such as endothelial cells and monocytes/macrophages [8]. Its major role is to regulate the catabolism of fatty acids, by increasing β -oxidation of fatty acids, gluconeogenesis and ketone body synthesis [13].

PPAR γ is highly expressed in adipocytes, but is also found in other cell types such as epithelial cells of the intestine and specific kinds of immune and inflammatory cells. PPAR γ enhances biological functions, which regulate adipogenesis, resulting in both adipocyte differentiation and an increase in small insulin-sensitive adipocytes [8]. In addition, PPAR γ is involved in lipid metabolism by maintaining the adipocyte-specific functions [9]. Experimental studies suggest that the activation of PPAR γ increase insulin sensitivity by affecting various genes in the glucose metabolism. Beneficial limiting processes of inflammation and atherosclerosis have also been reported [8, 14].

PPAR δ is ubiquitously expressed with high levels in heart, adipose tissue, skin and in skeletal muscle, where the relative expression of PPAR δ is 10- and 50-fold higher compared to PPAR α and PPAR γ , respectively. Given that skeletal muscles comprise the largest organ in the body, the expression of PPAR δ here may play an important physiological role with respect to the metabolic syndrome [10]. PPAR δ is involved in numerous biological functions, such as lipid and glucose homeostasis, cell differentiation, proliferation, apoptosis and immune regulation [8, 13, 15]. It is established that PPAR δ agonists may be effective in the treatment of the metabolic syndrome by increasing both HDL-cholesterol level and reverse cholesterol transport. This effect elevates the level of “good cholesterol” and reduces the amount of peripheral cholesterol by transporting it back to the liver for excretion, and hence preventing atherosclerosis. In addition, the benefits of PPAR δ activation on atherosclerosis have been reported as a consequence of its suppression of cytokine expression, and thus inflammatory response [7]. Furthermore, activation of PPAR δ in skeletal muscle and adipose tissue induces energy expenditure [9, 16]. Overall, it seems that activation of PPAR δ has beneficial effects in regulating the metabolic syndrome.

1.3 Endogenous ligands

PPARs have affinity for fatty acid-like molecules. Due to their hydrophobic ligand-binding pocket, it is not surprising that PPARs are activated by various fatty acids and eicosanoids, such as leukotrienes and prostaglandins, including PGA_1 and PGD_2 (Figure 3) [17]. According to current literature, $\text{PPAR}\delta$ also binds different saturated and unsaturated fatty acids such as palmitic acid and linolenic acid [12]. However, to activate $\text{PPAR}\delta$, these ligands would need to be present at high concentrations (in the micromolar range) and they are not always selective for the δ -subtype [18].

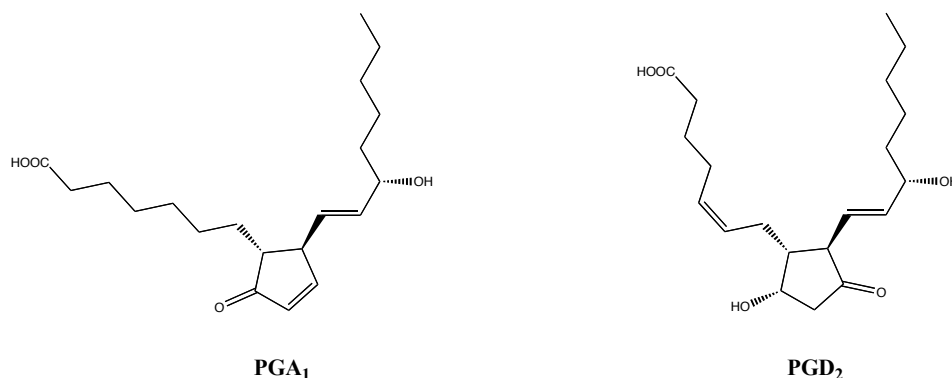


Figure 3. Structures of two prostaglandins, which are endogenous $\text{PPAR}\delta$ ligands.

1.4 Synthetic ligands in clinical use

To date, the only available drugs activate the α - or the γ -subtype. $\text{PPAR}\alpha$ activity can be modulated by a family of molecules called fibrates. These ligands were found to increase both VLDL and LDL-cholesterol with a following decrease of HDL-cholesterol. As mentioned in section 1.1, high levels of LDL are associated with increased risk of cardiovascular disease [4]. However, gemfibrozil (e.g. Lopid®) and fenofibrate (e.g. TriCor®) (Figure 4) are agonists in clinical use for reducing the cholesterol of patients at high risk of cardiovascular disease [14]. In Norway, marketing authorisations have not been issued for neither gemfibrozil nor fenofibrate, suggesting an unsatisfactory positive risk-benefit profile, and they are thus only available to Norwegian patients for compassionate use [19].

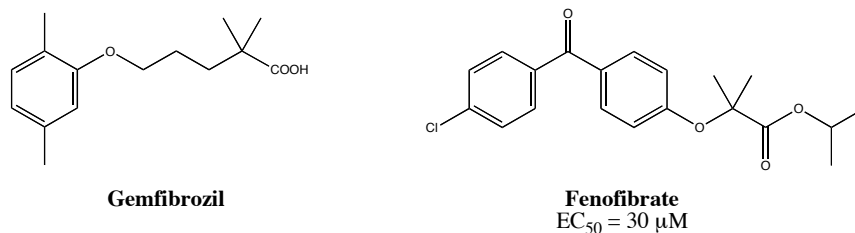


Figure 4. Synthetic PPAR α agonists (the fibrates) used in the treatment of hypertriglyceridemia. The EC₅₀-value is taken from reference [20].

PPAR γ is activated by the thiazolidinediones (TZDs) (Figure 5), which act as insulin sensitizers by reducing plasma glucose. Consequently, the TZDs are used in the treatment of type 2 diabetes. Troglitazone (e.g. ReZulin®) was the first substance to be marketed, but was withdrawn from the market as a result of idiosyncratic liver failures [14]. Rosiglitazone (e.g. Avandia®), belonging to the same class of drugs, has either been withdrawn from the market or sale has been restricted, due to increased risk of myocardial infarction [21, 22]. A third substance to be clinically used for the treatment of type 2 diabetes, namely pioglitazone (e.g. Actos®), is still marketed even though it may cause bladder tumours. However, this is not well-established [19].

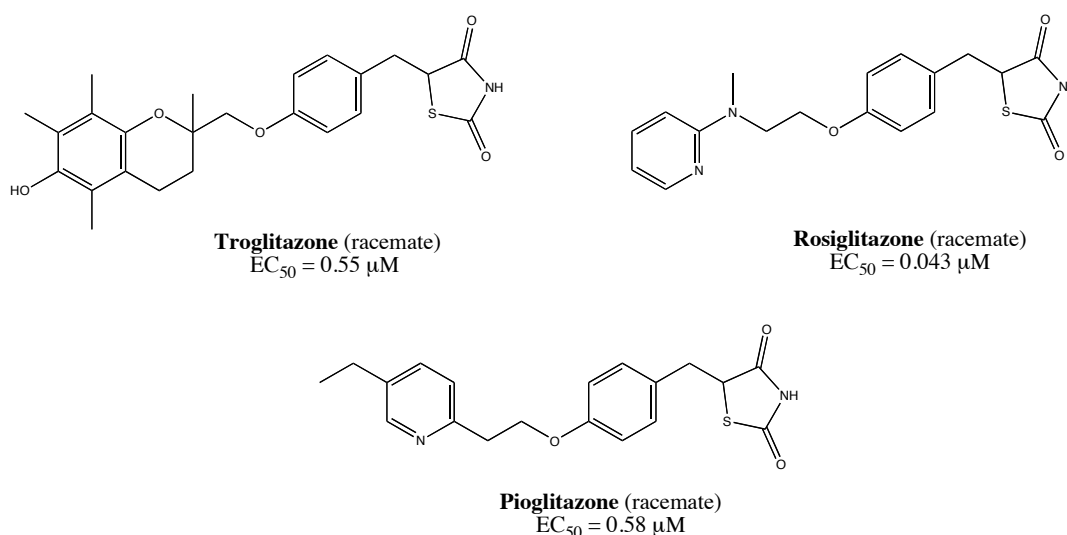


Figure 5. Synthetic PPAR γ agonists (TZDs). The EC₅₀-values are taken from reference [20].

1.5 PPAR δ as a therapeutic target

Nuclear receptors, and among them PPAR δ has gained more attention during the past 10-15 years. Its role as an important regulator in glucose and lipid homeostasis is established, especially in skeletal muscle, but also in adipose tissue and the liver. PPAR δ is therefore an interesting biological target in the research fields of the metabolic syndrome and type 2 diabetes. Despite research efforts, this receptor subtype remains the most poorly characterized and no synthetic ligands are yet developed for clinical use [23].

1.5.1 PPAR δ and its effects in skeletal muscle

PPAR δ plays an important role in skeletal muscle where it is expressed at 10- and 50-fold higher levels than PPAR α and PPAR γ , respectively. Skeletal muscle is made up of different fiber types with distinct metabolic and contractile characteristics. They are classified in three isoforms: oxidative slow-twitch (type I), mixed oxidative/glycolytic fast-twitch (type IIA) and glycolytic fast-twitch (type IIB) [10, 16, 24]. Oxidative slow-twitch fibers provide insulin-stimulated glucose transport as they contain more glucose transporters and insulin signaling intermediates. Thus, it is evident that high amounts of slow-twitch oxidative fibers are favourable in terms of improving the insulin sensitivity [11].

In addition, mitochondria, which oxidize fatty acids, are also found to be more abundantly expressed in oxidative slow-twitch fibers, increasing their potential for oxidation of fatty acids. For lipid catabolism to occur, the plasma-free fatty acids must penetrate the cell membrane by either diffusion or via receptor proteins, such as CD36 (Figure 6). In cytosol they react with CoA or ATP to form fatty acyl-CoA complexes, before entering the mitochondria, facilitated by carnityl palmitoyl transferase. Once inside the mitochondria, the free fatty acids can be oxidized [25]. PPAR δ is an important regulator of lipid catabolism, a process that mainly occurs in skeletal muscle. A number of genes involved in the regulation of cellular energy expenditure towards the use of fat as an energy source are PPAR δ -dependent, such as PDK4, which reduces glucose oxidation and thereby enhances lipid oxidation [26, 27]. This explains why PPAR δ activation has protective effects against the consequences of *dietary* lipid overload [28].

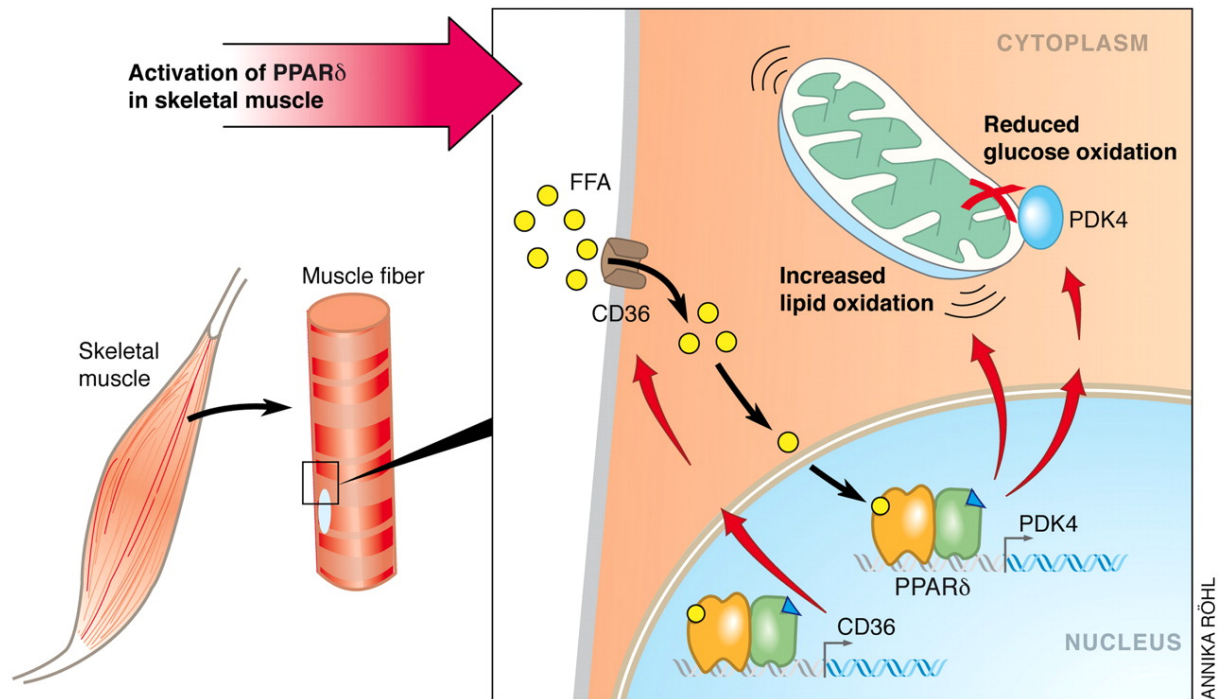


Figure 6. Decreased glucose oxidation in mitochondria and increased lipid oxidation, as a result of a change in gene expression governed by PPAR δ [11].

The increased lipid catabolism due to activation of PPAR δ may also indicate that PPAR δ alter skeletal muscle glucose *uptake*. However, experimental studies show varying results and further studies designed to examine the effects of PPAR δ -specific agonists on skeletal muscle glucose uptake are warranted [11].

Since PPAR δ is mainly expressed in slow-twitch oxidative fibers, it has also been proposed to play a role in fiber-type regulation. Overexpression of PGC1a, an important gene in fiber-type regulation (a coactivator of PPAR δ), promoted a full transformation of fast-twitch to slow-twitch muscle fibers in mice [29]. Furthermore, an activation of PPAR δ or inhibition of the *corepressor* RIP140 also favours the formation of slow-twitch muscle fibers in a similar manner [29, 30]. Interestingly, it was also found that PPAR δ overexpression mediates comparable biological effects as those induced by physical activity. Conversion of muscle fibers has also been discovered in humans as a result of endurance training. This raises the question of whether PPAR δ activation can mimic the beneficial effects of physical activity [31, 32].

1.5.2 PPAR δ and its effects in adipose tissue

As mentioned in the previous section, elevated proportions of slow-twitch fibers in skeletal muscle are found to increase the amount of PPAR δ receptors, leading to an increase in the uptake of fatty acids. As a result, lipid storage in adipocytes can be avoided [28], thus also obesity-induced insulin resistance. In addition, an expansion of adipocytes in a given tissue, which is often seen in connection to visceral obesity, may result in the recruitment of macrophages, which subsequently increases the production of cytokines. Cytokine-induced inflammation is implicated in the pathogenesis of insulin resistance [33, 34], as well as atherosclerosis. Consequently, the amount of macrophages is believed to correlate with the degree of insulin resistance. PPAR δ activation is suggested to be important in this pathophysiology by attenuating the production of inflammatory cytokines and is thus an important target for the prevention of insulin resistance [34].

1.5.3 PPAR δ and its effects in the liver

Based on the findings reported by Lee and co-workers, PPAR δ activation in liver has been suggested to ameliorate glucose tolerance and insulin sensitivity. Experiments have shown PPAR δ knockout mice to be glucose intolerant, whereas treatment of diabetic leptin-resistant (*db/db*) mice with a PPAR δ agonist, improved both insulin sensitivity and glucose tolerance. Decreased hepatic glucose output has been observed as a result of increased synthesis of fatty acids in the liver, the same metabolic effect as induced in skeletal muscle by exercise, fasting or cold exposure [7, 35, 36]. Furthermore, a recent study, reported by Serrano-Marco *et al.*, describes PPAR δ -mediated inhibition of proteins in the liver, which consequently leads to the prevention of cytokine-induced insulin resistance [37].

1.5.4 The toxicological effects of PPAR δ

Due to the wide tissue distribution of PPAR δ , toxicity and potential side effects of drug candidates have to be taken into account. Experiments with genetic mouse models for colorectal and intestinal cancer have shown results of increased polyp formation, indicating that PPAR δ may be involved in the up-regulation of intestinal adenoma growth [9]. Other investigations report the opposite results, claiming that PPAR δ attenuates polyp formation. Additionally, it is suggested that PPAR δ antagonists inhibit carcinogenesis in some tissues. In order to use agonists in the treatment of metabolic syndrome, it is clear that this topic needs

extensive research. More knowledge about the relationship of PPAR δ and carcinogenesis will aid the understanding of side effects of drug candidates [38].

1.5.5 Current PPAR δ agonists

PPAR δ agonists are currently not used clinically, despite the positive effects of PPAR δ activation. The identification of GW501516 ($EC_{50} = 1.1$ nM) and GW0742 ($EC_{50} = 1.0$ nM) as selective and potent PPAR δ agonists has been an important contribution to the investigation of the biological roles of the PPAR δ subtype (Figure 7) [39].

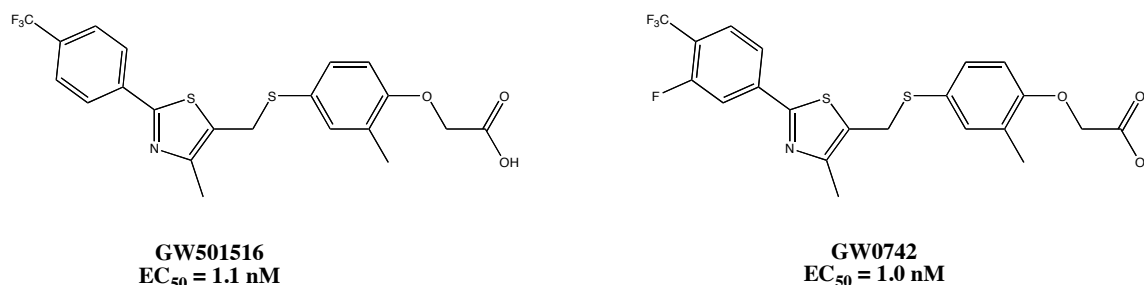


Figure 7. Structures of two synthetic PPAR δ agonists.

1.5.6 PPAR δ antagonism

The beneficial physiological effects of agonism in PPAR δ , especially in alleviating the symptoms of the metabolic syndrome, are well established [11, 40]. However, to date, there are no drugs available on the market targeting PPAR δ , owing partly to the fact that much remains to be discovered about the biological roles of this receptor. Recently, the focus has been extended to the development of PPAR δ antagonists, since the investigation of PPAR δ antagonism is of equal importance to the elucidation of the biological roles of PPAR δ .

There is a need for new molecules serving as pharmacological tools that enable the investigation of specific physiological functions governed by PPAR δ . In this context, the development of new high-affinity PPAR δ -selective antagonists can aid the understanding of the physiological effects of *repression* of the PPAR δ gene program. Given that antagonistic modulation of PPARs is indicated in both pro-inflammatory and obesogenic [41]

physiological responses, the synthesis of new antagonists to further elaborate on the mechanism behind these effects, is desirable.

Previously published inhibitors of PPAR δ

In 2008, a research group from GlaxoSmithKline (GSK) published GSK0660 ($IC_{50} = 300$ nM) as the first PPAR δ antagonist to be discovered (Figure 8). It was identified in a high-throughput screen and was found to be selective for the δ -subtype. Unfortunately, the oral bioavailability was rather poor [40].

Later, in 2009, the same research group identified GSK3787 (Figure 8), a selective and potent PPAR δ antagonist ($IC_{50} = 126$ nM) with enhanced bioavailability. This compound, with its electrophilic site *para* to the electron-withdrawing trifluoromethyl group (see Figure 8), is suggested to bind covalently with a nucleophilic cysteine residue within the LBD of the PPAR δ receptor [42].

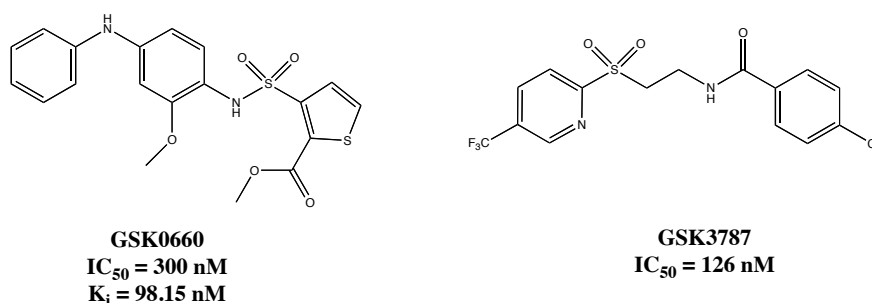


Figure 8. Structures of two synthetic PPAR δ antagonists.

The antagonistic effects of GSK3787 were studied in human skeletal muscle cells in the presence of an agonist (GW0742). GSK3787 was found to antagonize the agonist-induced gene transcription of two important PPAR δ genes, namely CPT1a and PDK4. These genes are involved in fatty acid β -oxidation and glucose metabolism, respectively. Interestingly, in the absence of the agonist, GSK3787 was only able to antagonize the basal expression of CPT1a. [42].

Another class of antagonists has also been identified, namely SR13904 (Figure 9). Zaveri *et al.* reported in 2009 that SR13904 inhibited cell proliferation by inhibition of the G₁/S cell cycle, various cell cycle-related proteins and thus an increase in apoptosis. This result has, however, not been reproduced in studies by other research groups and thus the role of PPAR δ antagonists as anticancer agents remains unclear [38, 42, 43].

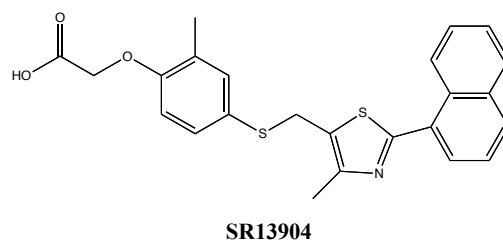


Figure 9. A synthetic PPAR δ antagonist suggested to inhibit cell proliferation.

In 2011, Müller and co-workers discovered two GSK0660-derived compounds, ST247 and PT-S58 (Figure 10), which exert inhibitory effects in PPAR δ . These compounds proved to have a significantly higher affinity ($IC_{50} = 93$ nM and 98 nM) than GSK0660 ($IC_{50} = 310$ nM) in an *in vitro* TR-FRET-based competitive ligand-binding assay. ST247 was reported to inhibit the agonist-induced expression of PPAR δ genes, in addition to actively recruit transcriptional corepressors and down-regulate the basal expression of PPAR δ genes. In view of these effects, the authors classified ST247 as an inverse agonist. The recruitment of corepressors was not found in the case of PT-S58, indicating that this compound is a true antagonist [44].

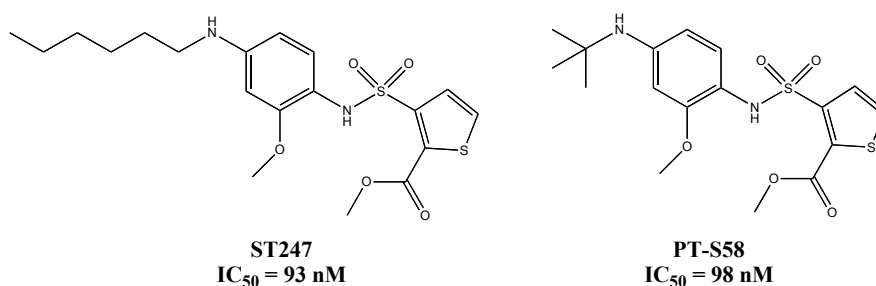


Figure 10. ST247 is reported as an inverse agonist, whereas PT-S58 is the first true antagonist.

In continuation, the Müller group also synthesized a series of compounds, again employing GSK0660 (Figure 8) as the lead compound in order to perform SAR studies. These studies revealed compounds **1a-1c** (Figure 11) to exhibit 10-fold higher binding affinities compared to GSK0660 [15]. The efficacies (e. g. IC_{50} values) of **1a-1c** have not been determined.

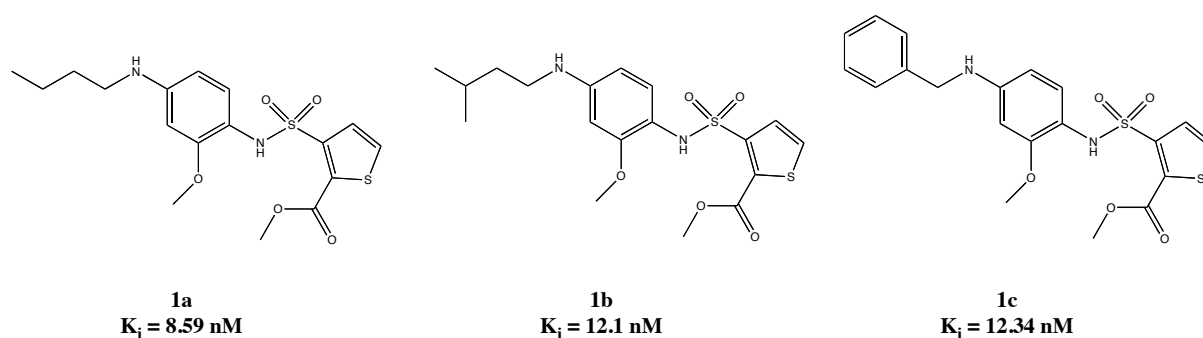
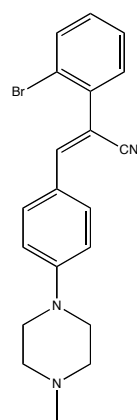


Figure 11. High-affinity compounds derived from GSK0660.

Recently, research by the same group revealed another inverse agonist, DG172 ($IC_{50} = 27$ nM) to be more potent than ST247 ($IC_{50} = 93$ nM) in an *in vitro* TR-FRET-based competitive ligand-binding assay (Figure 12). DG172 is also reported to be bioavailable after oral application to mice [45]. The acrylonitrile moiety in this molecule has an electrophilic site, as in GSK3787, indicating that this Michael-acceptor can be attacked by the nucleophilic cysteine residue in the LDB of the $PPAR\delta$ receptor. However that this reaction occurs, has yet to be established by LC-MS-MS, as it was in the case of GSK3787 [42].



DG172
 $IC_{50} = 27$ nM

Figure 12. The most potent $PPAR\delta$ inhibitor (DG172), with the best bioavailability.

Antagonism *versus* inverse agonism

The findings described above raise the question of whether the previously published antagonists in fact should be referred to as inverse agonists, given that their modes of action are similar to that of GSK3787, ST247 and DG172. However, given the complex nature of the transcriptional control exerted by PPARs and the incomplete knowledge about the mechanism of ligand-induced transcriptional repression, the ligands with inhibitory effects discussed in this thesis will consistently be referred to as antagonists.

1.6 Identification of GSK3787

A study of the structure-activity relationship (SAR) was carried out on a series of compounds focusing on the pyridyl ring, the aliphatic carbon chain and the aromatic moiety right-hand of the amide (Figure 13). Results from the studies suggested that an electron-withdrawing group such as trifluoromethyl (R_1), in the *para* position of the pyridyl ring, was crucial for obtaining the activity. In addition, the thioether analogue failed to produce any activity, and it was therefore proposed that a sulfone group in this position was required. Furthermore, the molecule was only active with a two-carbon chain ($n = 1$) between the sulfone and the amide group, indicating that the length of the chain is an important factor [42].

However, the differences in potency resulting from substitutions on the arylamide ring were minor. The analogue with a 4-chloro group on the aromatic moiety (R_2) was most preferable, even though this substitution only yielded the second highest potency compared to the 4- CF_3 group [42]. The fact that the published substitutions on the arylamide ring only resulted in minor changes in potency, suggests that the potency can be improved by other substitution patterns.

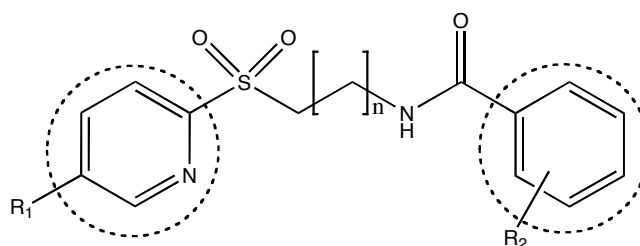


Figure 13. Important parts for SAR studies.

1.7 Aim of thesis

In this thesis, the focus was on the synthesis of more potent PPAR δ -selective antagonists, which hopefully can be used as tools for investigating the biological effects of PPAR δ antagonism.

The aims of this project where:

- i. To synthesize a series of first-generation analogues of GSK3787, partly by a reported procedure.
- ii. To synthesize a second-generation analogue with the emphasis on developing a new and efficient approach.

2 Results and discussions

2.1 Background for the first-generation analogues of GSK3787

Shearer *et al.* reported that the trifluoromethyl substituent, the two-carbon chain and the sulfone group are all important parts of the pharmacophore for GSK3787 [42]. We wanted to investigate how changes in the arylamide moiety affected the antagonistic effects (Figure 14).

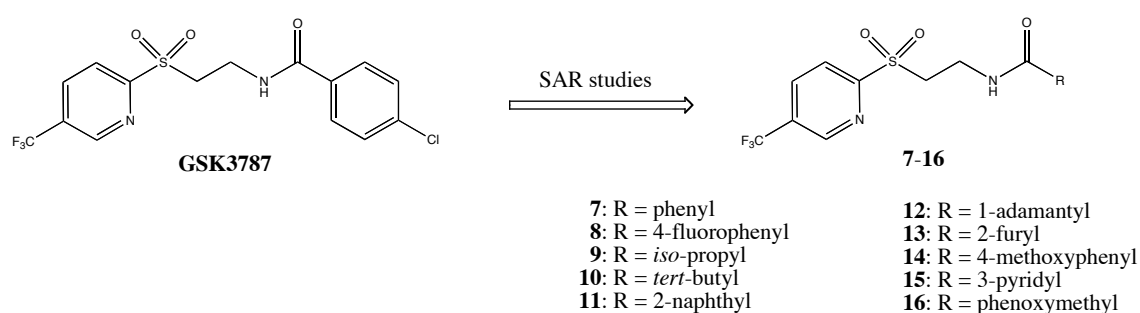
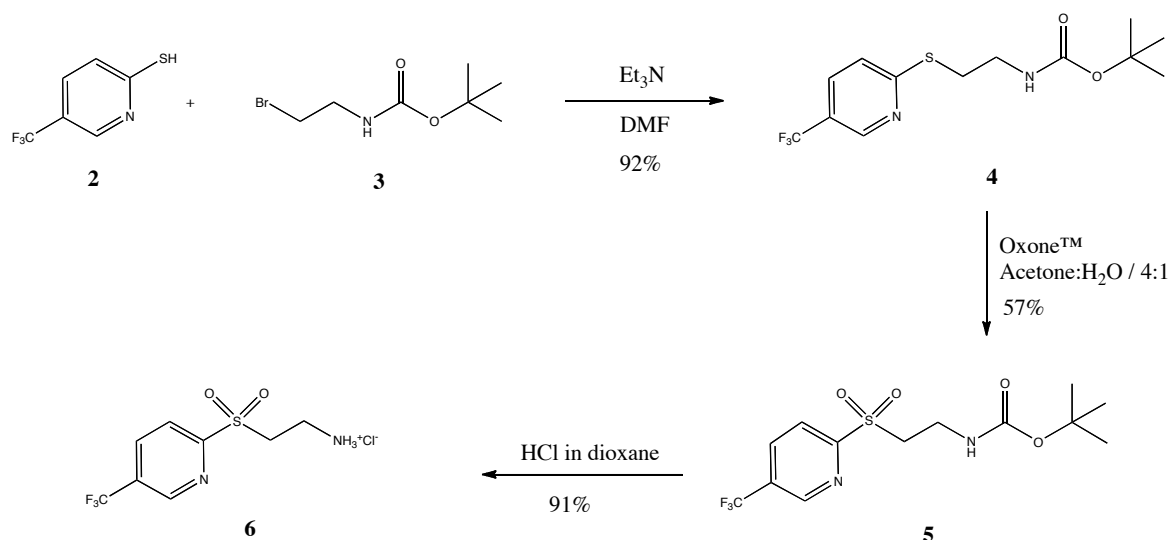


Figure 14. Structure of GSK3787 and the first-generation analogues 7-16.

2.2 Synthesis of first-generation analogues 7-16

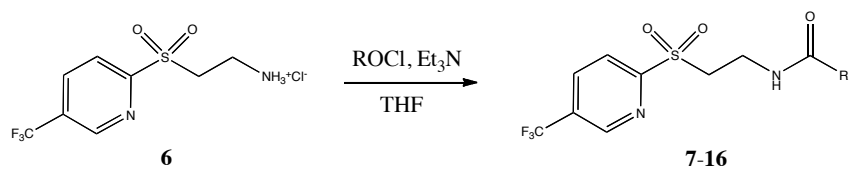
The key intermediate **6** was prepared over three steps according to a literature procedure, as reported by Shearer *et al.* (Scheme 1) [42].

The preparation of thioether **4** was achieved by reacting the thiol **2** with the alkyl bromide **3** through a nucleophilic substitution reaction (S_N2). Oxidation of thioether **4** using Oxone™ afforded the sulfone **5**. Removal of the Boc-group in **5** yielded the hydrochloride salt of the amine **6**, which would serve as a key intermediate for further acylations.



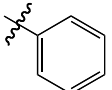
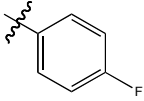
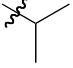

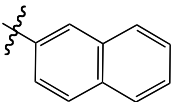
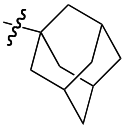
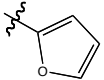
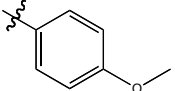
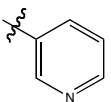
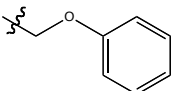
Scheme 1. Synthesis of the key intermediate **6**.

The final step involved an acylation of the primary amine **6** with various acid chlorides (Scheme 2). In total, 10 analogues **7-16** were prepared, with yields between 42% and 94% (Table 1).



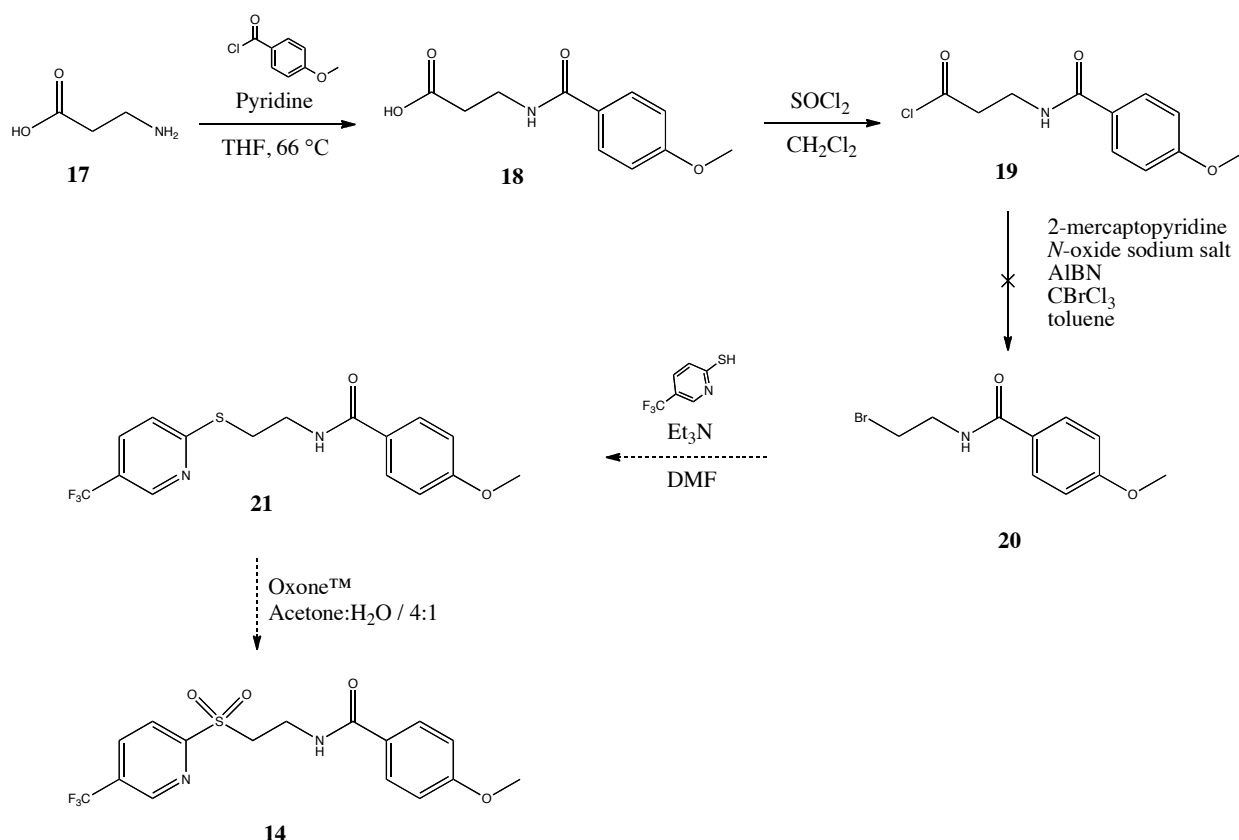
Scheme 2. The final step of the synthesis of the first-generation analogues of GSK3787.

Table 1. Results of the first-generation analogues of GSK3787.

Compound	Substituent name and structure	Yield of the final step
7	phenyl 	60%
8	4-fluorophenyl 	67%
9	<i>iso</i> -propyl 	42%
10	<i>tert</i> -butyl 	53%
11	2-naphthyl 	48%
12	1-adamantyl 	94%
13	2-furyl 	83%
14	4-methoxyphenyl 	82%
15	3-pyridyl 	69%
16	phenoxyethyl 	73%

2.3 Attempted synthesis of first-generation analogues

In an attempt to access our target molecules **7-16** by a different synthetic route, we decided to start from 3-aminopropanoic acid (**17**). The first step of this approach involved the acylation of the amine, with various acid chlorides, followed by a Barton radical decarboxylation (see Scheme 3 for the attempted synthesis of analogue **14**) [46, 47]. This reaction sequence was early found to be troublesome due to the poor solubility of 3-aminopropanoic acid and its derivatives in organic solvents, such as DMF, THF and acetone, which made the reactions difficult to monitor and to control. Therefore, all reactions were carried out without performing TLC. The intermediate alkyl bromide **20** was not detected in the ^1H NMR spectrum of the crude reaction mixture, and it could not be established which step that had failed. This approach was therefore abandoned.



Scheme 3. Attempted synthesis of the first-generation analogue **14**.

2.4 A second-generation analogue of GSK3787

By serendipity, an *N*-methylated analogue of GSK3787 was included in a molecular modelling study by our collaborators. This analogue was predicted to be more potent than GSK3787. Hence, the focus was later directed towards the synthesis of a second-generation of analogues of GSK3787. Therefore compound **23** (Figure 15) was prepared, in order to gain more information about the potency of *N*-methylated analogues of GSK3787. The 4-fluorophenyl group was chosen because of its similarities to GSK3787.

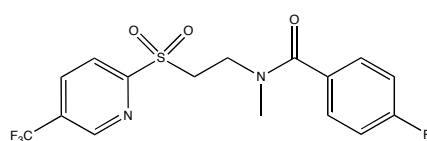


Figure 15. The second-generation analogue **23**.

In total, seven approaches towards the second-generation analogue **23** were attempted, where four of these possible strategies use the secondary amine **22** as a key intermediate (Figure 16), as it can be acylated with 4-fluorobenzoyl chloride (**41**) to afford the target molecule **23**.

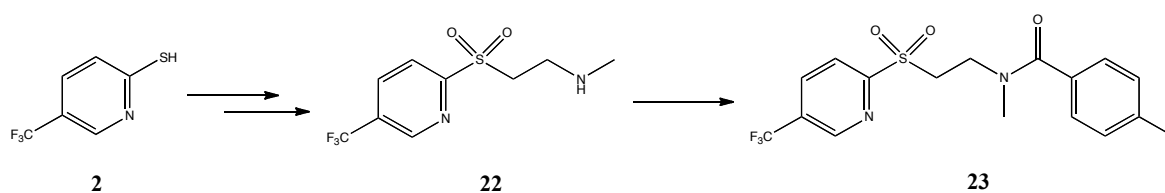


Figure 16. The starting material **2**, the key intermediate **22** and the target molecule **23**.

The four approaches towards the key intermediate **22**, and thus the second-generation analogue **23**, started with a nucleophilic substitution reaction (S_N2) between the thiol **2** and various commercially available alkyl bromides. An outline of the four approaches towards compound **22** is shown in Figure 17.

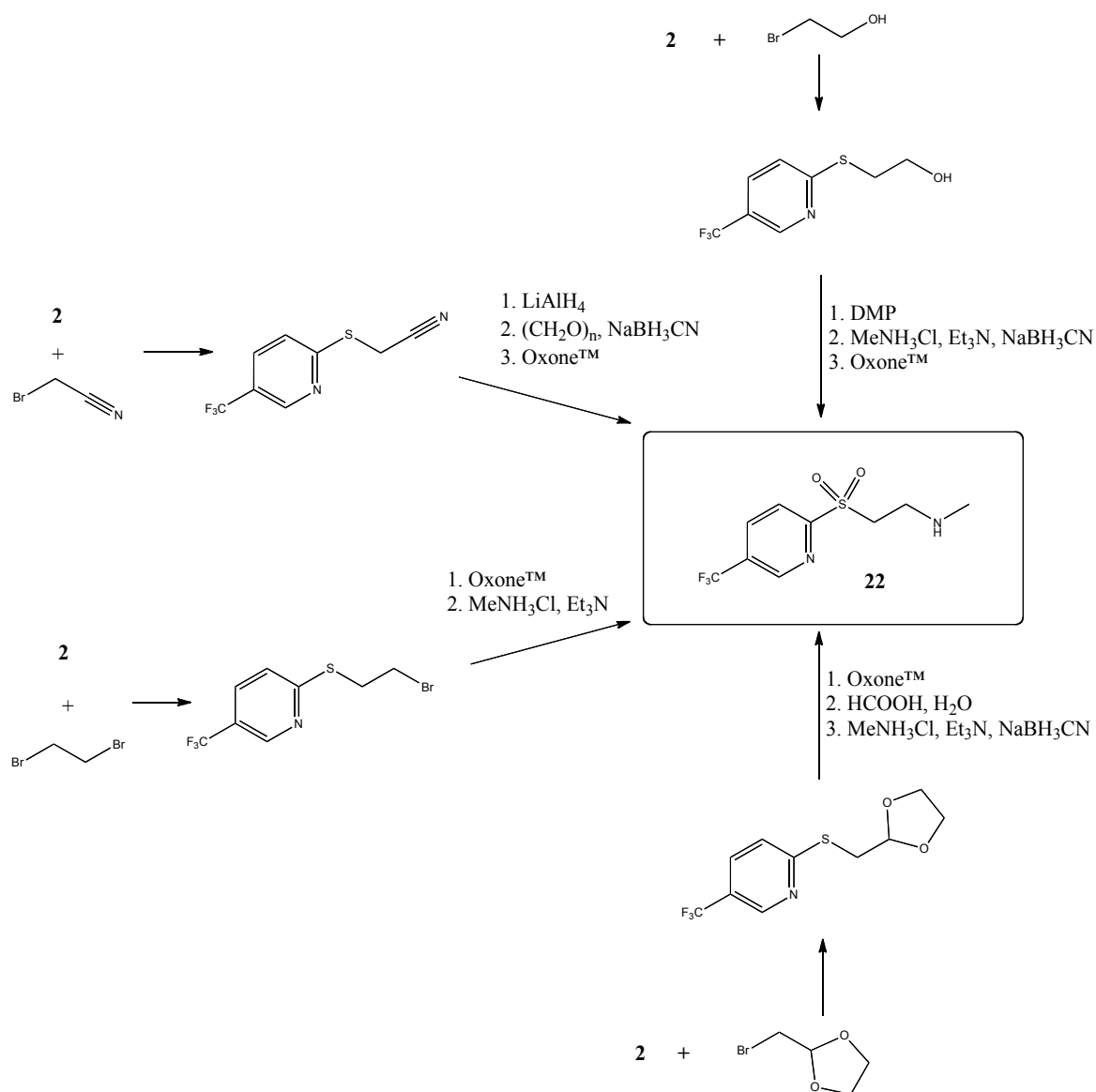


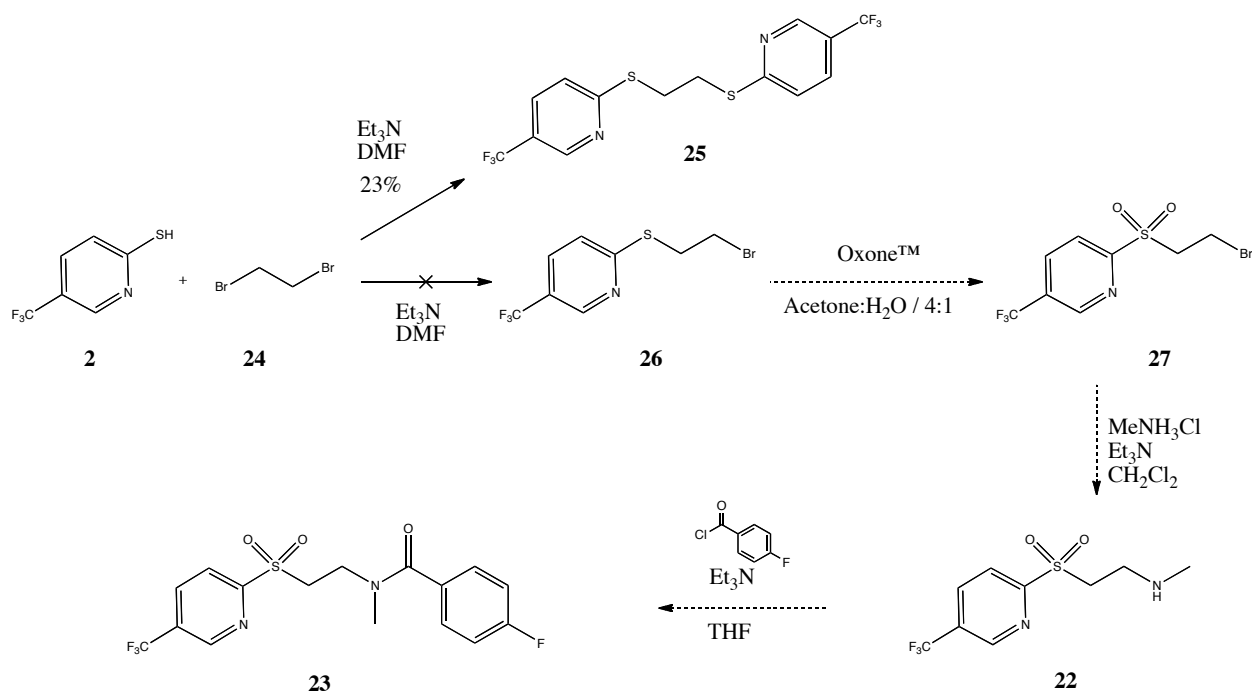
Figure 17. An outline of four approaches towards the key intermediate **22**.

In continuation, three approaches towards the second-generation analogue **23**, that did not include key intermediate **22**, were also attempted. The fifth approach was a direct *N*-alkylation of compound **8**, a prepared first-generation analogue, whereas the sixth approach differed from previously mentioned approaches, by using 4-fluorobenzoyl chloride (**41**) in the first step of the synthesis. The last approach was similar to the synthesis of the first-generation analogues, by using the same starting materials. All seven approaches will be described and discussed in more detail below (in section 2.5-2.6).

2.5 Attempted syntheses of *N*-methyl analogue 23

2.5.1 The first approach

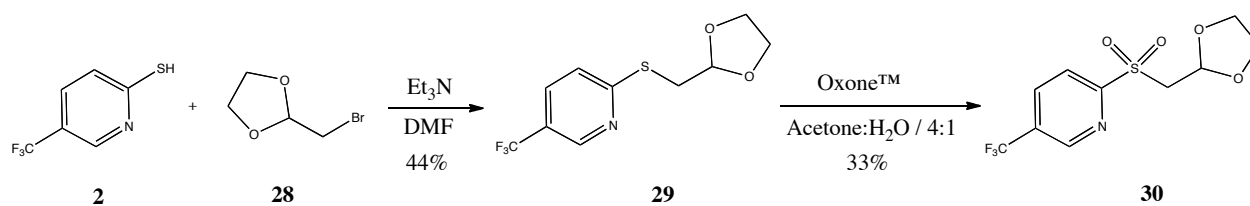
The thiol **2** was treated with 1,2-dibromoethane (**24**) in DMF (Scheme 4). This failed to give us the desired product, and instead we obtained the disubstituted product **25**, even though 1,2-dibromoethane (**24**) was added slowly (over 1.5 hours) to the thiolate. The structure of the disubstituted product **25** was confirmed by both ^1H and ^{13}C NMR spectra. The NMR spectra are shown in the appendix.



Scheme 4. An overview of the first approach towards **23**.

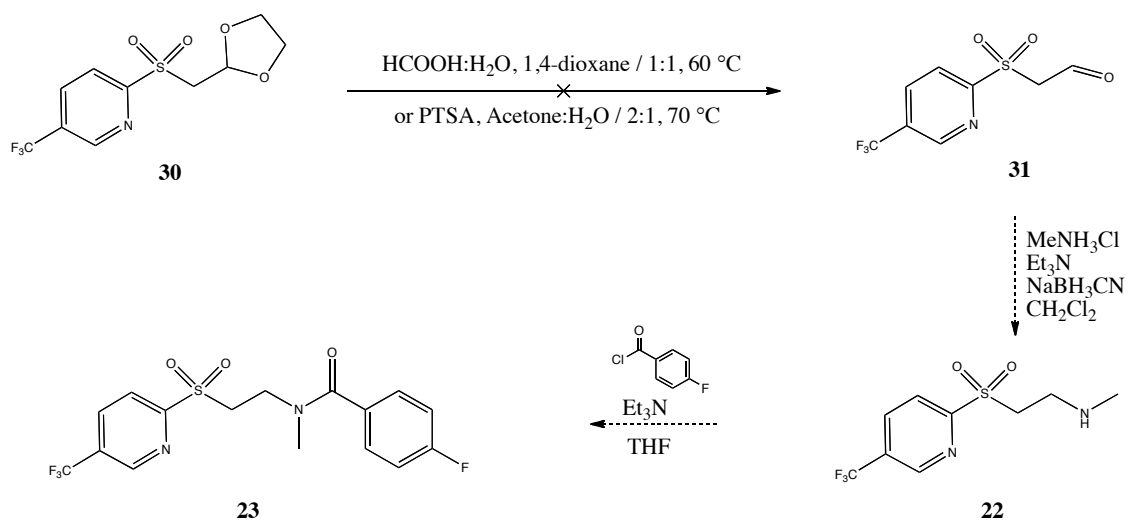
2.5.2 The second approach

In this approach, we intended to use an acetal as a protecting group to avoid the problem with dialkylation of 1,2-bromoethane (**24**), as in the first approach. The thiol **2** was treated with bromide **28** to afford thioether **29**, followed by the oxidation with OxoneTM in a 4:1 mixture of acetone and water, to yield sulfone **30** (Scheme 5).



Scheme 5. The two first steps of the second approach towards **23**.

Deprotection of the acetal in **30** in order to reveal the aldehyde was first attempted with formic acid and water in 1,4-dioxane at 60 °C (Scheme 6). However, the ^1H NMR spectrum showed no conversion of the starting material. Therefore, a new strategy with *p*-toluenesulfonic acid in acetone/water was attempted. This gave a complex mixture of products. Given the problems in obtaining the desired aldehyde, this approach was abandoned.

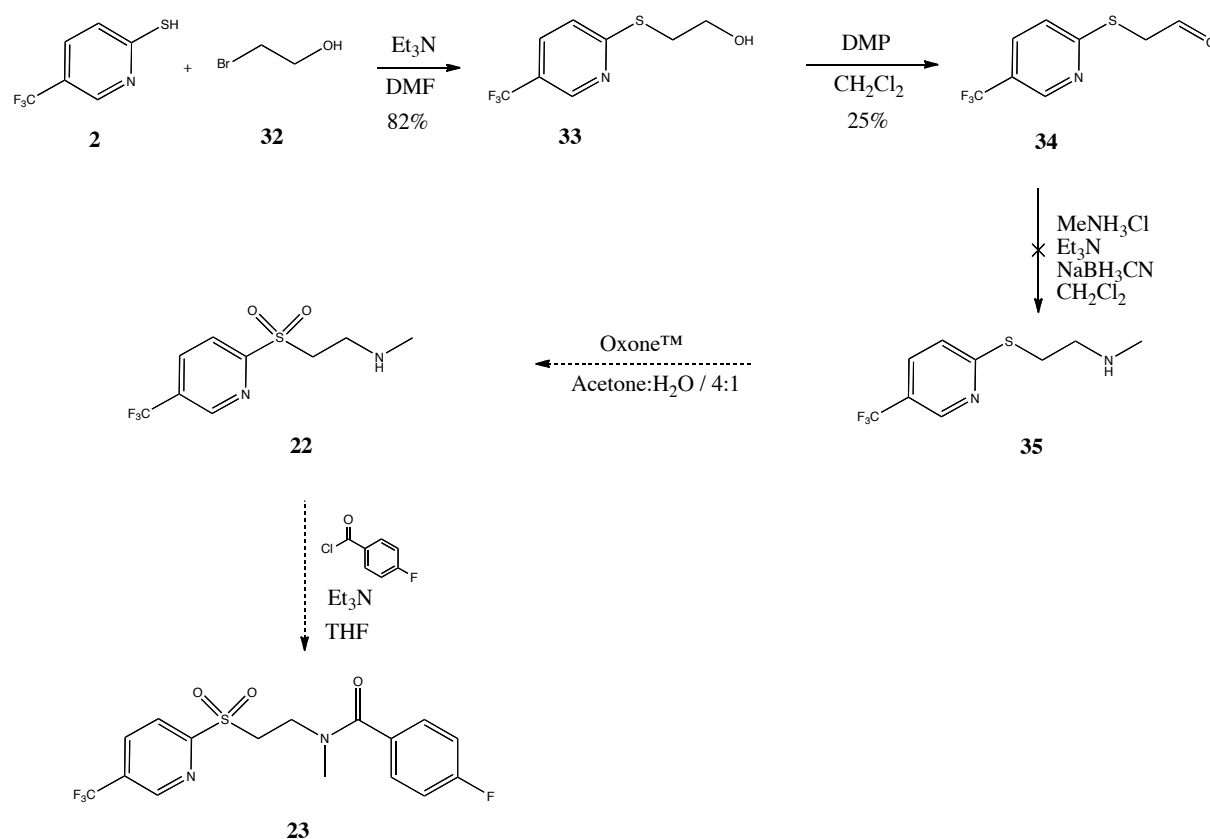


Scheme 6. Attempted deprotection of the acetal **30** and the intended final steps towards **23**.

The intended steps after preparing the aldehyde **31** were reductive amination with methylamine hydrochloride in the presence of sodium cyanoborohydride to yield secondary amine **22**, followed by acylation to afford **23**. ^1H , ^{13}C and DEPT135 NMR spectra for compound **30** are shown in the appendix.

2.5.3 The third approach

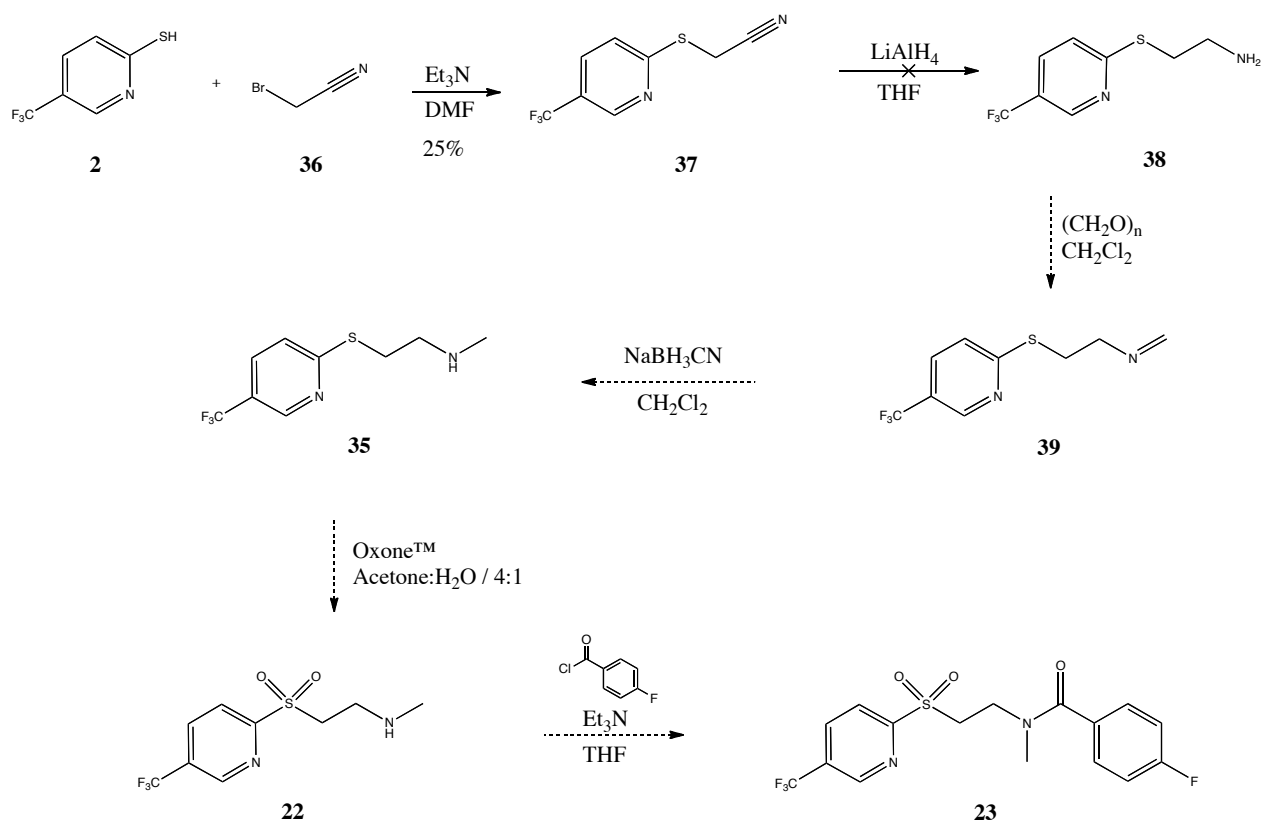
In an alternative approach, the aldehyde **34** could be accessed through oxidation of the alcohol **33** (Scheme 7). The thiol **2** was thus alkylated with bromoethanol **32** to give the alcohol **33** in 82% yield. The alcohol **33** was oxidized using DMP to yield the aldehyde **34** in a low yield (25%). Reductive amination on **34** was attempted, but the reaction was not successful, maybe due to the instability of the aldehyde. The ^1H NMR spectrum did not show the desired product, and the approach was thus abandoned.



Scheme 7. An overview of the third approach towards **23**.

2.5.4 The fourth approach

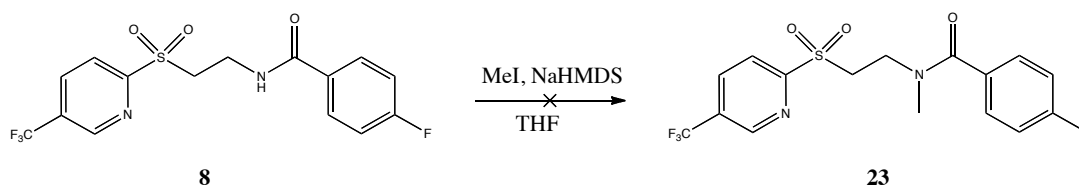
This approach avoided the problem of working with an aldehyde on the main skeleton by performing a reductive amination using paraformaldehyde and the primary amine **38** (Scheme 8). To reach the primary amine **38**, the thiol **2** was alkylated with bromoacetonitrile (**36**) to give the nitrile **37**, followed by reduction to yield the primary amine **38**. The reduction of the nitrile failed, perhaps due to an interaction between the pyridine and the aluminium in LiAlH_4 . During the reaction, the mixture turned from colourless to blue, indicating this possible complex. The use of a milder reducing agent was not investigated.



Scheme 8. An overview of the fourth approach towards **23**.

2.5.5 The fifth approach: a direct *N*-alkylation

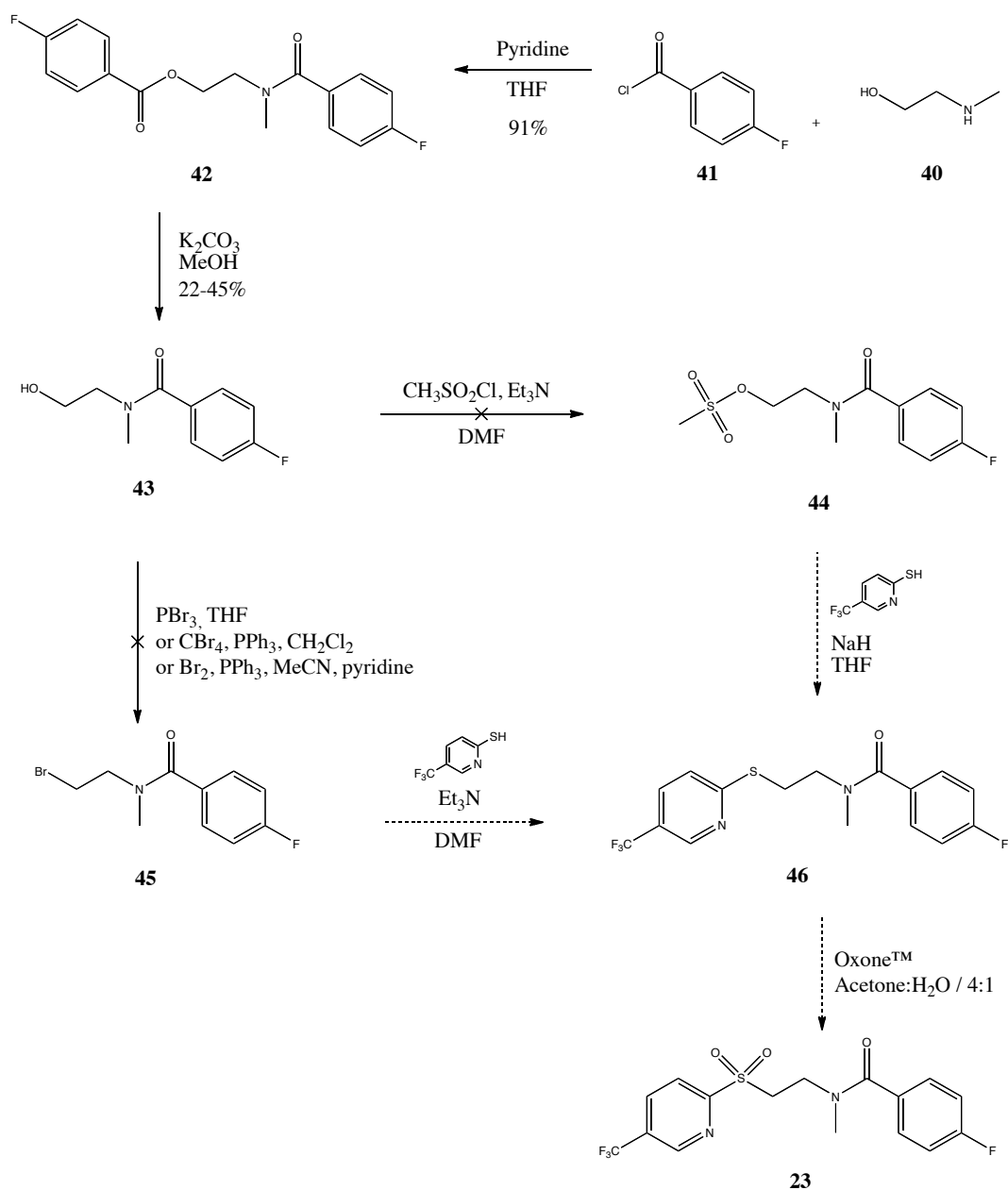
Starting with a secondary amide and thereby avoiding overalkylation [48], a direct *N*-alkylation was suggested to be a short route to **23**. A direct *N*-alkylation of the prepared first-generation analogue **8** was attempted, using NaHMDS as a base, with a large excess of MeI in THF (Scheme 9). The reaction did not provide the desired product. However, this result could have been caused by the difficulty of using the volatile MeI on a small scale. The acidic α -protons of the sulfone may also contribute to potential problems in this reaction, giving the α -alkylated product instead of the desired *N*-methylation.



Scheme 9. An attempted direct *N*-alkylation of compound **8** to yield **23**.

2.5.6 The sixth approach

This approach employed the commercially available *N*-methyl aminoethanol (**40**) as a starting material (Scheme 10). The double *N,O*-acylation afforded the amidoester **42**, in which the benzoic ester could be selectively hydrolysed in a subsequent step, yielding the alcohol **43**. In this fashion the *N*-methylated arylamide moiety could be obtained in a reliable acylation reaction, in excellent yields (91%).



Scheme 10. An overview of the sixth approach towards **23**.

The benzoic ester was hydrolysed using K_2CO_3 in MeOH, to afford the alcohol **43** in a low yield. Attempts were made to improve the yield by increasing the reaction time. Monitoring the reaction with TLC confirmed full conversion of starting material **42**, but it was still difficult to obtain a high yield of **43** after purification. Due to the low yields (between 22% and 45%), this reaction was also attempted with LiOH in a 4:1 mixture of THF and water, but these conditions failed to improve the yield. The bromination of alcohol **43** to afford bromide **45** was attempted by three different strategies. All reactions were unsuccessful, even though

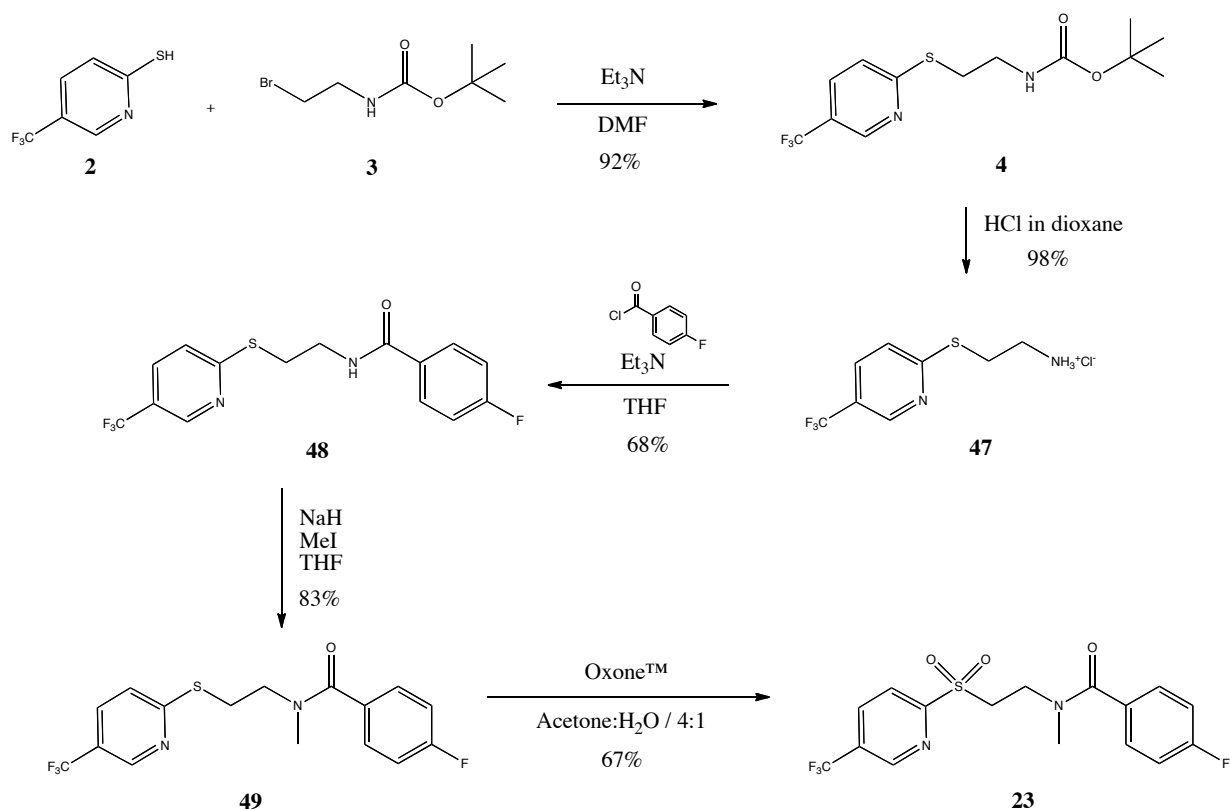
this approach seemed very promising on paper. In a final attempt, a substitution reaction between the thiol **2** and the mesylate **44** was hampered by the failure to obtain the mesylate **44** from the alcohol **43** and mesyl chloride. On the basis of the described difficulties, the abovementioned strategies were also abandoned. ¹H, ¹³C and DEPT135 NMR spectra of the amidoester **42**, as well as a ¹H NMR spectrum of alcohol **43**, are shown in the appendix. The experimental procedures for these compounds (**42** and **43**) are listed in section 5.4.

2.6 Successful synthesis of the *N*-methyl analogue **23**

The synthetic approach, which afforded compound **23** (Scheme 11), included five steps.

The synthesis started similarly to the abovementioned approaches, with a nucleophilic substitution reaction (S_N2) to yield the thioether **4**. Instead of oxidizing thioether **4** to the sulfone group with acidic α -protons, the compound was directly *N*-deprotected using HCl in dioxane to yield the amine hydrochloride salt **47**. The following acylation with the acid chloride **41** was performed in the same manner as earlier, to give the amide **48**. The yield over the three steps was 66%.

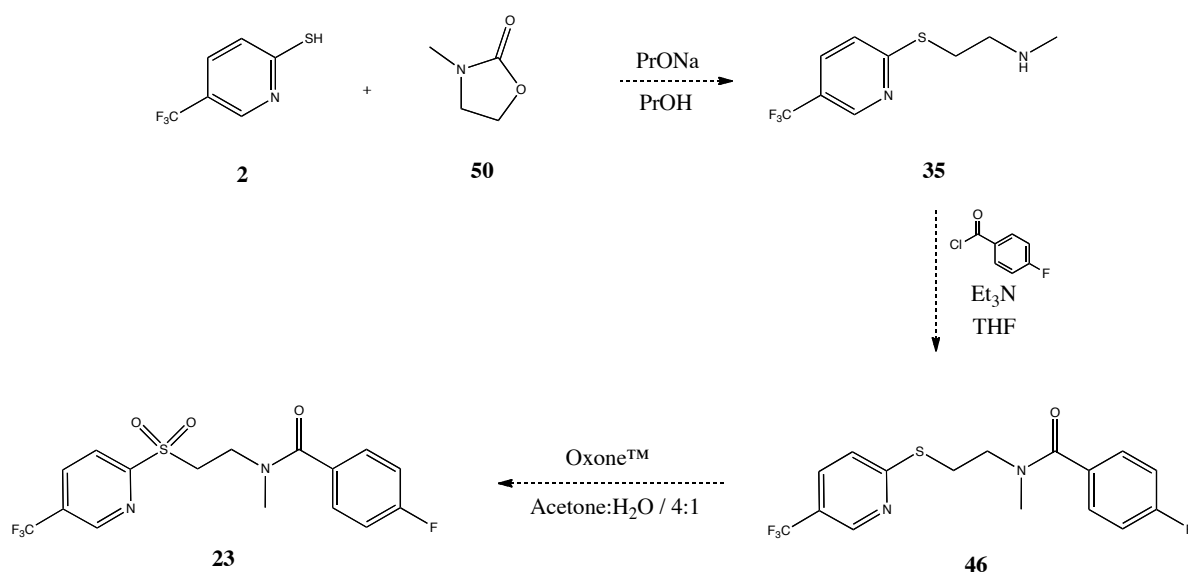
The *N*-methylated compound **49** was achieved by using a great excess of MeI as the methylation reagent in THF in the presence of NaH. The following oxidation of the thioether group, yielded sulfone **23**. When monitoring the reaction, the *N*-methyl amide **49** was expected to be more lipophilic than its *N*-H analogue **48**. However, this was not the case, and could be explained by an intramolecular hydrogen bond between the nitrogen atom in the pyridine ring and the amide *N*-H, which would make thioether **48** more lipophilic than **49**, due to the masking of its polar groups. In sum, this approach was successful and provided the desired product. Due to time constraints, only one analogue of the second generation was prepared.



Scheme 11. The successful synthesis of the second-generation analogue **23**.

2.7 Alternative synthesis of compound **23**

In a paper published by Ishibashi and colleagues, a nucleophilic substitution reaction between an arylthiolate and *N*-methyl-2-oxazolidinone (**50**) in PrOH was able to afford the secondary ethylamine in 98% yield. It was reported to be a reaction completed within 30 minutes [49]. The same approach was therefore suggested for the thiol **2** and the methyl oxazolidinone **50** to yield the secondary amine **35** (Scheme 12). An acylation of the secondary amine **35**, followed by oxidation with Oxone™ could yield the target molecule **23**. This approach was not explored due to the fact that a successful approach was already achieved.



Scheme 12. An alternative synthesis of compound **23**, using thiol **2** and methyl oxazolidinone **50** as starting materials.

2.8 Molecular modelling

Molecular modelling studies were performed by Ph.D. student Åsmund Kaupang. The prepared compounds **7-16** and **23** were docked into the LBD of PPAR δ . The findings from these studies showed that compound **23** of the synthesized analogues (Figure 18 and 19) has the highest docking score, followed by compound **11** (Figure 18 and 20). The docking score indicates that the compounds exhibit favourable interactions within the PPAR δ LBD, and thus that they should have affinity for the binding pocket. Compound **8**, which is the *N*-H analogue of **23**, scored significantly lower in the docking studies. Since the *N*-methyl substitution was beneficial for the binding properties, an *N*-methyl analogue of **11** was also submitted to docking. This compound displayed even better binding properties than both **11** and **23**. Currently, further molecular modelling studies are ongoing aiming at generating new lead compounds as selective PPAR δ antagonists.

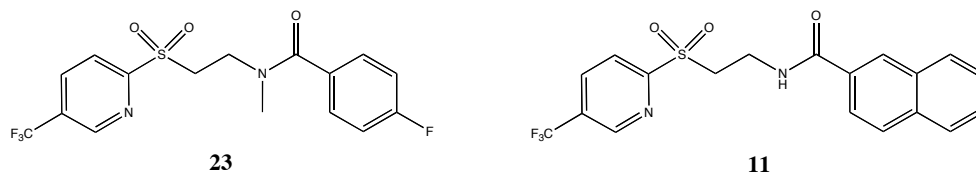


Figure 18. The two prepared compounds **23** and **11** displayed the best binding properties in the molecular modelling studies.

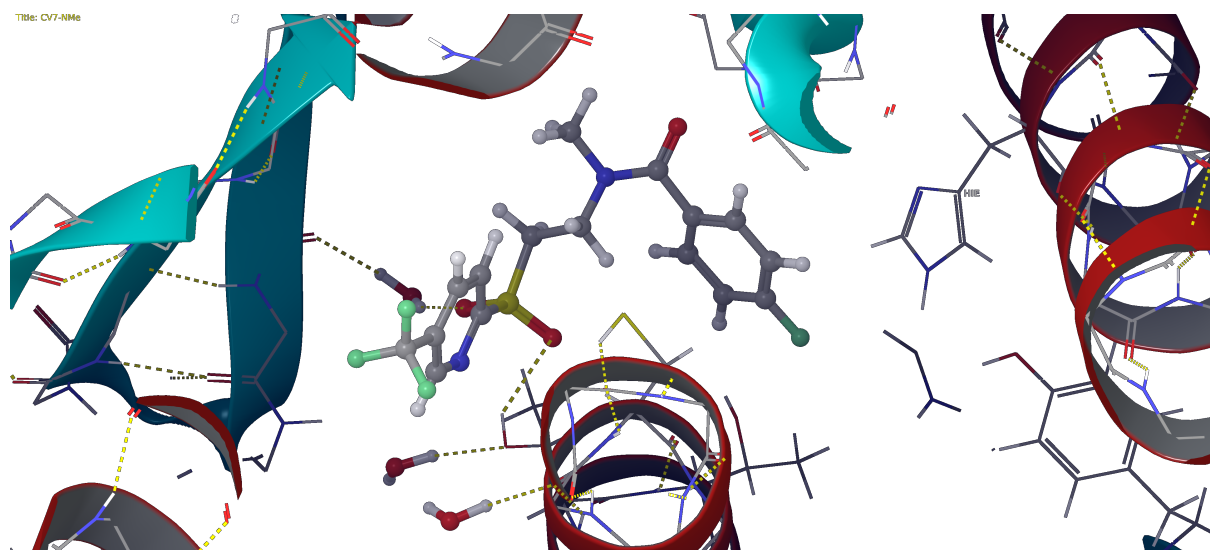


Figure 19. Molecular modeling of compound **23** in the PPAR δ LBD.

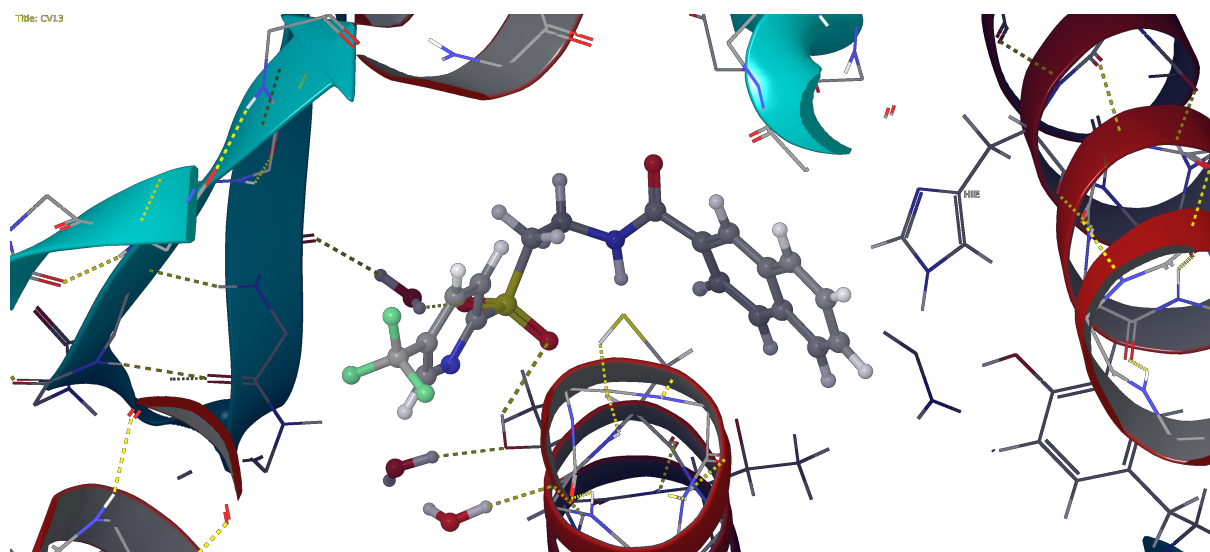


Figure 20. Molecular modelling of compound **11** in the PPAR δ LBD.

3 Conclusion and future work

Synthesis

The synthetic efforts resulted in eleven putative antagonists of PPAR δ . The first-generation analogues **7-16** were synthesized in part by a known synthetic method, followed by an acylation reaction. An efficient approach for the second-generation analogues was developed, which afforded compound **23**. This method may prove useful for the synthesis of additional analogues suitable for SAR studies.

Biological studies

The biological studies of compounds **7-16** and **23** are currently ongoing. The *in vitro* testing will reveal the potency of the prepared analogues, and an initial structure activity relationship can be established when the biological results are available.

Molecular modelling

Molecular modelling studies were performed and indicate that the second-generation compound **23** outperform the first-generation compounds. Since compound **11** showed to have the best binding properties among the first-generation analogues, an *N*-methyl analogue of **11** was also submitted to docking. This compound displayed even better binding properties than both **11** and **23**. This finding suggests that the *N*-methyl analogue of **11** should be synthesized and biologically evaluated.

4 Spectroscopic elucidation and characterization of compounds

4.1 General characterization of intermediates and analogues

The prepared analogues and intermediates **4-16**, **23** and **37-39** share a common moiety, and will therefore be discussed in general (Figure 21).

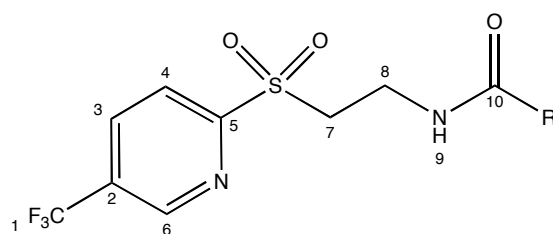


Figure 21. General structure of prepared analogues and their intermediates. The numerations are not in accordance with the IUPAC rules.

The recorded ¹H NMR spectra show characteristic signals for aromatic protons, which typically occur between 6 ppm and 8 ppm. The proton with the highest chemical shift value, furthest downfield, is likely to be the proton in position 6 (Figure 21). This is explained by the deshielding effect of the electronegative trifluoromethyl group and the nitrogen atom in the pyridine ring. According to the literature, the coupling constants in a benzene ring system are $J = 7.5$ Hz for *ortho* coupling, $J = 1.5$ Hz for *meta* coupling and $J = 0.7$ Hz for *para* coupling [50]. These coupling constants will be used as guidelines in the structure elucidation of the prepared compounds. The aromatic protons in position 3 and 4 will occur as a double doublet and a doublet, with an *ortho* and a *meta* coupling, and an *ortho* coupling, respectively. The protons (in position 7 and 8) in the alkyl chain typically appear at 3-4 ppm, due to the lower electron density around them, caused by the electron withdrawing sulfone and amide group. The proton in position 9 occurs as a triplet, typically at 6-8 ppm. However, the chemical shift values for the N-H protons vary with different solvents and concentrations.

The ^{13}C NMR spectra obtained for all compounds show two important and characteristic signals at 120-130 ppm. Each of these two signals is split into a quartet, explained by the three fluorine atoms coupled to the carbon in position 1. These quartets are therefore assigned to the carbons in position 1 and 2. However, the quartet assigned to the carbon in position 2 has a lower coupling constant and a higher chemical shift value, caused by the electron withdrawing sulfone group.

Typically, the most downfield signals are assigned to the carbon atoms in position 10 and 5, where the carbonyl in position 10 has the highest chemical shift value. The carbon in position 6 generally appears more downfield compared to the carbon in position 3 and 4, which is due to the electron withdrawing effects of the trifluoromethyl group and the nitrogen atom in the pyridine ring. As expected from the literature, the carbons in the alkyl chain (in position 7 and 8) are detected as the most upfield signals.

All compounds, except **4-6**, have to the best of our knowledge not previously been reported or characterized in the literature.

4.2 Spectroscopic characterization of first-generation analogues 7-16 and their intermediates 4-6

4.2.1 Characterization of compound 4

Compound **4** has already been characterized in the literature by Shearer and co-workers and the obtained ^1H NMR spectrum is in accordance with the published data [42]. However, this compound does not apply to the general rule discussed in section 4.1, owing to the fact that the thioether group is less electron withdrawing than the sulfone group. Therefore, the quaternary carbon at position 1 has a higher chemical shift value than the carbon at position 2. The ^1H NMR and ^{13}C NMR chemical shifts are assigned to the numbered positions in Figure 22 and Table 2. The ^1H and ^{13}C NMR spectra are shown in the appendix.

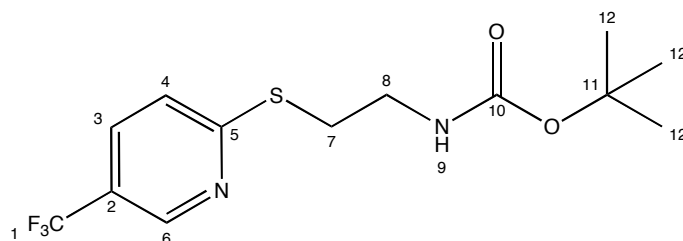


Figure 22. Atom numbering of compound 4.

Table 2. Assignment of chemical shift values for compound 4.

Position	δ_{H}	Multiplicity	Coupling constant(s) (<i>J</i> Hz)	δ_{C}	Multiplicity	Coupling constant (<i>J</i> Hz)
1	-	-	-	123.93	q	271.7
2	-	-	-	121.01	q	32.6
3	7.97	dd	8.6, 2.5	133.33	d	3.2
4	7.53	d	8.5	121.73	-	-
5	-	-	-	163.95	-	-
6	8.77	s	-	145.90	-	-
7	3.32 – 3.13	m	-	39.42	-	-
8	3.32 – 3.13	m	-	29.30	-	-
9	7.05	m	-	-	-	-
10	-	-	-	155.53	-	-
11	-	-	-	77.73	-	-
12	1.37	d	4.8	28.17	-	-

4.2.2 Characterization of compound 5

Compound **5** has already been characterized in the literature by Shearer and co-workers and the obtained ^1H NMR spectrum is in accordance with the published data [42]. The ^1H NMR and ^{13}C NMR chemical shifts are assigned to the numbered positions in Figure 23 and Table 3. The ^1H and ^{13}C NMR spectra are shown in the appendix.

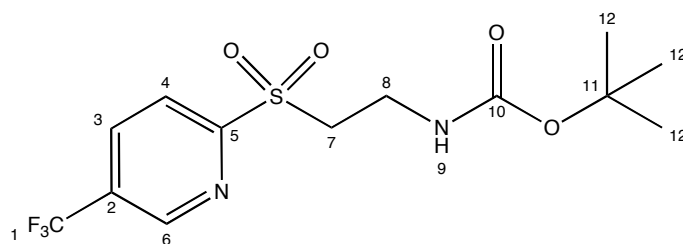


Figure 23. Atom numbering of compound **5**.

Table 3. Assignment of chemical shift values for compound **5**.

Position	δ_{H}	Multiplicity	Coupling constant (J Hz)	δ_{C}	Multiplicity	Coupling constant (J Hz)
1	-	-	-	122.85	q	273.3
2	-	-	-	128.38	q	32.9
3	8.62	dd	-	137.03	d	3.5
4	8.25	d	8.2	122.29	-	-
5	-	-	-	160.09	-	-
6	9.23	s	-	148.84 – 146.23	m	-
7	3.68	t	6.4	50.90	-	-
8	3.31	q	5.9	34.33	-	-
9	6.79	t	5.2	-	-	-
10	-	-	-	155.06	-	-
11	-	-	-	78.00	-	-
12	1.27	s	-	27.99	-	-

4.2.3 Characterization of compound **6**

Shearer and co-workers have earlier performed the ^1H NMR characterization of compound **6** [42]. The obtained ^1H NMR spectrum is roughly in accordance with the published data, except for the broad singlet, which is shifted upfield from 8.11 ppm to 8.48 ppm. Given that both spectra are recorded in $\text{DMSO-}d_6$, this inconsistency may be caused by a difference in concentration of the NMR sample. The ^1H NMR and ^{13}C NMR chemical shifts are assigned to the numbered positions in Figure 24 and Table 4. The ^1H , ^{13}C and DEPT135 NMR spectra are shown in the appendix.

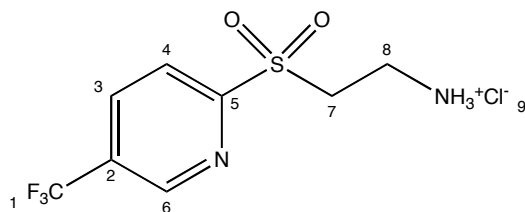


Figure 24. Atom numbering of compound 6.

Table 4. Assignment of chemical shift values to compound 6.

Position	δ_H	Multiplicity	Coupling constant (J Hz)	δ_C	Multiplicity	Coupling constant (J Hz)
1	-	-	-	122.75	q	273.4
2	-	-	-	128.85	q	33.1
3	8.76 – 8.56	m	-	137.42	q	3.4
4	8.31	d	8.2	122.48	-	-
5	-	-	-	159.16	-	-
6	9.27	s	-	147.57	q	3.6
7	4.07 – 3.81	m	-	49.04	-	-
8	3.32 – 3.06	m	-	32.85	-	-
9	8.48	bs	-	-	-	-

4.2.4 Characterization of compound 7

The chemical shift values for the atoms at position 1-8 share the same characteristics as described in section 4.1, except the protons in position 3 and 4, which occur as multiplets. The five protons in the arylamide moiety appear between 7.26 ppm and 7.66 ppm, as expected for aromatic protons. The ^1H NMR and ^{13}C NMR chemical shifts are assigned to the numbered positions in Figure 25 and Table 5. The ^1H , ^{13}C and DEPT135 NMR spectra are shown in the appendix.

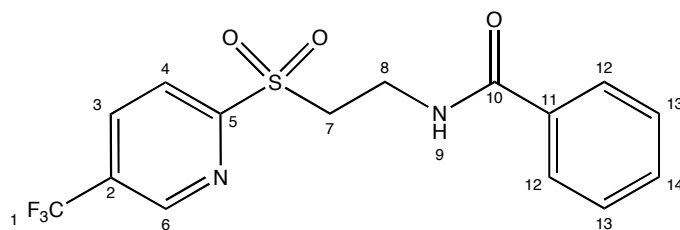


Figure 25. Atom numbering of compound 7.

Table 5. Assignment of chemical shift values to compound 7.

Position	δ_H	Multiplicity	Coupling constant (J Hz)	δ_C	Multiplicity	Coupling constant (J Hz)
1	-	-	-	122.63	q	273.2
2	-	-	-	128.23	q	33.00
3	8.60 – 8.39	m	-	136.86	q	3.4
4	8.60 – 8.39	m	-	122.18	-	-
5	-	-	-	160.01	-	-
6	9.08	s	-	147.20	q	3.8
7	3.89	t	6.2	50.34	-	-
8	3.66	q	6.0	33.76	-	-
9	8.24	m	-	-	-	-
10	-	-	-	165.94	-	-
11	-	-	-	133.29	-	-
12	7.66 – 7.26	m	-	126.83	-	-
13	7.66 – 7.26	m	-	128.09	-	-
14	7.66 – 7.26	m	-	131.32	-	-

4.2.5 Characterization of compound 8

The ^1H and ^{13}C NMR chemical shifts are assigned to the numbered positions in Figure 26 and Table 6. The ^{13}C NMR spectra display a double doublet and a multiplet for the carbons in position 12 and 13, respectively, due to the substituted aromatic fluorine atom. The ^1H , ^{13}C and DEPT135 NMR spectra are shown in the appendix.

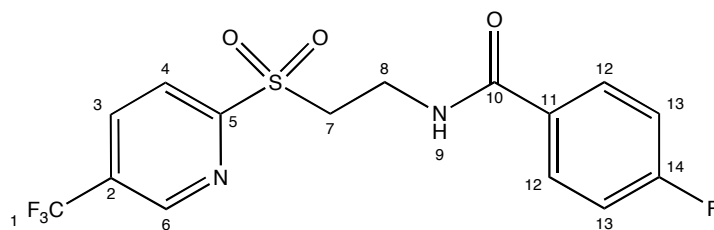


Figure 26. Atom numbering of compound **8**.

Table 6. Assignment of chemical shift values to compound **8**.

Position	δ_H	Multiplicity	Coupling constant(s) (J Hz)	δ_C	Multiplicity	Coupling constant (J Hz)
1	-	-	-	122.61	q	273.2
2	-	-	-	128.15	q	32.9
3	7.75 – 7.58	m	-	136.85	q	3.4
4	7.75 – 7.58	m	-	122.13	-	-
5	-	-	-	160.05	d	160.9
6	9.12 – 8.95	m	-	147.17	q	3.8
7	3.89	t	6.1	50.22	-	-
8	3.64	m	-	33.87	-	-
9	8.22	m	-	-	-	-
10	-	-	-	164.78	-	-
11	-	-	-	129.67	d	2.9
12	8.47	dd	8.0, 2.3	129.49	d	9.1
13	7.32 – 7.10	m	-	115.03	d	21.8
14	-	-	-	163.95	d	248.8

4.2.6 Characterization of compound 9

The ^1H and ^{13}C NMR chemical shifts are assigned to the numbered positions in Figure 27 and Table 7. The CH_3 -groups in position 12 appear at 0.85 ppm, as expected for aliphatic protons. The proton in position 11 occurs as a heptet at 2.07 ppm, which is in accordance with the literature value. The ^1H , ^{13}C and DEPT135 NMR spectra are shown in the appendix.

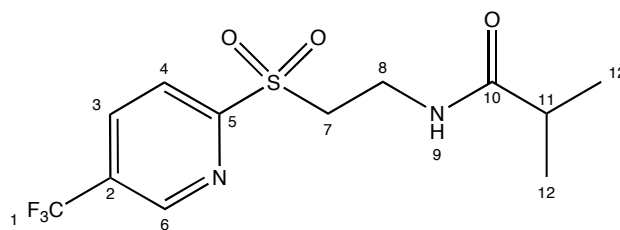


Figure 27. Atom numbering of compound **9**.

Table 7. Assignment of chemical shift values to compound **9**.

Position	δ_{H}	Multiplicity	Coupling constant(s) (<i>J</i> Hz)	δ_{C}	Multiplicity	Coupling constant (<i>J</i> Hz)
1	-	-	-	122.82	q	273.3
2	-	-	-	128.48	q	33.0
3	8.62	dd	8.4, 1.7	137.08	-	-
4	8.26	d	8.2	122.28	-	-
5	-	-	-	160.01	-	-
6	9.24	s	-	147.39	-	-
7	3.69	t	6.5	50.66	-	-
8	3.41	q	6.3	32.83	-	-
9	7.83	t	5.7	-	-	-
10	-	-	-	176.20	-	-
11	2.07	h	6.9	33.69	-	-
12	0.85	d	6.9	19.17	-	-

4.2.7 Characterization of compound 10

The ^1H NMR and ^{13}C NMR chemical shifts are assigned to the numbered positions in Figure 28 and Table 8. The observed doublet at 0.85 ppm, which integrates for nine protons, indicates the three CH_3 -groups in position 12. The ^1H , ^{13}C and DEPT135 NMR spectra are shown in the appendix.

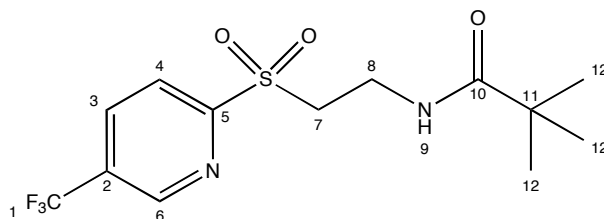


Figure 28. Atom numbering of compound **10**.

Table 8. Assignment of chemical shift values to compound **10**.

Position	δ_{H}	Multiplicity	Coupling constant(s) (J Hz)	δ_{C}	Multiplicity	Coupling constant (J Hz)
1	-	-	-	122.81	q	273.2
2	-	-	-	128.51	q	33.0
3	8.62	dd	8.5, 1.9	137.10	q	3.6
4	8.26	d	8.2	122.30	-	-
5	-	-	-	159.95	-	-
6	9.25	s	-	147.42	q	3.8
7	3.70	t	6.6	50.63	-	-
8	3.42	q	6.5	33.16	-	-
9	7.55	t	5.4	-	-	-
10	-	-	-	177.61	-	-
11	-	-	-	33.16	-	-
12	0.93	s	-	27.06	-	-

4.2.8 Characterization of compound **11**

Most of the ^1H and ^{13}C NMR chemical shifts are assigned to the numbered positions in Figure 29 and Table 9. However, the chemical shift values for the naphthalene ring are difficult to assign. Instead, a range of chemical shifts is assigned to the aromatic protons and carbons, except position 6. The ^1H , ^{13}C and DEPT135 spectra are shown in the appendix.

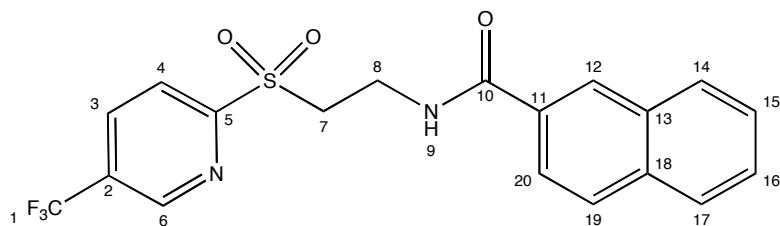


Figure 29. Atom numbering of compound **11**.

Table 9. Assignment of chemical shift values to compound **11**.

Position	δ_{H}	Multiplicity	Coupling constant (J Hz)	δ_{C}	Multiplicity	Coupling constant (J Hz)
1	-	-	-	122.50	q	273.4
2	-	-	-	128.19	q	33.1
3	*	-	-	136.84	q	3.4
4	*	-	-	122.18	-	-
5	-	-	-	160.29 – 159.58	m	-
6	9.05	-	-	147.19	q	3.8
7	3.94	t	6.0	50.38	-	-
8	3.72	q	5.6	33.88	-	-
9	8.66	t	4.8	-	-	-
10	-	-	-	165.98	-	-
11	-	-	-	131.92	-	-
12	8.46	-	-	128.75	-	-
13	-	-	-	134.17	-	-
14	*	-	-	**	-	-
15	*	-	-	**	-	-
16	*	-	-	**	-	-
17	*	-	-	**	-	-
18	-	-	-	130.63	-	-
19	*	-	-	**	-	-
20	*	-	-	**	-	-

* the chemical shift value for this proton is in the range of 7.52 - 8.27 ppm.

** the chemical shift value for this carbon is in the range of 123.61 - 127.74 ppm.

4.2.9 Characterization of compound **12**

The ^1H and ^{13}C NMR chemical shifts are assigned the numbered positions in Figure 30 and Table 10. The ^1H , ^{13}C and DEPT135 NMR spectra are shown in the appendix.

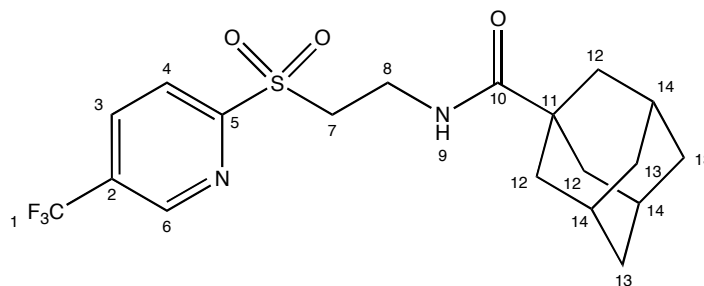


Figure 30. Atom numbering of compound **12**.

Table 10. Assignment of chemical shift values to compound **12**.

Position	δ_{H}	Multiplicity	Coupling constant (<i>J</i> Hz)	δ_{C}	Multiplicity	Coupling constant (<i>J</i> Hz)
1	-	-	-	122.51	q	273.4
2	-	-	-	130.41	q	33.9
3	8.25	s	-	136.16	q	3.3
4	8.25	s	-	121.93	-	-
5	-	-	-	160.48	-	-
6	9.00	s	-	147.44	q	3.8
7	3.71 – 3.59	m	-	51.90	-	-
8	3.79	q	5.8	33.12	-	-
9	6.42	t	-	-	-	-
10	-	-	-	178.36	-	-
11	-	-	-	40.69	-	-
12	1.80	s	-	39.13	-	-
13	1.77 – 1.62	m	-	36.54	-	-
14	2.02	s	-	28.13	-	-

4.2.10 Characterization of compound **13**

The ^1H NMR and ^{13}C NMR chemical shifts are assigned to the numbered positions in Figure 31 and Table 11. The ^1H , ^{13}C NMR and DEPT135 NMR spectra are shown in the appendix.

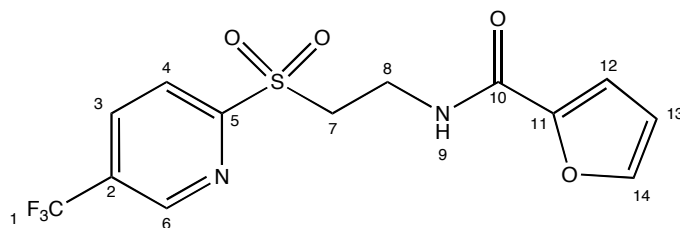


Figure 31. Atom numbering of compound **13**.

Table 11. Assignment of chemical shift values to compound **13**.

Position	δ_{H}	Multiplicity	Coupling constant (J Hz)	δ_{C}	Multiplicity	Coupling constant (J Hz)
1	-	-	-	122.48	q	273.5
2	-	-	-	130.30	q	33.8
3	7.41	s	-	136.04	q	3.4
4	8.45 – 8.01	m	-	121.89	-	-
5	-	-	-	158.33	-	-
6	8.92	s	-	147.48 – 147.17	m	-
7	4.01 – 3.92	m	-	51.93	-	-
8	3.84 – 3.71	m	-	33.29	-	-
9	6.95	t	-	-	-	-
10	-	-	-	160.61	-	-
11	-	-	-	158.33	-	-
12	7.05	d	3.4	114.89	-	-
13	6.60 – 6.41	m	-	112.38	-	-
14	8.45 – 8.01	m	-	144.3	-	-

4.2.11 Characterization of compound **14**

The ^1H NMR and ^{13}C NMR chemical shifts are assigned to the numbered positions in Figure 32 and Table 12. The four protons in position 12 and 13 occur as doublets, and the coupling constants indicate both positions to be *ortho* coupled with the vicinal protons. The signal at 3.78 ppm integrates for three protons, and is assigned to position 15, typical for O-methyl. The ^1H and ^{13}C NMR spectra are shown in the appendix.

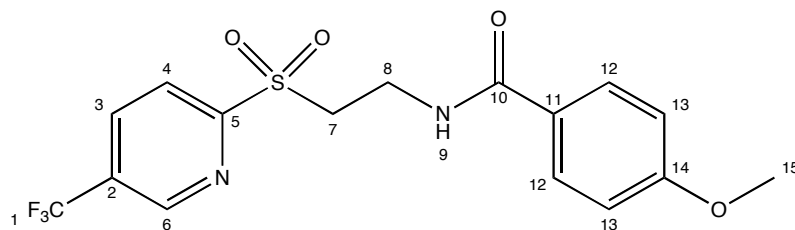


Figure 32. Atom numbering of compound **14**.

Table 12. Assignment of chemical shift values to compound **14**.

Position	δ_{H}	Multiplicity	Coupling constant(s) (J Hz)	δ_{C}	Multiplicity	Coupling constant (J Hz)
1	-	-	-	122.63	q	273.3
2	-	-	-	128.13	q	33.0
3	8.46	dd	8.3, 1.8	136.81	q	3.3
4	8.22	d	8.2	122.10	-	-
5	-	-	-	160.03	-	-
6	9.04	s	-	147.14	q	3.7
7	3.87	t	6.2	55.26	-	-
8	3.62	q	6.0	33.73	-	-
9	8.29	t	5.3	-	-	-
10	-	-	-	165.38	-	-
11	-	-	-	125.47	-	-
12	7.55	d	8.9	128.66	-	-
13	6.89	d	8.9	113.27	-	-
14	-	-	-	161.66	-	-
15	3.78	s	-	50.39	-	-

4.2.12 Characterization of compound 15

The ^1H NMR and ^{13}C NMR chemical shifts are assigned to the numbered positions in Figure 33 and Table 13. The ^1H , ^{13}C , DEPT135 and COSY45 NMR spectra are shown in the appendix.

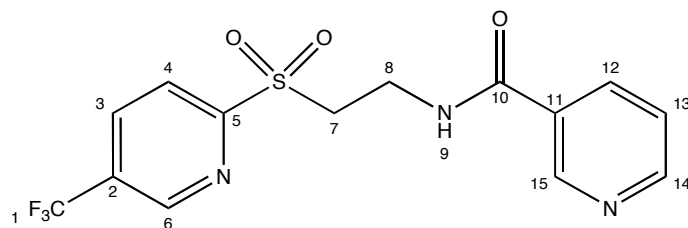


Figure 33. Atom numbering of compound **15**.

Table 13. Assignment of chemical shift values to compound **15**.

Position	δ_{H}	Multiplicity	Coupling constant(s) (J Hz)	δ_{C}	Multiplicity	Coupling constant (J Hz)
1	-	-	-	122.58	q	273.4
2	-	-	-	128.23	q	33.1
3	8.25	d	8.2	136.89	q	3.3
4	8.55 – 8.45	m	-	122.18	-	-
5	-	-	-	160.02	-	-
6	8.80 – 8.73	m	-	148.00	-	-
7	3.90	t	6.2	50.16	-	-
8	3.67	q	5.9	33.76	-	-
9	8.73 – 8.62	m	-	-	-	-
10	-	-	-	164.52	-	-
11	-	-	-	128.70	-	-
12	7.94	m	-	134.53	-	-
13	7.42	m	-	123.23	-	-
14	8.73 – 8.62	m	-	147.20	q	3.6
15	9.08	-	-	151.98	-	-

4.2.13 Characterization of compound 16

The ^1H NMR and ^{13}C NMR chemical shifts are assigned to the numbered positions in Figure 34 and Table 14. The signal assigned to the protons at position 11 display as a singlet. The chemical shift values for the five aromatic protons in position 13-15 are in accordance with the shift range for aromatic protons. The ^1H , ^{13}C NMR and DEPT135 NMR spectra are shown in the appendix.

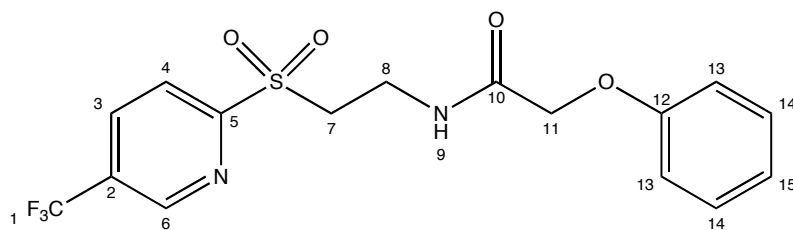


Figure 34. Atom numbering of compound 16.

Table 14. Assignment of chemical shift values to compound 16.

Position	δ_{H}	Multiplicity	Coupling constant(s) (J Hz)	δ_{C}	Multiplicity	Coupling constant (J Hz)
1	-	-	-	122.73	q	273.3
2	-	-	-	128.49	q	33.1
3	8.57	dd	8.2, 1.8	137.06	q	3.5
4	8.26	d	8.2	122.32	-	-
5	-	-	-	157.37	-	-
6	9.22	s	-	147.36	q	3.8
7	3.77	t	6.6	50.48	-	-
8	3.54	q	6.4	32.58	-	-
9	8.14	t	5.6	-	-	-
10	-	-	-	167.75	-	-
11	4.28	s	-	66.61	-	-
12	-	-	-	159.85	-	-
13	7.28	dd	8.6, 7.4	114.65	-	-
14	7.05 – 6.81	m	-	129.45	-	-
15	7.05 – 6.81	m	-	121.27	-	-

4.3 Spectroscopic characterization of the second-generation analogue 23 and its intermediates 48-49

4.3.1 Characterization of compound 48

The ^1H NMR chemical shifts are assigned to the numbered positions in Figure 35 and Table 15. The proton in position 9 occurs as a broad singlet, which can be explained by the low concentration of the NMR sample. The ^1H NMR spectrum is shown in the appendix.

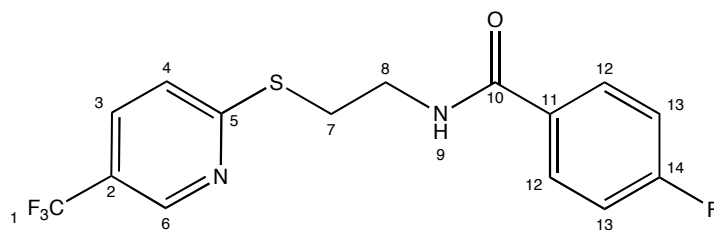


Figure 35. Atom numbering of compound **48**.

Table 15. Assignment of ^1H NMR chemical shift values to compound **48**.

Position	δ_{H}	Multiplicity	Coupling constant (J Hz)
1	-	-	-
2	-	-	-
3	7.95 – 7.60	m	-
4	7.34	d	8.3
5	-	-	-
6	8.63	s	-
7	3.49	t	6.1
8	3.79	q	6.5
9	7.23	bs	-
10	-	-	-
11	-	-	-
12	7.95 – 7.60	-	-
13	7.06	m	-
14	-	-	-

4.3.2 Characterization of compound **49**

The ^1H NMR chemical shifts are assigned to the numbered positions in Figure 36 and Table 16. The singlet at 3.08 ppm is in accordance with a typical chemical shift of an *N*-methyl group. The signals at 6.34-7.96 ppm are assigned to the four aromatic protons in the 4-fluorophenyl moiety. The ^1H NMR spectrum is shown in the appendix.

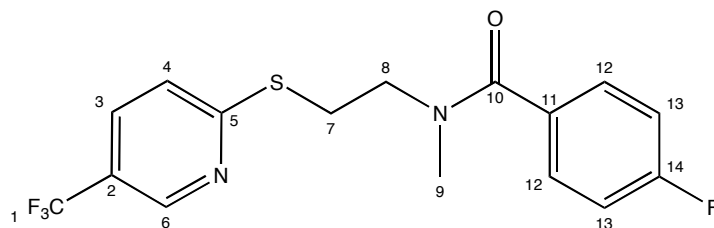


Figure 36. Atom numbering of compound **49**.

Table 16. Assignment of ^1H NMR chemical shift values to compound **49**.

Position	δ_{H}	Multiplicity	Coupling constant (J Hz)
1	-	-	-
2	-	-	-
3	7.96 – 6.34	m	-
4	7.96 – 6.34	m	-
5	-	-	-
6	8.53	d	115.9
7	4.31 – 3.16	m	-
8	4.31 – 3.16	m	-
9	3.08	s	-
10	-	-	-
11	-	-	-
12	7.96 – 6.34	m	-
13	7.96 – 6.34	m	-
14	-	-	-

4.3.3 Characterization of compound **23**

The ^1H NMR and ^{13}C NMR chemical shifts are assigned to the numbered positions in Figure 37 and Table 17. The characteristic splitting patterns (doublets) caused by the substituted fluorine atom in the 4-fluorophenyl moiety are visible in the ^{13}C NMR spectra. The ^1H , ^{13}C and DEPT135 NMR spectra are shown in the appendix.

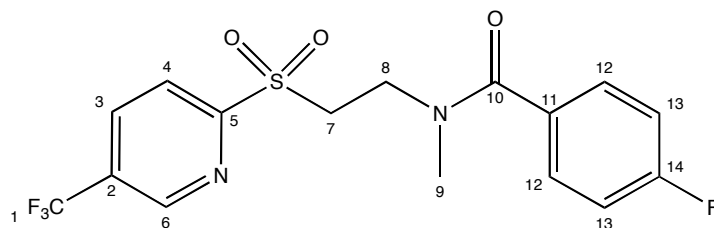


Figure 37. Atom numbering of compound **23**.

Table 17. Assignment of chemical shift values to compound **23**.

Position	δ_{H}	Multiplicity	Coupling constant (J Hz)	δ_{C}	Multiplicity	Coupling constant (J Hz)
1	-	-	-	122.53	q	273.5
2	-	-	-	130.34	q	34.0
3	7.50 – 7.34	m	-	136.84 – 135.36	m	-
4	7.50 – 7.34	m	-	121.96	-	-
5	-	-	-	160.46	-	-
6	8.99	s	-	147.91 – 146.71	m	-
7	3.92	d	51.1	49.34	-	-
8	3.92	d	51.1	42.46	-	-
9	3.09	s	-	39.05	-	-
10	-	-	-	171.01	-	-
11	-	-	-	131.63	d	3.5
12	8.24	s	-	129.49	d	6.8
13	7.08	m	-	115.66	d	21.9
14	-	-	-	163.63	d	250.6

4.4 Spectroscopic characterization of compounds from attempted approaches

4.4.1 Characterization of intermediates from the sixth approach

Characterization of compound **42**

The ^1H NMR and ^{13}C NMR chemical shifts are assigned to the numbered positions in Figure 38 and Table 18. The ^1H and ^{13}C NMR spectra are shown in the appendix.

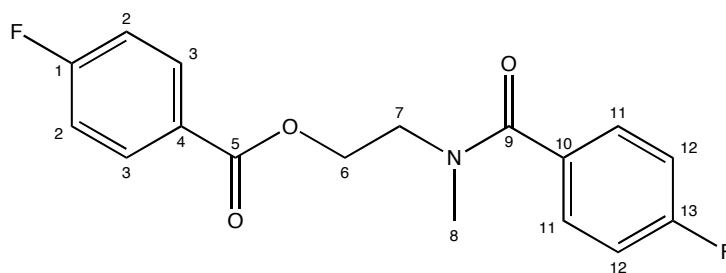


Figure 38. Atom numbering of compound **42**.

Table 18. Assignment of chemical shift values to compound **42**.

Position	δ_{H}	Multiplicity	Coupling constant(s) (J Hz)	δ_{C}	Multiplicity	Coupling constant(s) (J Hz)
1	-	-	-	156.06	-	-
2	7.20 – 6.96	m	-	115.71	dd	21.9, 12.9
3	7.39	dd	8.4, 5.3	132.31	d	9.5
4	-	-	-	126.10	-	-
5	-	-	-	164.33	-	-
6	4.88 – 4.28	m	-	62.22	-	-
7	4.09 – 3.63	m	-	46.94	-	-
8	3.11	-	-	38.99	-	-
9	-	-	-	167.70	-	-
10	-	-	-	132.17	d	3.5
11	8.25 – 7.87	m	-	129.30	d	8.4
12	7.20 – 6.96	m	-	115.71	dd	21.9, 12.9
13	-	-	-	161.75	-	-

Characterization of compound **43**

The ^1H NMR chemical shifts are assigned to the numbered positions in Figure 39 and Table 19. The ^1H NMR spectrum is shown in the appendix.

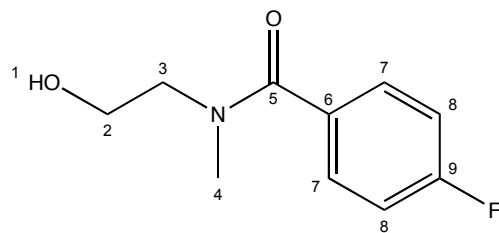


Figure 39. Atom numbering of compound **43**.

Table 19. Assignment of ^1H NMR chemical shift values to compound **43**.

Position	δ_{H}	Multiplicity	Coupling constant (J Hz)
1	4.03 – 3.29	m	-
2	4.03 – 3.29	m	-
3	4.03 – 3.29	m	-
4	3.03	s	-
5	-	-	-
6	-	-	-
7	7.43	s	-
8	7.06	s	-
9	-	-	-

5 Experimental section

5.1 General

Unless noted otherwise, all reagents and solvents were used as purchased without further purification. Thin layer chromatography (TLC) was performed using silica gel 60 F₂₅₄-plates. Flash column chromatography was performed on silica gel 60 (40-63 μm , Fluka). Hexane was distilled prior to use.

To record the NMR spectra, Bruker Advance DPX-300 MHz spectrometer or Bruker Advance DPX 400 Fourier Transform spectrometer were used. Coupling constants (J) are reported in hertz, while the chemical shift values are reported in parts per million (ppm, δ), relative to CDCl_3 (7.26 ppm for ^1H and 77.16 ppm for ^{13}C) and $\text{DMSO-}d_6$ (2.50 ppm for ^1H and 39.52 ppm for ^{13}C). Some of the spectra contain an additional singlet at 0.00 ppm representing TMS added to the solvent as an internal standard.

5.2 First-generation analogues

5.2.1 Synthesis of intermediates

Synthesis of *tert*-butyl (2-((5-(trifluoromethyl)pyridin-2-yl)thio)ethyl)carbamate (4)

To a stirred solution of 5-(trifluoromethyl)pyridine-2-thiol (2.00 g, 11.1 mmol) in DMF (40 mL) was added Et_3N (4.0 mL, 28.8 mmol), followed by a solution of 2-(*N*-Boc-amino)ethyl bromide (2.72 g, 12.1 mmol) in DMF (20 mL). The mixture was stirred for 1 hour and monitored with TLC. After completion of the reaction, the mixture was poured into water (100 mL) and extracted with EtOAc (3 x 50 mL). The combined organic phases were washed with water (2 x 50 mL) and brine (50 mL), dried (MgSO_4) and the solvent was removed under reduced pressure. The remaining colourless solid was obtained in 97% yield (3.46 g, 10.7 mmol) and used without further purification. ^1H NMR (300 MHz, $\text{DMSO-}d_6$): δ 8.77 (s, 1H), 7.97 (dd, $J = 8.6, 2.5$ Hz, 1H), 7.53 (d, $J = 8.5$ Hz, 1H), 7.05 (m, 1H), 3.32 – 3.13 (m, 4H), 1.37 (d, $J = 4.8$ Hz, 9H). ^{13}C NMR (75 MHz, $\text{DMSO-}d_6$): δ 163.95, 155.53, 145.90, 133.33 (d, $J = 3.2$ Hz), 123.93 (q, $J = 271.7$ Hz), 121.73, 121.01 (q, $J = 32.6$ Hz), 77.73, 39.42, 29.30, 28.17.

Synthesis of *tert*-butyl (2-((5-(trifluoromethyl)pyridin-2-yl)sulfonyl)ethyl)carbamate (**5**)

To a mixture of compound **4** (2.00 g, 6.2 mmol) in acetone and water (4:1, 10 mL) was added Oxone™ (15.0 g, 24.4 mmol) and the reaction was stirred overnight. Acetone was removed under reduced pressure and the remaining aqueous suspension was poured into water (10 mL) and extracted with EtOAc (20 mL). The combined organic phases were washed with brine (20 mL), dried (MgSO₄) and the solvent was removed under reduced pressure. The remaining solid was purified using column chromatography, which afforded **5** as a colourless solid in 57% yield (1.25 g, 3.5 mmol). Mp 146-169 °C. R_f = 0.20 (4:6 EtOAc:hexane). ¹H NMR (300 MHz, DMSO-*d*₆): δ 9.23 (s, 1H), 8.62 (dd, 1H), 8.25 (d, *J* = 8.2 Hz, 1H), 6.79 (t, *J* = 5.2 Hz, 1H), 3.68 (t, *J* = 6.4 Hz, 2H), 3.31 (q, *J* = 5.9 Hz, 2H), 1.27 (s, 7H). ¹³C NMR (75 MHz, DMSO-*d*₆): δ 160.09, 155.06, 148.84 – 146.23 (m), 137.03 (d, *J* = 3.5 Hz), 128.38 (q, *J* = 32.9 Hz), 122.85 (q, *J* = 273.3 Hz), 122.29, 78.00, 50.90, 34.33, 27.99.

Synthesis of 2-((5-(trifluoromethyl)pyridin-2-yl)sulfonyl)ethanaminium chloride (**6**)

To compound **5** (2.10 g, 5.9 mmol) was added HCl in dioxane (50 mL) and the reaction was stirred for 3 hours. The suspension was diluted with Et₂O (50 mL) and stirred for 10 minutes. The resulting precipitate was filtered, rinsed with Et₂O (20 mL) and the solid was collected. The residual solvent was removed under reduced pressure and the solid was dried under reduced pressure overnight. This afforded the colourless hydrochloride salt **6** in 91% yield (1.57 g, 5.4 mmol), which was used without further purification. Mp 193-195 °C. ¹H NMR (400 MHz, DMSO-*d*₆): δ 9.27 (s, 1H), 8.76 – 8.56 (m, 1H), 8.48 (s, 3H), 8.31 (d, *J* = 8.2 Hz, 1H), 4.07 – 3.81 (m, 2H), 3.32 – 3.06 (m, 2H). ¹³C NMR (101 MHz, DMSO-*d*₆): δ 159.16, 147.57 (q, *J* = 3.6 Hz), 137.42 (q, *J* = 3.4 Hz), 128.85 (q, *J* = 33.1 Hz), 122.75 (q, *J* = 273.4 Hz), 122.48, 49.04, 32.85.

5.2.2 General procedure for the synthesis of first-generation analogues

To a stirred solution of 2-((5-(trifluoromethyl)pyridin-2-yl)sulfonyl)ethanaminium chloride (**6**) (0.87 mmol) in dry THF (10 mL) at 0 °C was added Et₃N (0.6 mL, 4.0 mmol). To this solution, the acid chloride (2.0 mmol) in dry THF (4 mL) was added dropwise. The mixture was stirred at room temperature for 1 hour, then poured into water (50 mL) and extracted with

EtOAc (3 x 20 mL). The combined organic phases were washed with saturated aqueous NH₄Cl (3 x 20 mL), water (20 mL), brine (20 mL), dried (MgSO₄) and evaporated under reduced pressure. The crude products were purified using column chromatography on silica gel and dried under reduced pressure overnight.

Synthesis of *N*-(2-((5-(trifluoromethyl)pyridin-2-yl)sulfonyl)ethyl)benzamide (7)

The title compound was obtained as a colourless solid in 60% yield (185 mg, 0.5 mmol) from **6** (254 mg, 0.87 mmol) and benzoyl chloride (324 mg, 2.0 mmol) according to the general procedure. Mp 156-158 °C. R_f = 0.09 (1:99 MeOH:CH₂Cl₂). ¹H NMR (300 MHz, DMSO-*d*₆): δ 9.08 (s, 1H), 8.60 – 8.39 (m, 2H), 8.24 (m, 1H), 7.66 – 7.26 (m, 5H), 3.89 (t, *J* = 6.2 Hz, 2H), 3.66 (q, *J* = 6.0 Hz, 2H). ¹³C NMR (75 MHz, DMSO-*d*₆): δ 165.94, 160.01, 147.20 (q, *J* = 3.8 Hz), 136.86 (q, *J* = 3.4 Hz), 133.29, 131.32, 128.23 (q, *J* = 33.0 Hz), 128.09, 126.83, 122.63 (q, *J* = 273.2 Hz), 122.18, 50.34, 33.76.

Synthesis of 4-fluoro-*N*-(2-((5-(trifluoromethyl)pyridin-2-yl)sulfonyl)ethyl)benzamide (8)

The title compound was obtained as a colourless solid in 67% yield (219 mg, 0.6 mmol) from **6** (254 mg, 0.87 mmol) and 4-fluorobenzoyl chloride (0.25 ml, 2.0 mmol) according to the general procedure. Mp 164-167 °C. R_f = 0.1 (1:99 MeOH:CH₂Cl₂). ¹H NMR (300 MHz, DMSO-*d*₆): δ 9.12 – 8.95 (m, 1H), 8.47 (dd, *J* = 8.0, 2.3 Hz, 2H), 8.22 (m, 1H), 7.75 – 7.58 (m, 2H), 7.32 – 7.10 (m, 2H), 3.89 (t, *J* = 6.1 Hz, 2H), 3.64 (q, *J* = 5.9 Hz, 2H). ¹³C NMR (75 MHz, DMSO-*d*₆): δ 164.78, 163.95 (d, *J* = 248.8 Hz), 160.05 (d, *J* = 160.9 Hz), 147.17 (q, *J* = 3.8 Hz), 136.85 (q, *J* = 3.4 Hz), 129.67 (d, *J* = 2.9 Hz), 129.49 (d, *J* = 9.1 Hz), 128.15 (q, *J* = 32.9 Hz), 122.61 (q, *J* = 273.2 Hz), 122.13, 115.03 (d, *J* = 21.8 Hz), 50.22, 33.87.

Synthesis of *N*-(2-((5-(trifluoromethyl)pyridin-2-yl)sulfonyl)ethyl)isobutyramide (9)

The title compound was obtained as a colourless solid in 42% yield (119 mg, 0.36 mmol) from **6** (255 mg, 0.87 mmol) and isobutyryl chloride (0.21 ml, 2.0 mmol) according to the general procedure. Mp 162-165 °C. R_f = 0.17 (2:98 MeOH:CH₂Cl₂). ¹H NMR (300 MHz, DMSO-*d*₆): δ 9.24 (s, 1H), 8.62 (dd, *J* = 8.4, 1.7 Hz, 1H), 8.26 (d, *J* = 8.2 Hz, 1H), 7.83 (t, *J* =

5.7 Hz, 1H), 3.69 (t, $J = 6.5$ Hz, 2H), 3.41 (q, $J = 6.3$ Hz, 2H), 2.07 (h, $J = 6.9$ Hz, 1H), 0.85 (d, $J = 6.9$ Hz, 6H). ^{13}C NMR (75 MHz, DMSO- d_6): δ 176.20, 160.01, 147.39 (q, $J = 3.9$ Hz), 137.08 (q, $J = 3.5$ Hz), 128.48 (q, $J = 33.0$ Hz), 122.82 (q, $J = 273.3$ Hz), 122.28, 50.66, 33.69, 32.83, 19.17.

Synthesis of *N*-(2-((5-(trifluoromethyl)pyridin-2-yl)sulfonyl)ethyl)pivalamide (10)

The title compound was obtained as a colourless solid in 53% yield (163 mg, 0.48 mmol) from **6** (263 mg, 0.9 mmol) and pivaloyl chloride (0.22 ml, 2.0 mmol) according to the general procedure. Mp 172-174 °C. $R_f = 0.25$ (1.5:98.5 MeOH:CH₂Cl₂). ^1H NMR (300 MHz, DMSO- d_6): δ 9.25 (s, 1H), 8.62 (dd, $J = 8.5, 1.9$ Hz, 1H), 8.26 (d, $J = 8.2$ Hz, 1H), 7.55 (t, $J = 5.4$ Hz, 1H), 3.70 (t, $J = 6.6$ Hz, 2H), 3.42 (q, $J = 6.5$ Hz, 2H), 0.93 (s, 9H). ^{13}C NMR (75 MHz, DMSO- d_6): δ 177.61, 159.95, 147.42 (q, $J = 3.8$ Hz), 137.10 (q, $J = 3.6$ Hz), 128.51 (q, $J = 33.0$ Hz), 122.81 (q, $J = 273.2$ Hz), 122.30, 50.63, 37.82, 33.16, 27.06.

Synthesis of *N*-(2-((5-(trifluoromethyl)pyridin-2-yl)sulfonyl)ethyl)-2-naphthamide (11)

The title compound was obtained as a colourless solid in 48% yield (163 mg, 0.4 mmol) from **6** (268 mg, 0.92 mmol) and pivaloyl chloride (0.22 ml, 2.0 mmol) according to the general procedure. Mp 176-178 °C. $R_f = 0.14$ (1:99 MeOH:CH₂Cl₂). ^1H NMR (300 MHz, DMSO- d_6): δ 9.05 (s, 1H), 8.66 (t, $J = 4.8$ Hz, 1H), 8.46 (d, $J = 8.0$ Hz, 1H), 8.27 (d, $J = 8.2$ Hz, 1H), 8.19 (s, 1H), 7.92 (dd, $J = 11.9, 7.9$ Hz, 3H), 7.76 – 7.52 (m, 3H), 3.94 (t, $J = 6.0$ Hz, 2H), 3.72 (q, $J = 5.6$ Hz, 2H). ^{13}C NMR (75 MHz, DMSO- d_6): δ 165.98, 160.29 – 159.58 (m), 147.19 (q, $J = 3.8$ Hz), 136.84 (q, $J = 3.4$ Hz), 134.17, 131.92, 130.63, 128.75, 128.19 (q, $J = 33.1$ Hz), 127.74, 127.63, 127.53, 127.28, 126.66, 123.61, 122.50 (q, $J = 273.4$ Hz), 122.18, 50.38, 33.88.

Synthesis of *N*-(2-((5-(trifluoromethyl)pyridin-2-yl)sulfonyl)ethyl)adamantane-1-carboxamide (12)

The title compound was obtained as a colourless solid in 94% yield (339 mg, 0.81 mmol) from **6** (254 mg, 0.87 mmol) and 1-adamantanecarbonyl chloride (400 mg, 2.0 mmol) according to the general procedure. Mp 185-186 °C. $R_f = 0.25$ (5:95 MeOH:CH₂Cl₂). ¹H NMR (400 MHz, CDCl₃): δ 9.00 (s, 1H), 8.25 (s, 2H), 6.42 (t, 1H), 3.79 (q, $J = 5.8$ Hz, 2H), 3.71 – 3.59 (m, 2H), 2.02 (s, 3H), 1.80 (s, 6H), 1.77 – 1.62 (m, 6H). ¹³C NMR (101 MHz, CDCl₃): δ 178.36, 160.48, 147.44 (q, $J = 3.8$ Hz), 136.16 (q, $J = 3.3$ Hz), 130.41 (q, $J = 33.9$ Hz), 122.51 (q, $J = 273.4$ Hz), 121.93, 51.90, 40.69, 39.13, 36.54, 33.12, 28.13.

Synthesis of *N*-(2-((5-(trifluoromethyl)pyridin-2-yl)sulfonyl)ethyl)furan-2-carboxamide (13)

The title compound was obtained as a colourless solid in 83% yield (252 mg, 0.72 mmol) from **6** (254 mg, 0.87 mmol) and 2-furoyl chloride (0.20 ml, 2.0 mmol) according to the general procedure. Mp 129-131 °C. $R_f = 0.27$ (5:95 MeOH:CH₂Cl₂). ¹H NMR (400 MHz, CDCl₃): δ 8.92 (s, 1H), 8.45 – 8.01 (m, 2H), 7.41 (s, 1H), 7.05 (d, $J = 3.4$ Hz, 1H), 6.95 (t, 1H), 6.60 – 6.41 (m, 1H), 4.01 – 3.92 (m, 2H), 3.84 – 3.71 (m, 2H). ¹³C NMR (101 MHz, CDCl₃): δ 160.61, 158.33, 147.48 – 147.17 (m), 144.3, 136.04 (q, $J = 3.4$ Hz), 130.30 (q, $J = 33.8$ Hz), 122.48 (q, $J = 273.5$ Hz), 121.89, 114.89, 112.38, 51.93, 33.29.

Synthesis of 4-methoxy-*N*-(2-((5-(trifluoromethyl)pyridin-2-yl)sulfonyl)ethyl)benzamide (14)

The title compound was obtained as a colourless solid in 82% yield (275 mg, 0.7 mmol) from **6** (254 mg, 0.87 mmol) and 4-methoxybenzoyl chloride (0.27 ml, 2.0 mmol) according to the general procedure. Mp 167-168 °C. $R_f = 0.22$ (5:95 MeOH:CH₂Cl₂). ¹H NMR (300 MHz, DMSO-*d*₆): δ 9.04 (s, 1H), 8.46 (dd, $J = 8.3, 1.8$ Hz, 1H), 8.29 (t, $J = 5.3$ Hz, 1H), 8.22 (d, $J = 8.2$ Hz, 1H), 7.55 (d, $J = 8.9$ Hz, 2H), 6.89 (d, $J = 8.9$ Hz, 2H), 3.87 (t, $J = 6.2$ Hz, 2H), 3.78 (s, 3H), 3.62 (q, $J = 6.0$ Hz, 2H). ¹³C NMR (75 MHz, DMSO-*d*₆): δ 165.38, 161.66, 160.03, 147.14 (q, $J = 3.7$ Hz), 136.81 (q, $J = 3.3$ Hz), 128.66, 128.13 (q, $J = 33.0$ Hz), 125.47, 122.63 (q, $J = 273.3$ Hz), 122.10, 113.27, 55.26, 50.39, 33.73.

Synthesis of *N*-(2-((5-(trifluoromethyl)pyridin-2-yl)sulfonyl)ethyl)nicotinamide (15)

The title compound was obtained as a colourless solid in 69% yield (214 mg, 0.6 mmol) from **6** (254 mg, 0.87 mmol) and nicotinoyl chloride (356 mg, 2.0 mmol) according to the general procedure. Mp 174-176 °C. $R_f = 0.26$ (10:90 MeOH:CH₂Cl₂). ¹H NMR (400 MHz, DMSO-*d*₆): δ 9.08 (s, 1H), 8.80 – 8.73 (m, 1H), 8.73 – 8.62 (m, 2H), 8.55 – 8.45 (m, 1H), 8.25 (d, $J = 8.2$ Hz, 1H), 7.94 (m, 1H), 7.42 (m, 1H), 3.90 (t, $J = 6.2$ Hz, 2H), 3.67 (q, $J = 5.9$ Hz, 2H). ¹³C NMR (101 MHz, DMSO-*d*₆): δ 164.52, 160.02, 151.98, 148.0, 147.20 (q, $J = 3.6$ Hz), 136.89 (q, $J = 3.3$ Hz), 134.53, 128.7, 128.23 (q, $J = 33.1$ Hz), 123.23, 122.58 (q, $J = 273.4$ Hz), 122.18, 50.16, 33.76.

Synthesis of 2-phenoxy-*N*-(2-((5-(trifluoromethyl)pyridin-2-yl)sulfonyl)ethyl)acetamide (16)

The title compound was obtained as a colourless solid in 73% yield (202 mg, 0.52 mmol) from **6** (206 mg, 0.71 mmol) and phenoxyacetyl chloride (0.22 ml, 1.6 mmol) according to the general procedure. Mp 126-129 °C. $R_f = 0.24$ (5:95 MeOH:CH₂Cl₂). ¹H NMR (300 MHz, DMSO-*d*₆): δ 9.22 (s, 1H), 8.57 (dd, $J = 8.2, 1.8$ Hz, 1H), 8.26 (d, $J = 8.2$ Hz, 1H), 8.14 (t, $J = 5.6$ Hz, 1H), 7.28 (dd, $J = 8.6, 7.4$ Hz, 2H), 7.05 – 6.81 (m, 3H), 4.28 (s, 2H), 3.77 (t, $J = 6.6$ Hz, 2H), 3.54 (q, $J = 6.4$ Hz, 2H). ¹³C NMR (75 MHz, DMSO-*d*₆): δ 167.75, 159.85, 157.37, 147.36 (q, $J = 3.8$ Hz), 137.06 (q, $J = 3.5$ Hz), 129.45, 128.49 (q, $J = 33.1$ Hz), 122.73 (q, $J = 273.3$ Hz), 122.32, 121.27, 114.65, 66.61, 50.48, 32.58.

5.3 Second-generation analogue

5.3.1 Synthesis of intermediates

Synthesis of 2-((5-(trifluoromethyl)pyridin-2-yl)thio)ethanaminium chloride (47)

A mixture of **4** (680 mg, 2.1 mmol) and HCl in dioxane (17 mL) was stirred at room temperature for 3 hours. The suspension was diluted with Et₂O (17 mL) and stirred for 10 minutes. The resulting precipitate was filtered, rinsed with Et₂O (10 mL) and the solid was collected. The residual solvent was removed under reduced pressure and the solid was dried

under reduced pressure overnight. The compound **47** was obtained as a colourless solid in 98% yield (535 mg, 2.0 mmol) and used without further purification.

Synthesis of 2-((5-(trifluoromethyl)pyridin-2-yl)thio)ethanamine (48)

To a stirred solution of **47** (530 mg, 2.05 mmol) in dry THF (30 mL) at 0 °C was added Et₃N (1.8 mL, 10.5 mmol). To this solution, 4-fluorobenzoyl chloride (0.62 mL, 5.3 mmol) was added dropwise. The mixture was stirred at room temperature for 1 hour, then poured into water (100 mL) and extracted with EtOAc (3 x 40 mL). The combined organic phases were washed with saturated aqueous NH₄Cl (3 x 40 mL), water (40 mL), brine (40 mL), dried (MgSO₄) and evaporated under reduced pressure. The crude product was purified using column chromatography on silica gel with 1-5% MeOH in CH₂Cl₂ as eluent to afford **48** as a colourless solid in 68% yield. Mp 115-118 °C. R_f = 0.4. ¹H NMR (400 MHz, CDCl₃): δ 8.63 (s, 1H), 7.95 – 7.60 (m, 3H), 7.34 (d, *J* = 8.3 Hz, 1H), 7.23 (s, 1H), 7.06 (m, 2H), 3.79 (q, *J* = 5.6 Hz, 2H), 3.49 (t, *J* = 6.1 Hz, 2H).

Synthesis of 4-fluoro-*N*-methyl-*N*-(2-((5-(trifluoromethyl)pyridin-2-yl)thio)ethyl)benzamide (49)

To a stirred solution of **48** (450 mg, 1.3 mmol) in dry THF (5 mL) at room temperature was added a 60% dispersion of NaH in mineral oil (68 mg, 1.7 mmol). After 10 minutes, the MeI (0.8 mL, 13.0 mmol) was added to the mixture and stirred at 40 °C for 5 hours. The reaction was quenched with saturated aqueous NH₄Cl (2 mL), extracted with Et₂O (30 mL) and the organic layer was washed with brine (10 mL). The crude product was purified using column chromatography on silica gel to afford **49** as a colourless solid in 83% yield. Mp 86-88 °C. R_f = 0.15 (2:3 EtOAc:hexane). ¹H NMR (400 MHz, CDCl₃): δ 8.53 (d, *J* = 115.9 Hz, 1H), 7.96 – 6.34 (m, 6H), 4.31 – 3.16 (m, 4H), 3.08 (s, 3H).

5.3.2 Synthesis of the second-generation analogue

Synthesis of 4-fluoro-*N*-methyl-*N*-(2-((5-(trifluoromethyl)pyridin-2-yl)sulfonyl)ethyl)benzamide (23)

To a stirred solution of **49** (336 mg, 0.93 mmol) in acetone and water (4:1, 3 mL) was added Oxone™ (2.25 g, 3.66 mmol), and the mixture was stirred overnight before evaporating the

acetone under reduced pressure. The remaining aqueous suspension was poured into water (10 mL) and extracted with EtOAc (2 x 30 mL). The organic layer was washed with brine (10 mL) and dried (MgSO₄). The crude product was purified using column chromatography on silica gel and dried under reduced pressure overnight. The title compound **23** was afforded in 67% yield (243 mg, 0.62 mmol) as a colourless solid. Mp 119-122 °C. R_f = 0.24 (3:2 EtOAc:hexane). ¹H NMR (400 MHz, CDCl₃): δ 8.99 (s, 1H), 8.24 (s, 2H), 7.50 – 7.34 (m, 2H), 7.08 (m, 2H), 3.92 (d, *J* = 52.1 Hz, 4H), 3.09 (s, 3H). ¹³C NMR (101 MHz, CDCl₃): δ 171.01, 163.63 (d, *J* = 250.6 Hz), 160.46, 147.91 – 146.71 (m), 136.84 – 135.36 (m), 131.63 (d, *J* = 3.5 Hz), 130.34 (q, *J* = 34.0 Hz), 129.49 (d, *J* = 6.8 Hz), 122.53 (q, *J* = 273.5 Hz), 121.96, 115.66 (d, *J* = 21.9 Hz), 49.34, 42.46, 39.05.

5.4 Synthesis of intermediates from the sixth approach

Synthesis of 2-(4-fluoro-*N*-methylbenzamido)ethyl 4-fluorobenzoate (**42**)

To a solution of 2-(methylamino)ethanol **40** (0.4 mL, 5.0 mmol) and pyridine (4 mL, 50 mmol) in dry THF (20 mL) was added 4-fluorobenzoyl chloride **41** (3 mL, 25.0 mmol) at 0 °C. The mixture was stirred at room temperature overnight and monitored with TLC. Upon completion, the reaction was poured into saturated aqueous NH₄Cl (60 mL) and extracted with EtOAc (3 x 40 mL). The combined organic phases were washed with saturated aqueous NH₄Cl (3 x 40 mL), saturated aqueous NaHCO₃ (3 x 40 mL), brine (40 mL) and dried (MgSO₄). The crude product was purified using column chromatography on silica gel to afford **42** as a colourless solid in 91% yield. R_f = 0.16 (7:3 EtOAc:hexane). ¹H NMR (300 MHz, CDCl₃): δ 8.25 – 7.87 (m, 2H), 7.39 (dd, *J* = 8.4, 5.3 Hz, 2H), 7.20 – 6.96 (m, 4H), 4.88 – 4.28 (m, 2H), 4.09 – 3.63 (m, 2H), 3.11 (s, 3H). ¹³C NMR (75 MHz, CDCl₃): δ 167.70, 165.06, 164.33, 161.75, 132.31 (d, *J* = 9.5 Hz), 132.17 (d, *J* = 3.5 Hz), 129.30 (d, *J* = 8.4 Hz), 126.10, 115.71 (dd, *J* = 21.9, 12.9 Hz), 62.22, 46.94, 38.99.

Synthesis of 4-fluoro-*N*-(2-hydroxyethyl)-*N*-methylbenzamide (**43**)

Compound **42** (1.00 g, 3.15 mmol) was dissolved in MeOH (20 mL), and K₂CO₃ (2.0 g, 14.7 mmol) was added. The reaction was stirred at room temperature for 45 minutes and monitored

with TLC. Upon completion, the mixture was poured into water (100 mL), extracted with EtOAc (6 x 30 mL), washed with water (3 x 30 mL), dried (Na_2SO_4) and the solvent was evaporated under reduced pressure. The crude product was purified using column chromatography on silica gel with 10% EtOH in EtOAc as eluent, to afford **43** as a colourless oil in 45% yield. $R_f = 0.24$. $^1\text{H NMR}$ (400 MHz, CDCl_3): δ 7.43 (s, 2H), 7.06 (s, 2H), 4.03 – 3.29 (m, 5H), 3.03 (s, 3H).

References

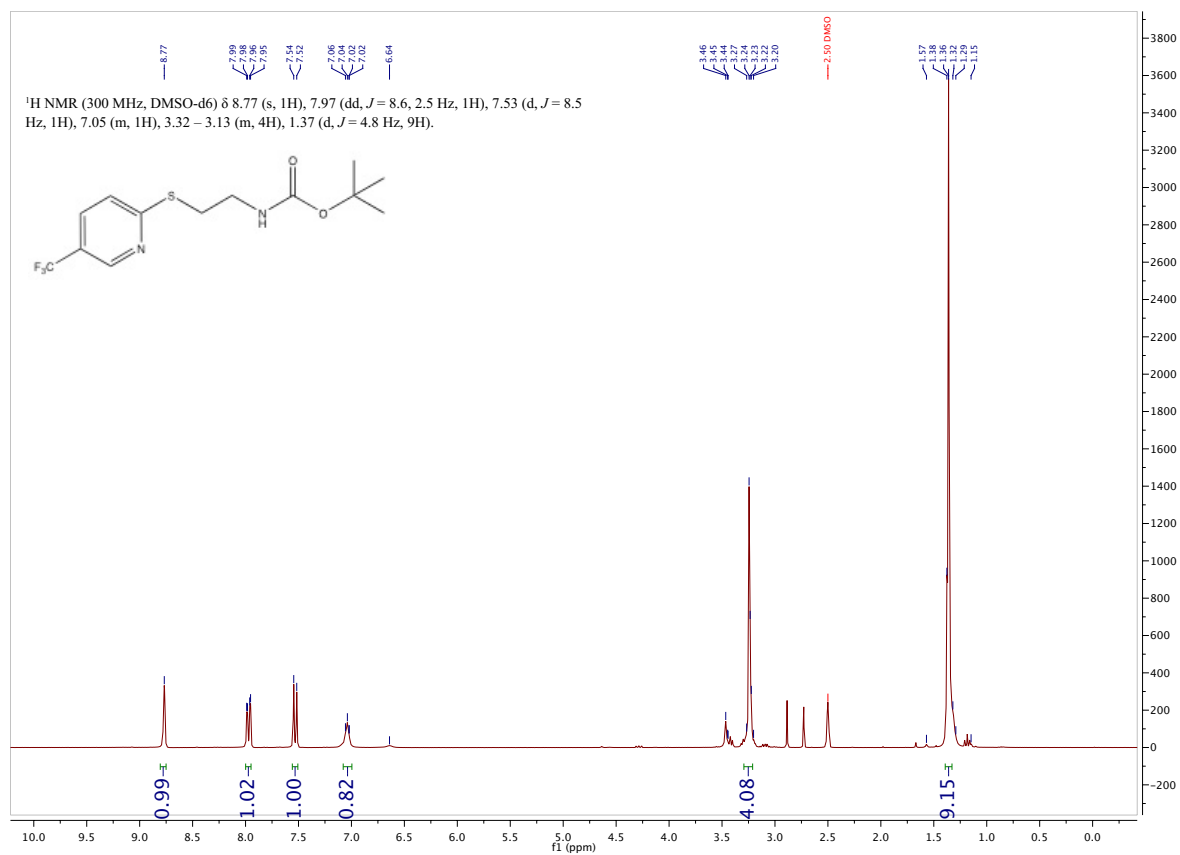
1. <http://www.nhi.no> (accessed 26. March 2012).
2. Grimaldi, P. A. *Biochimie* **2005**, *87*, 5.
3. Rang, H. P.; Dale, M. M.; Ritter, J. M.; Flower, R. J. In *Rang and Dale's Pharmacology*, 6th ed.; Elsevier, 2007, pp 397-401.
4. <http://www.legemiddelhandboka.no> (accessed 23. April 2012).
5. Rang, H. P.; Dale, M. M.; Ritter, J. M.; Flower, R. J. In *Rang and Dale's Pharmacology*, 6th ed.; Elsevier, 2007, pp 321-325.
6. <http://www.who.org> (accessed 22. March 2012).
7. Takahashi, S.; Tanaka, T.; Sakai, J. *Endocr. J.* **2007**, *54*, 347.
8. Kota, B. P.; Huang, T. H.; Roufogalis, B. D. *Pharmacol. Res.* **2005**, *51*, 85.
9. Zhang, F.; Lavan, B.; Gregoire, F. M. *Drug News Perspect.* **2004**, *17*, 661.
10. Barish, G. D.; Narkar, V. A.; Evans, R. M. *J. Clin. Invest.* **2006**, *116*, 590.
11. Ehrenborg, E.; Krook, A. *Pharmacol. Rev.* **2009**, *61*, 373.
12. Weindl, G.; Schäfer-Korting, M.; Schaller, M.; Korting, H. C. *Drugs* **2005**, *65*, 1919.
13. Michalik, L.; Auwerx, J.; Berger, J. P.; Chatterjee, V. K.; Glass, C. K.; Gonzalez, F. J.; Grimaldi, P. A.; Kadowaki, T.; Lazar, M. A.; O'Rahilly, S.; Palmer, C. N.; Plutzky, J.; Reddy, J. K.; Spiegelman, B. M.; Staels, B.; Wahli, W. *Pharmacol. Rev.* **2006**, *58*, 726.
14. Plutzky, J. *PPARs and Their Emerging Role in Vascular Biology, Inflammation, and Atherosclerosis*, In *Contemporary Cardiology: Diabetes and Cardiovascular Disease*. 2nd ed.; Humana Press, 2005, pp 93-101.
15. Toth, P. M.; Naruhn, S.; Pape, V. F.; Dörr, S. M.; Klebe, G.; Müller, R.; Diederich, W. E. *ChemMedChem* **2012**, *7*, 159.
16. Seedorf, U.; Aberle, J. *Biochim. Biophys. Acta* **2007**, *1771*, 1125.
17. Zoete, V.; Grosdidier, A.; Michielin, O. *Biochim. Biophys. Acta* **2007**, *1771*, 915.
18. Wang, Y. X. *Cell Res.* **2010**, *20*, 124.
19. <http://www.legemiddelverket.no> (accessed 29. March 2012).
20. Willson, T. M.; Brown, P. J.; Sternbach, D. D.; Henke, B. R. *J. Med. Chem.* **2000**, *43*, 527.
21. Nissen, S. E.; Wolski, K. *Arch. Intern. Med.* **2010**, *170*, 1191.
22. Friedland, S. N.; Leong, A.; Fillion, K. B.; Genest, J.; Lega, I. C.; Mottillo, S.; Poirier, P.; Reoch, J.; Eisenberg, M. J. *Am. J. Med.* **2012**, *125*, 126.
23. Willson, T. M.; Wahli, W. *Curr. Opin. Chem. Biol.* **1997**, *1*, 235.
24. Brooke, M. H.; Kaiser, K. K. *Arch. Neurol.* **1970**, *23*, 369.
25. Kiens, B. *Physiol. Rev.* **2006**, *86*, 205.
26. Muoio, D. M.; MacLean, P. S.; Lang, D. B.; Li, S.; Houmard, J. A.; Way, J. M.; Winegar, D. A.; Corton, J. C.; Dohm, G. L.; Kraus, W. E. *J. Biol. Chem.* **2002**, *277*, 26089.
27. Kleiner, S.; Nguyen-Tran, V.; Bare, O.; Huang, X.; Spiegelman, B.; Wu, Z. *J. Biol. Chem.* **2009**, *284*, 18624.
28. Tanaka, T.; Yamamoto, J.; Iwasaki, S.; Asaba, H.; Hamura, H.; Ikeda, Y.; Watanabe, M.; Magoori, K.; Ioka, R. X.; Tachibana, K.; Watanabe, Y.; Uchiyama, Y.; Sumi, K.; Iguchi, H.; Ito, S.; Doi, T.; Hamakubo, T.; Naito, M.; Auwerx, J.; Yanagisawa, M.; Kodama, T.; Sakai, J. *Proc. Natl. Acad. Sci. U. S. A.* **2003**, *100*, 15924.
29. Luquet, S.; Lopez-Soriano, J.; Holst, D.; Fredenrich, A.; Melki, J.; Rassoulzadegan, M.; Grimaldi, P. A. *FASEB J.* **2003**, *17*, 2299.

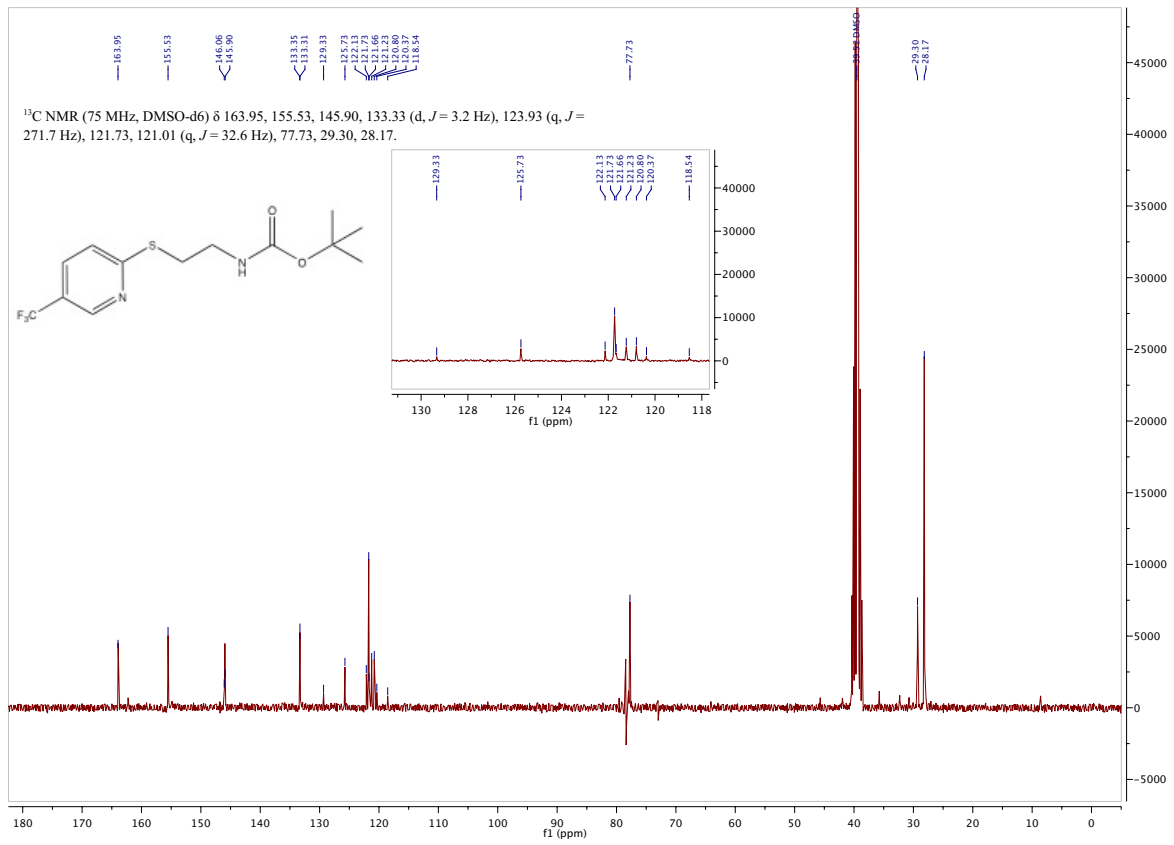
30. Seth, A.; Steel, J. H.; Nichol, D.; Pocock, V.; Kumaran, M. K.; Fritah, A.; Mobberley, M.; Ryder, T. A.; Rowlerson, A.; Scott, J.; Poutanen, M.; White, R.; Parker, M. *Cell Metab.* **2007**, *6*, 236.
31. Knowler, W. C.; Barrett-Connor, E.; Fowler, S. E.; Hamman, R. F.; Lachin, J. M.; Walker, E. A.; Nathan, D. M. *N. Engl. J. Med.* **2002**, *346*, 393.
32. McCall, G. E.; Byrnes, W. C.; Dickinson, A.; Pattany, P. M.; Fleck, S. J. *J. Appl. Physiol.* **1996**, *81*, 2004.
33. Shoelson, S. E.; Herrero, L.; Naaz, A. *Gastroenterology* **2007**, *132*, 2169.
34. Salvadó, L.; Serrano-Marco, L.; Barroso, E.; Palomer, X.; Vázquez-Carrera, M. *Expert Opin. Ther. Targets* **2012**, *16*, 209.
35. Lee, C. H.; Olson, P.; Hevener, A.; Mehl, I.; Chong, L. W.; Olefsky, J. M.; Gonzalez, F. J.; Ham, J.; Kang, H.; Peters, J. M.; Evans, R. M. *Proc. Natl. Acad. Sci. U. S. A.* **2006**, *103*, 3444.
36. Liu, S.; Hatano, B.; Zhao, M.; Yen, C. C.; Kang, K.; Reilly, S. M.; Gangl, M. R.; Gorgun, C.; Balschi, J. A.; Ntambi, J. M.; Lee, C. H. *J. Biol. Chem.* **2011**, *286*, 1237.
37. Serrano-Marco, L.; Barroso, E.; El Kochairi, I.; Palomer, X.; Michalik, L.; Wahli, W.; Vázquez-Carrera, M. *Diabetologia* **2012**, *55*, 743.
38. Peters, J. M.; Shah, Y. M.; Gonzalez, F. J. *Nat. Rev. Cancer* **2012**, *12*, 181.
39. Sznajdman, M. L.; Haffner, C. D.; Maloney, P. R.; Fivush, A.; Chao, E.; Goreham, D.; Sierra, M. L.; LeGrumelec, C.; Xu, H. E.; Montana, V. G.; Lambert, M. H.; Willson, T. M.; Oliver, W. R., Jr.; Sternbach, D. D. *Bioorg. Med. Chem. Lett.* **2003**, *13*, 1517.
40. Shearer, B. G.; Steger, D. J.; Way, J. M.; Stanley, T. B.; Lobe, D. C.; Grillot, D. A.; Iannone, M. A.; Lazar, M. A.; Willson, T. M.; Billin, A. N. *Mol. Endocrinol.* **2008**, *22*, 523.
41. Desvergne, B.; Feige, J. N.; Casals-Casas, C. *Mol. Cell. Endocrinol.* **2009**, *304*, 43.
42. Shearer, B. G.; Wiethe, R. W.; Ashe, A.; Billin, A. N.; Way, J. M.; Stanley, T. B.; Wagner, C. D.; Xu, R. X.; Leesnitzer, L. M.; Merrihew, R. V.; Shearer, T. W.; Jeune, M. R.; Ulrich, J. C.; Willson, T. M. *J. Med. Chem.* **2010**, *53*, 1857.
43. Zaveri, N. T.; Sato, B. G.; Jiang, F.; Calaoagan, J.; Laderoute, K. R.; Murphy, B. J. *Cancer Biol. Ther.* **2009**, *8*, 1252.
44. Naruhn, S.; Toth, P. M.; Adhikary, T.; Kaddatz, K.; Pape, V.; Dörr, S.; Klebe, G.; Müller-Brüsselbach, S.; Diederich, W. E.; Müller, R. *Mol. Pharmacol.* **2011**, *80*, 828.
45. Lieber, S.; Scheer, F.; Meissner, W.; Naruhn, S.; Adhikary, T.; Müller-Brüsselbach, S.; Diederich, W. E.; Müller, R. *J. Med. Chem.* **2012**, *55*, 2858.
46. Kürti, L.; Czako, B. In *Strategic applications of named reactions in organic synthesis* Elsevier, 2005, pp 33.
47. Barton, D. H. R.; Crich, D.; Motherwell, W. B. *Tetrahedron Lett.* **1983**, *24*, 4979.
48. Warren, S.; Wyatt, P. In *Organic synthesis. The disconnection approach*, 2nd ed.; Wiley, 2008, pp 53.
49. Ishibashi, H.; Uegaki, M.; Sakai, M.; Takeda, Y. *Tetrahedron* **2001**, *57*, 2115.
50. Breitmaier, E. In *Structure Elucidation by NMR in Organic Chemistry: A Practical Guide*, 3rd ed.; Wiley, 2002, pp 11-25.

6 Appendix

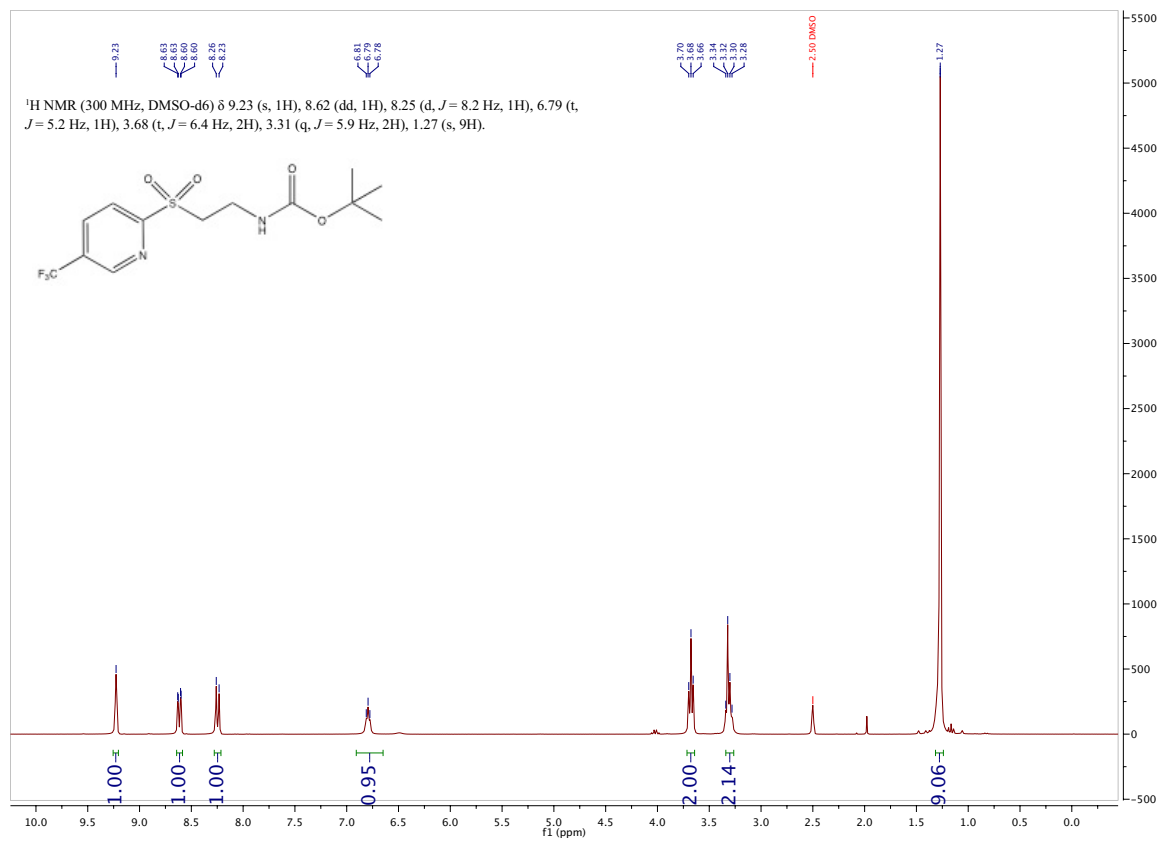
6.1 Spectra of prepared analogues and their intermediates

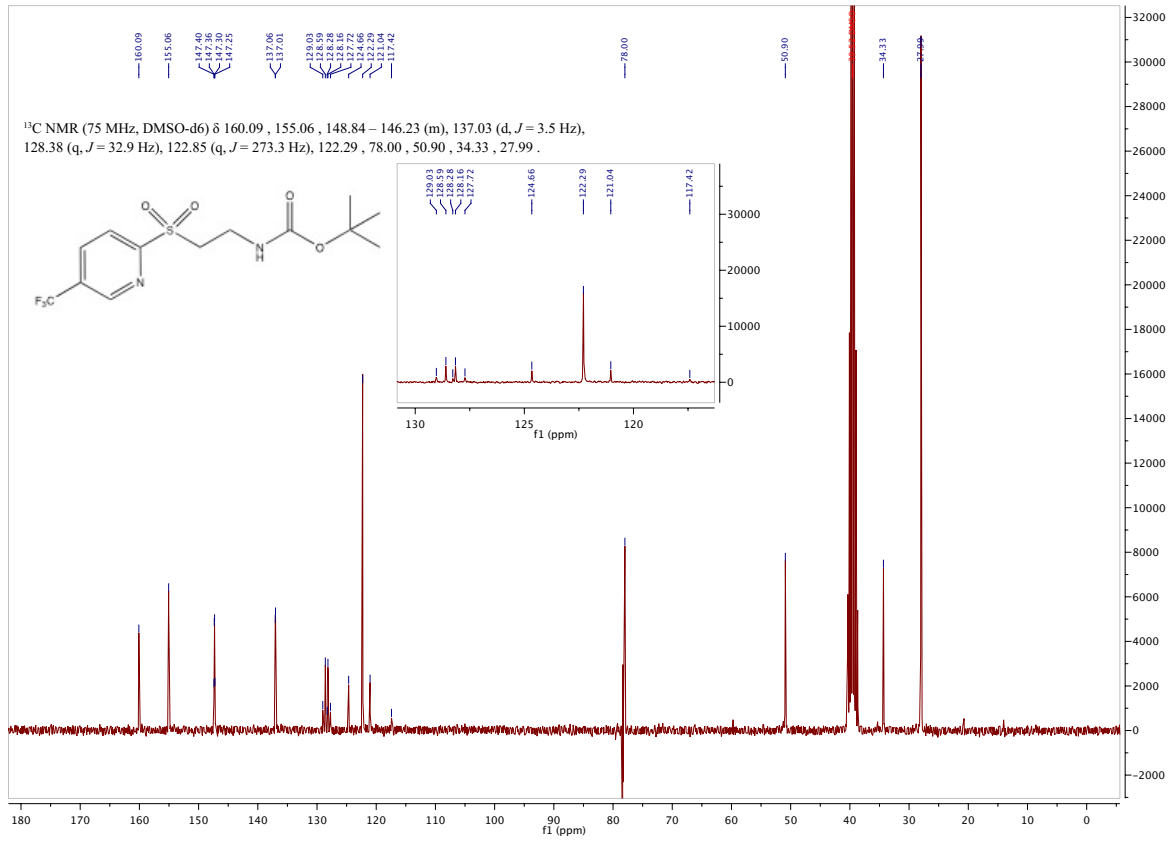
^1H and ^{13}C NMR spectra of compound 4



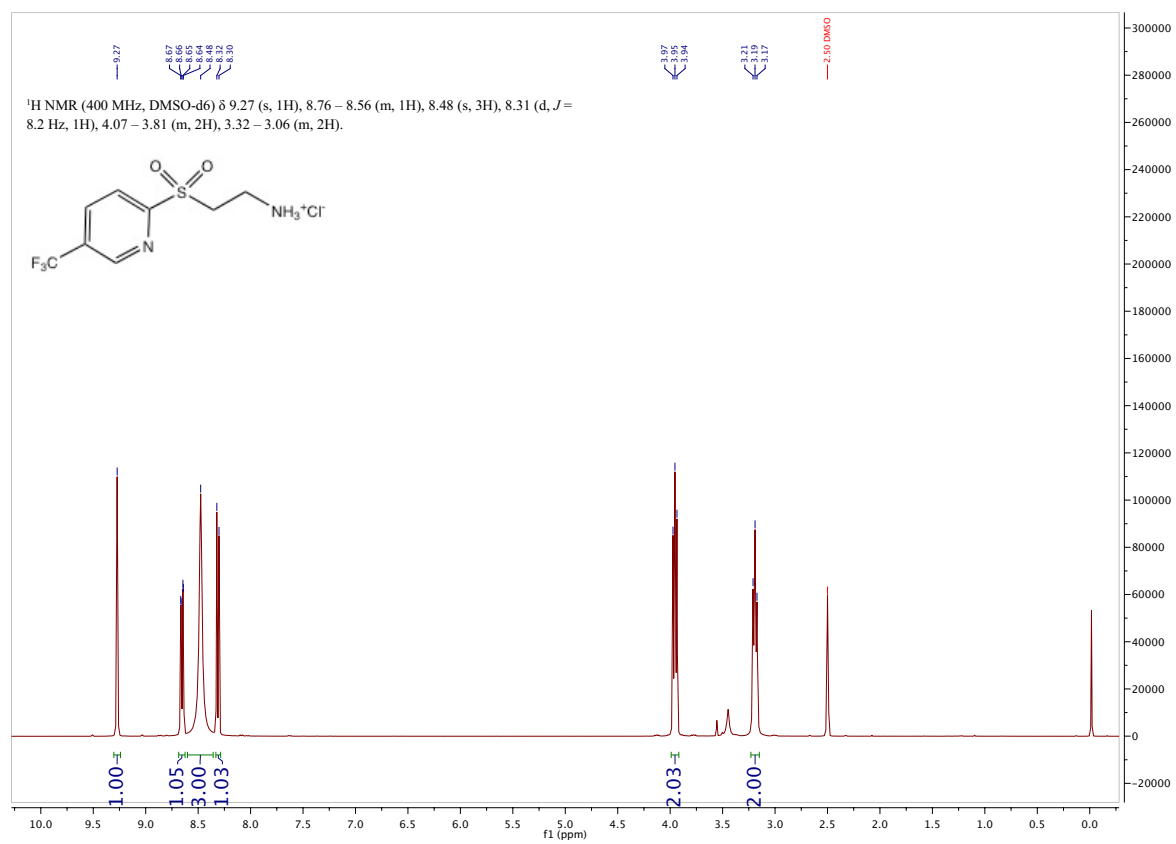


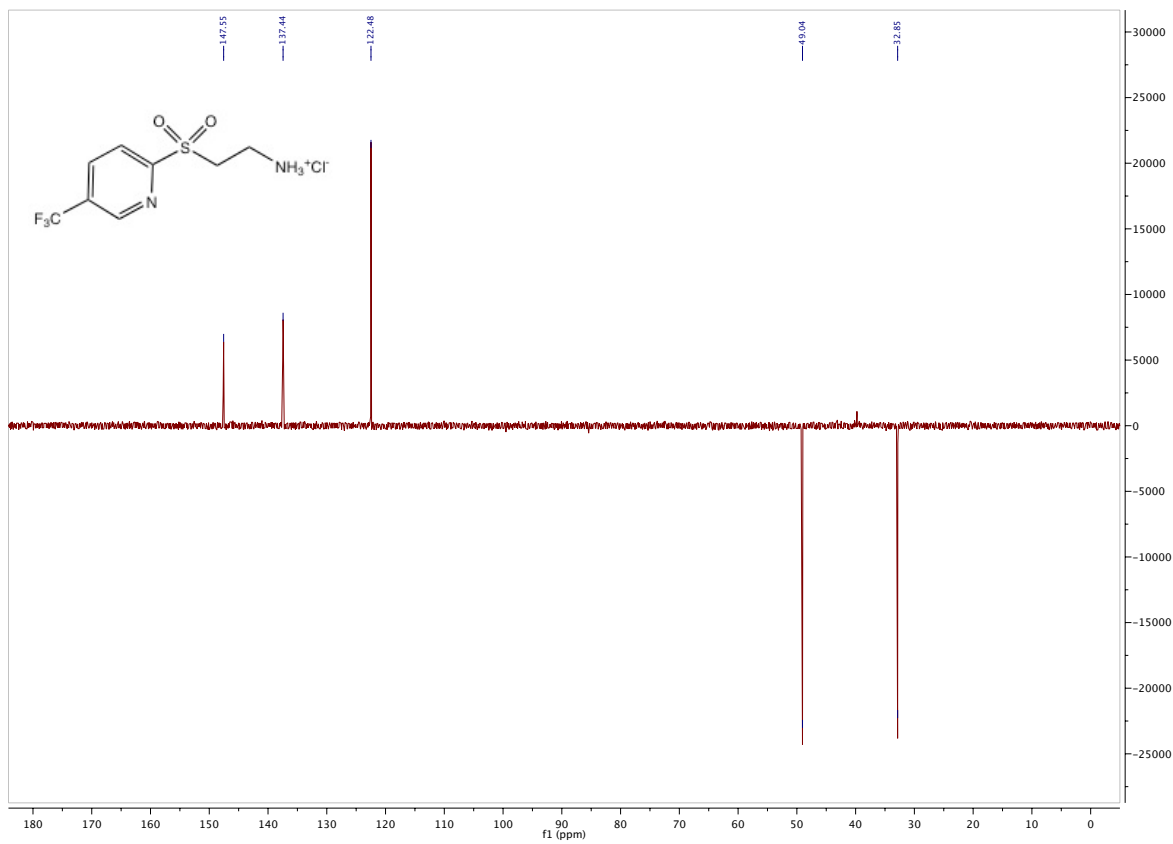
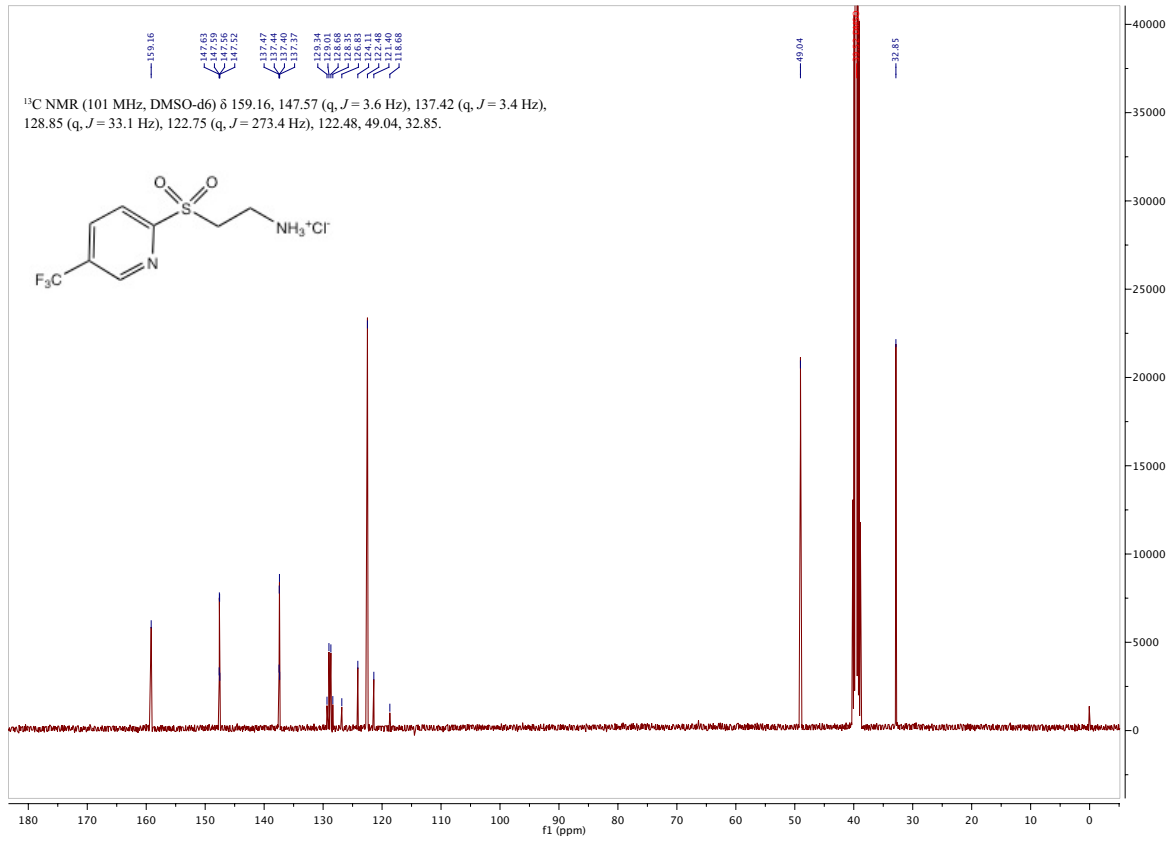
¹H and ¹³C NMR spectra of compound 5



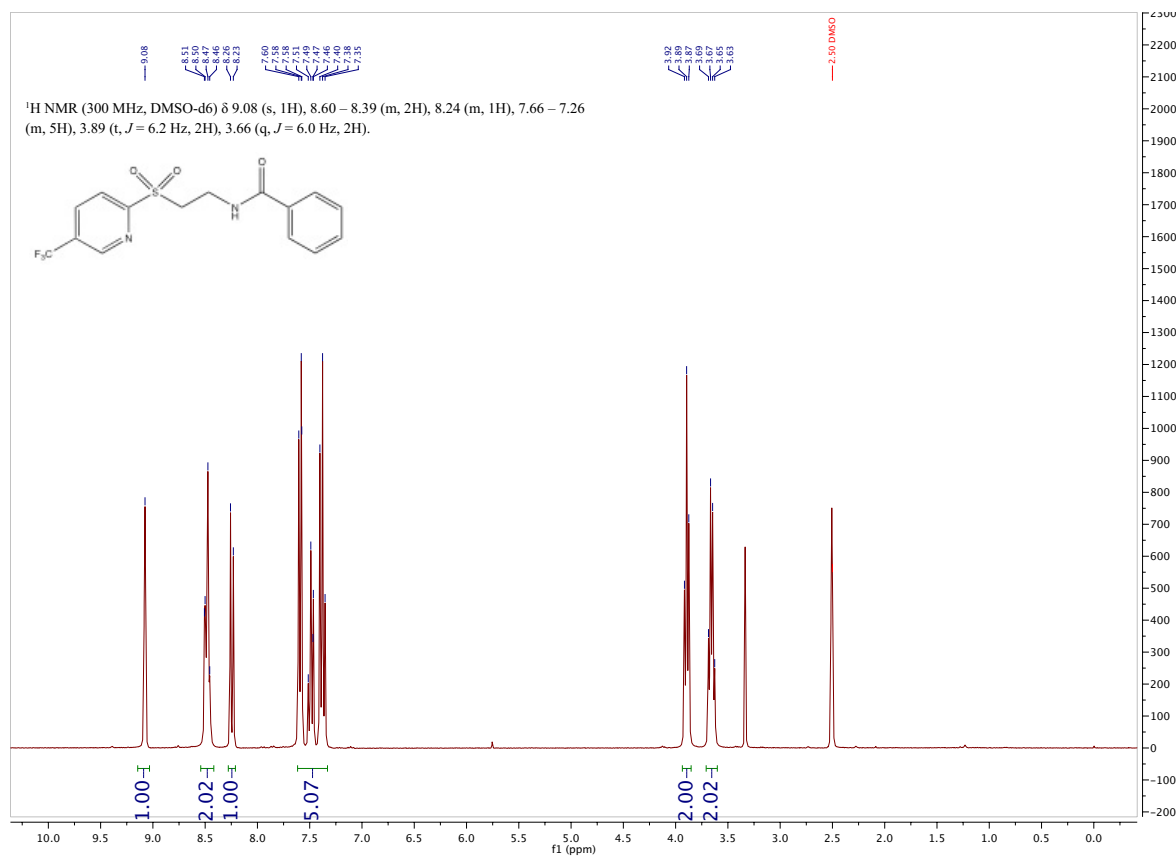


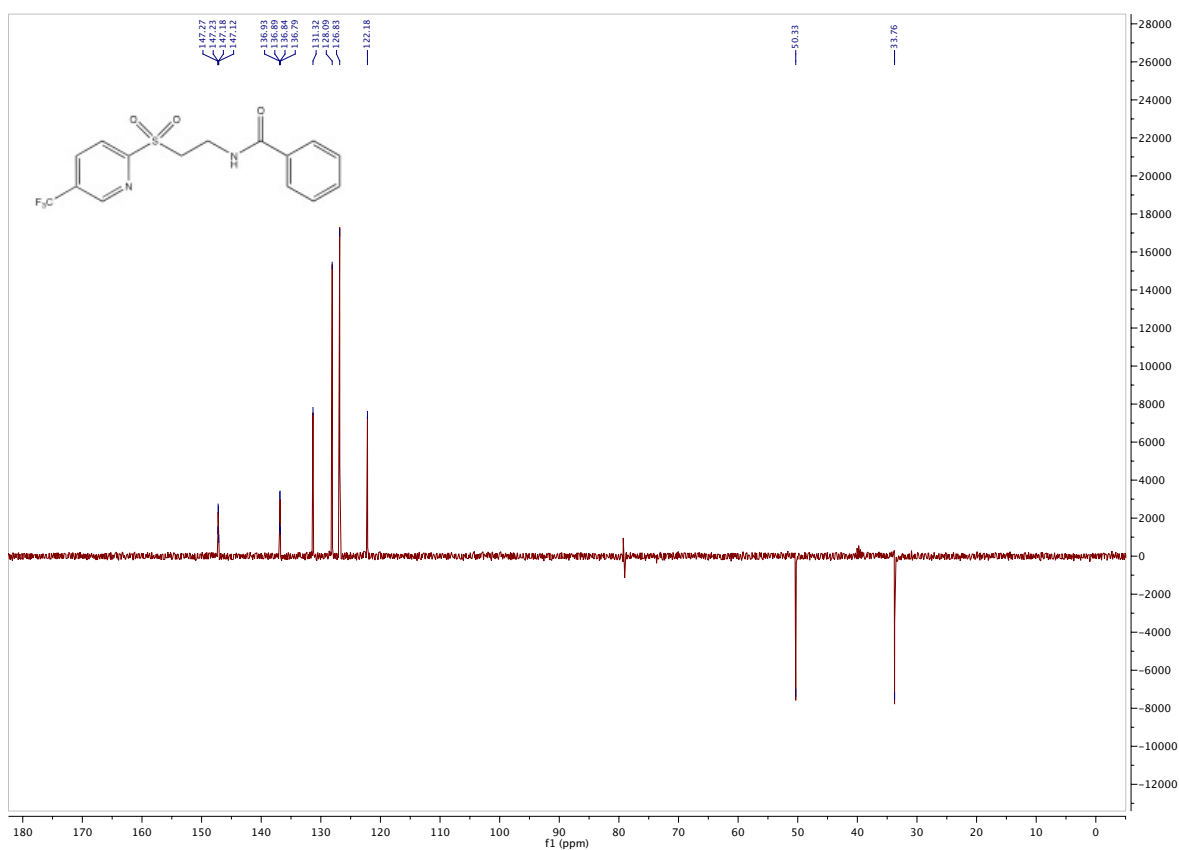
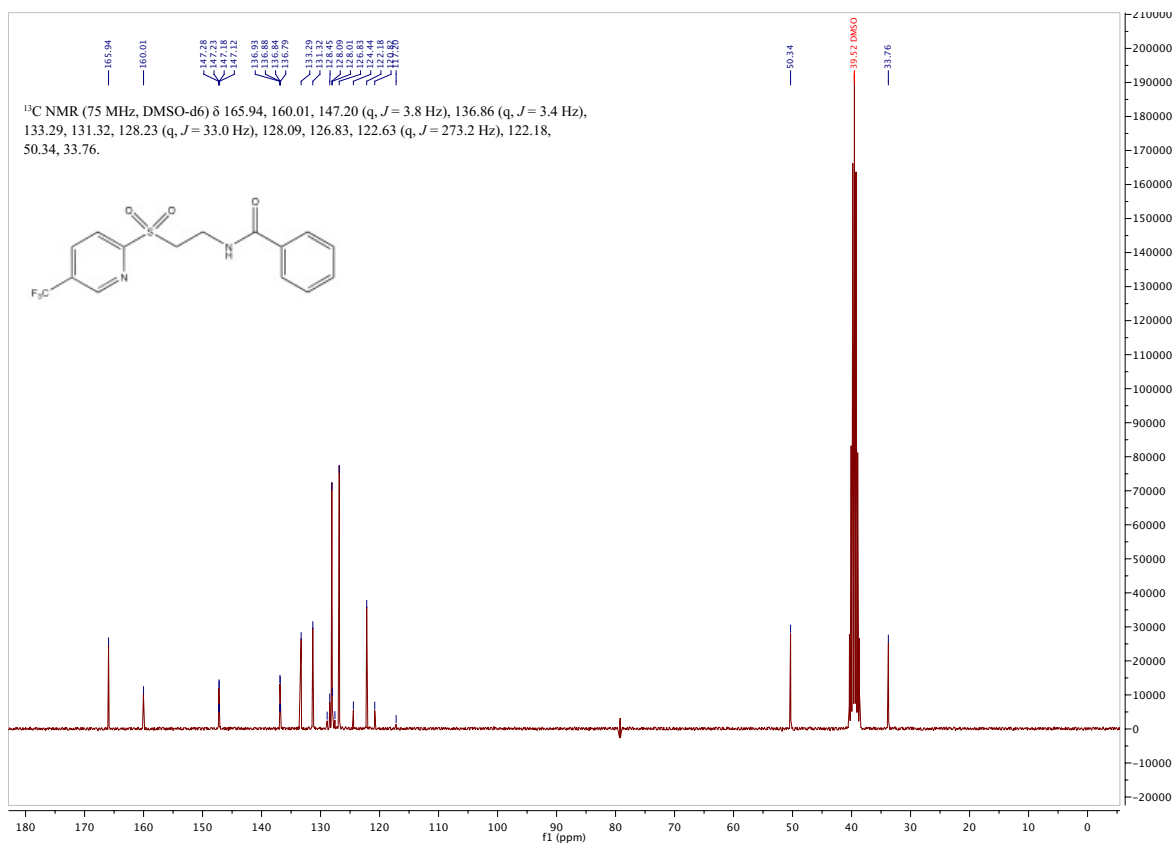
^1H , ^{13}C and DEPT135 spectra of compound CV3



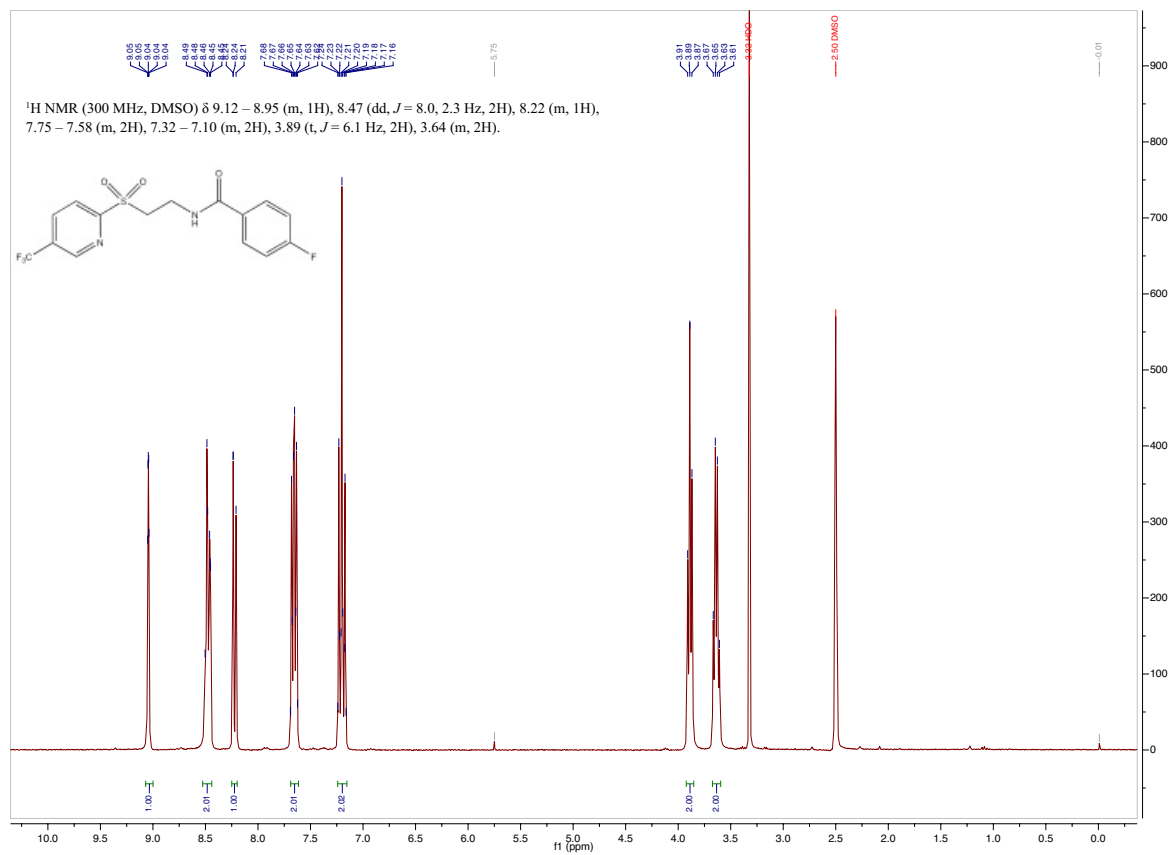


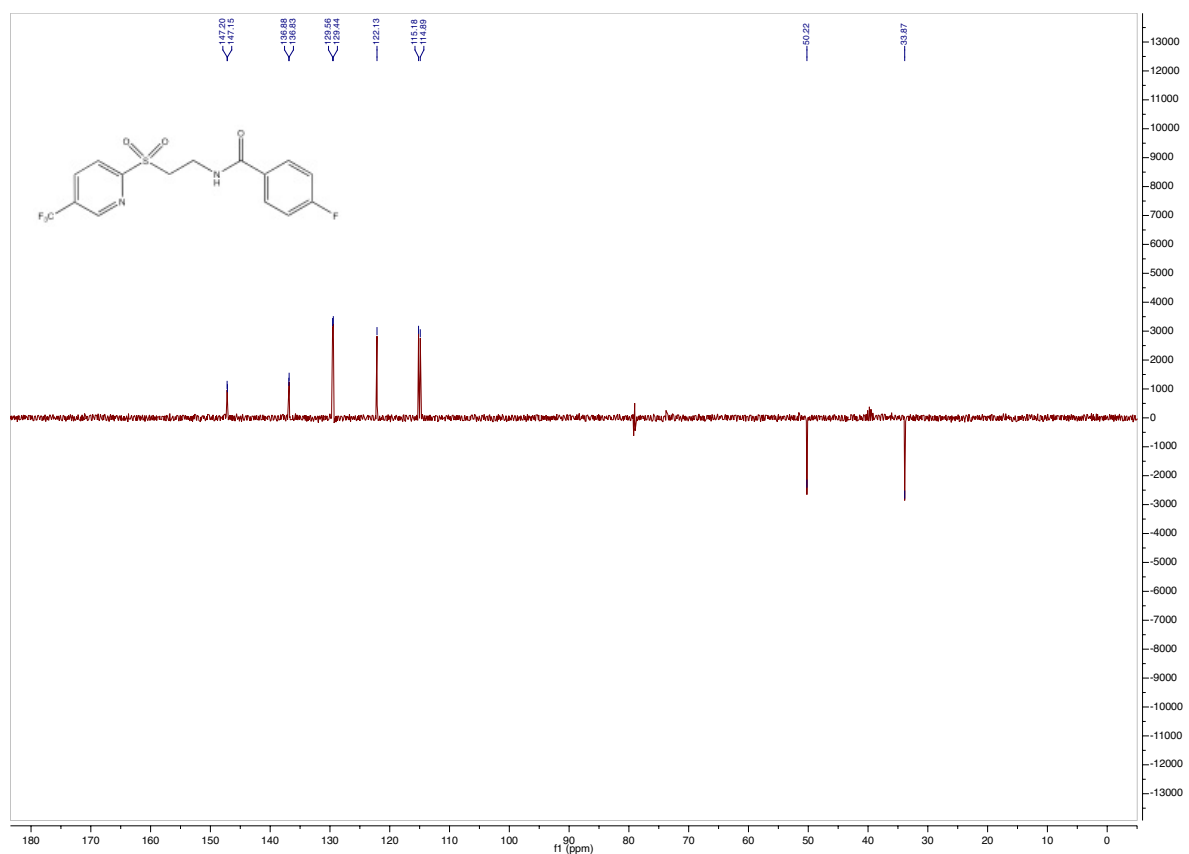
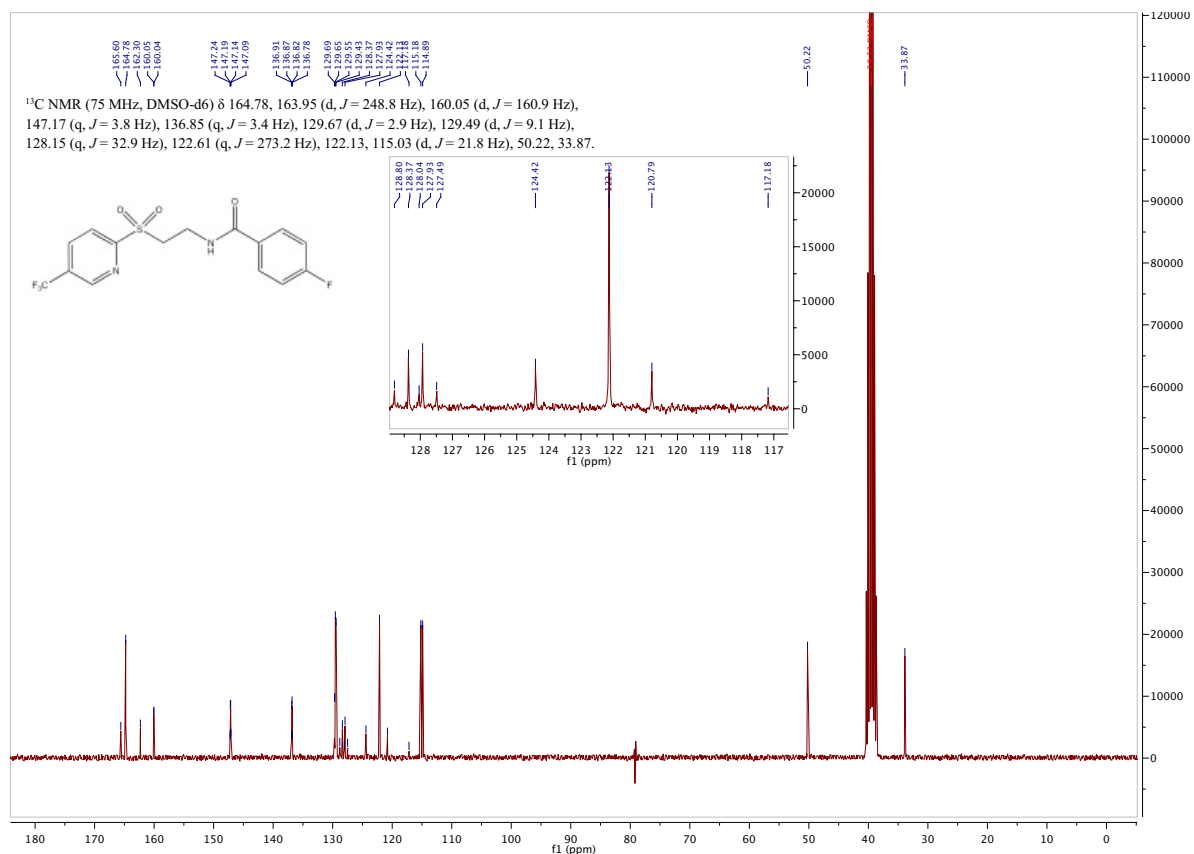
^1H , ^{13}C and DEPT135 spectra of compound 7



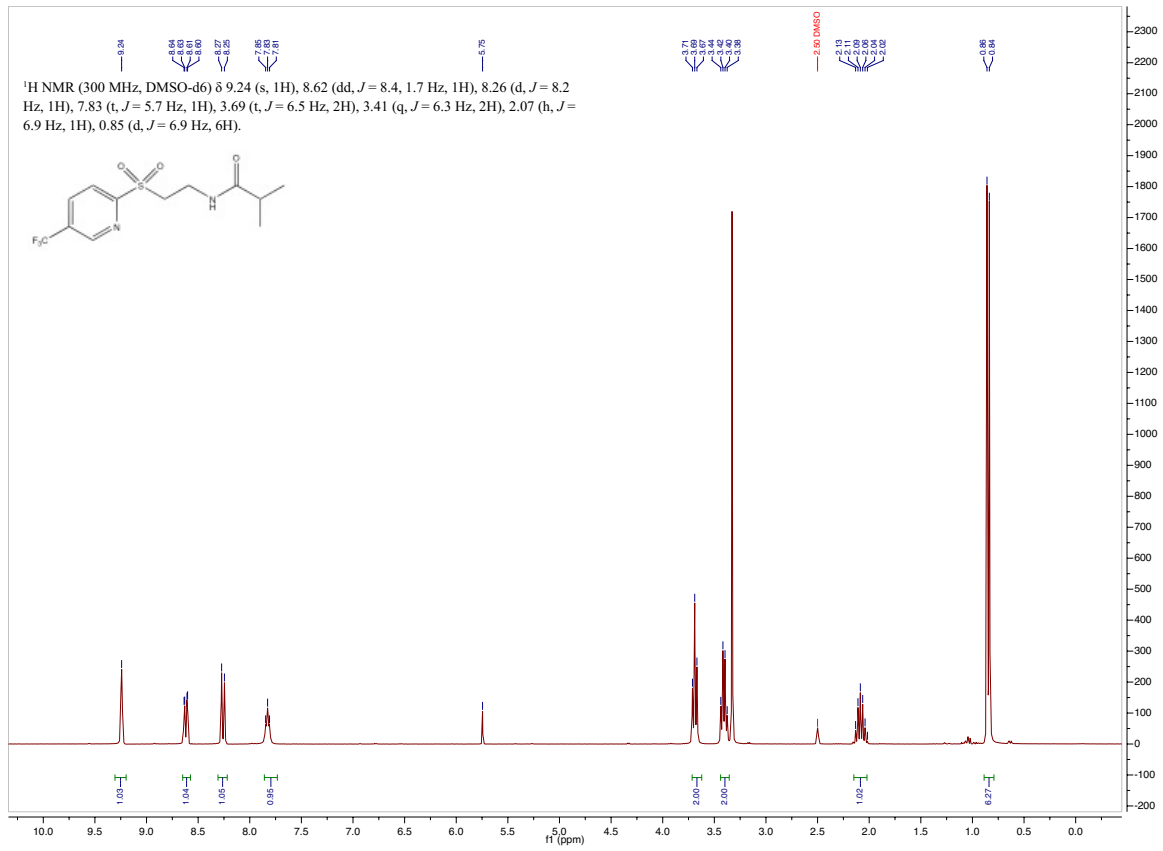


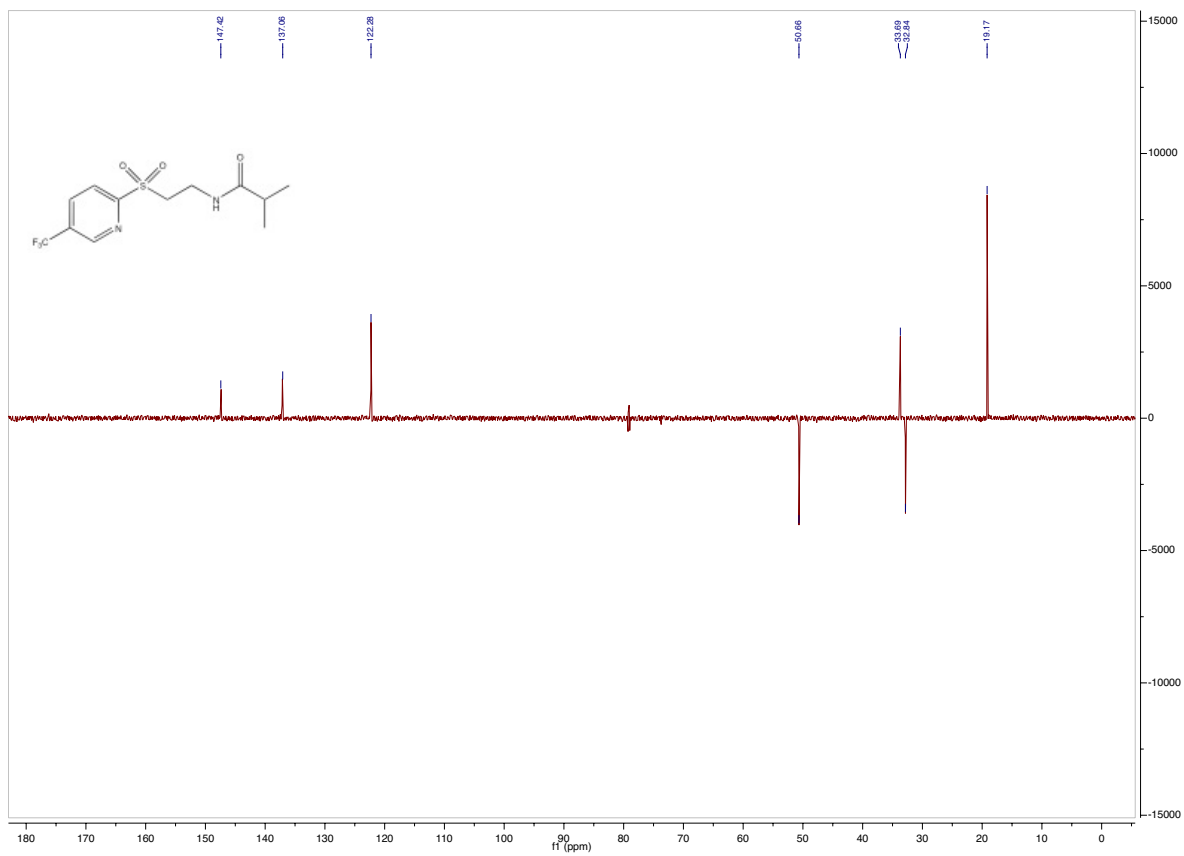
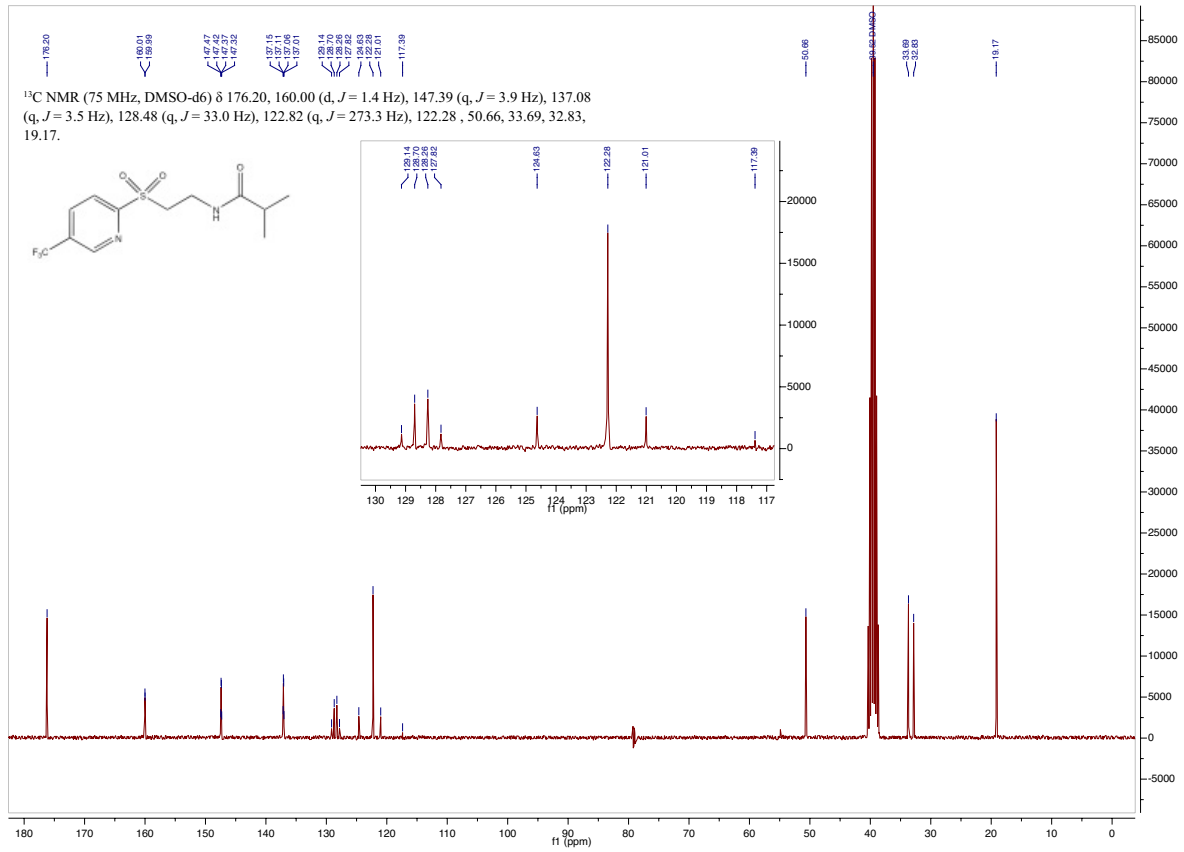
^1H , ^{13}C and DEPT135 spectra of compound 8



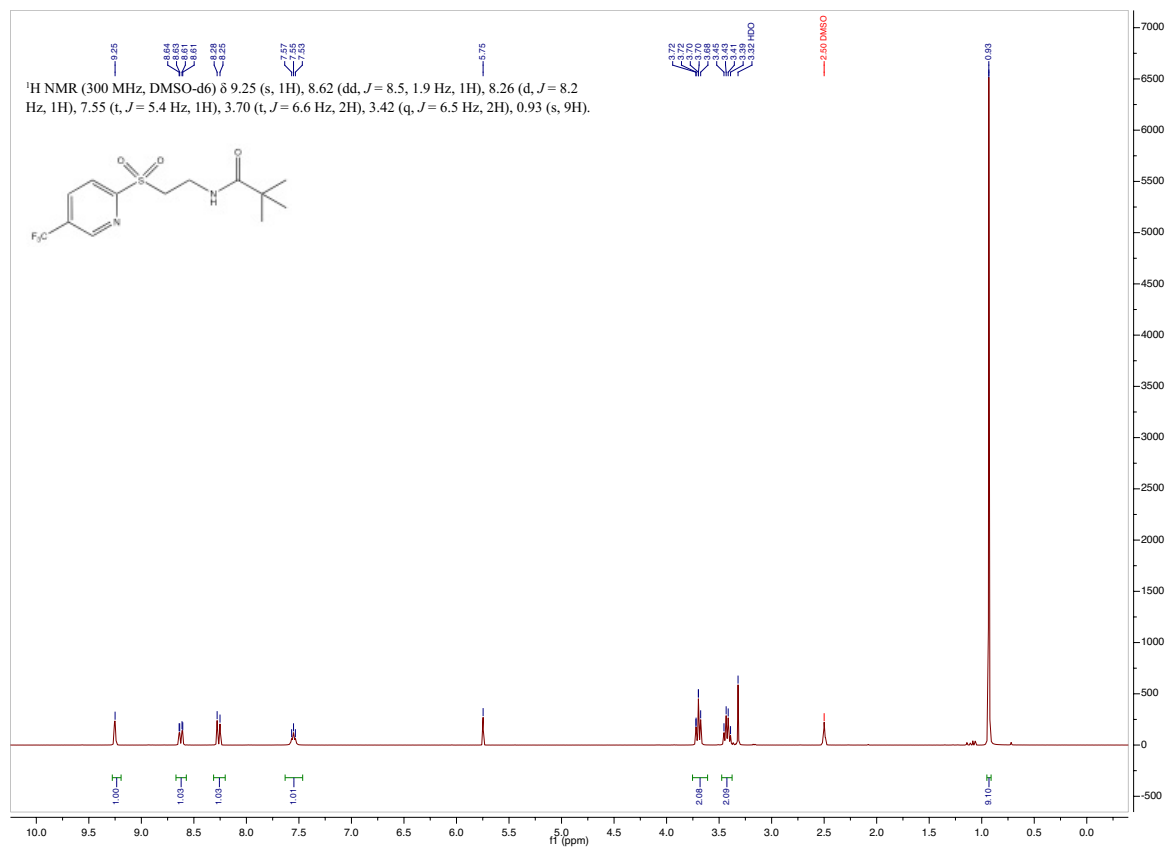


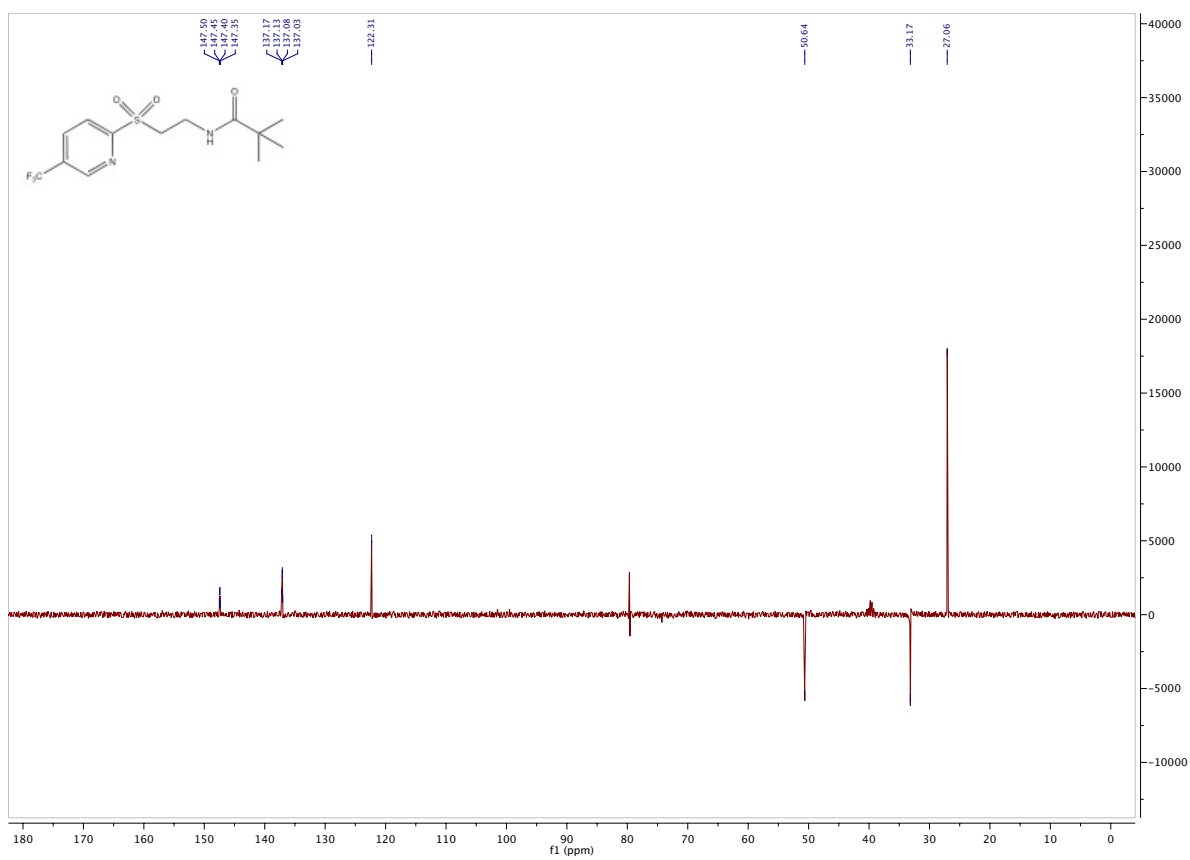
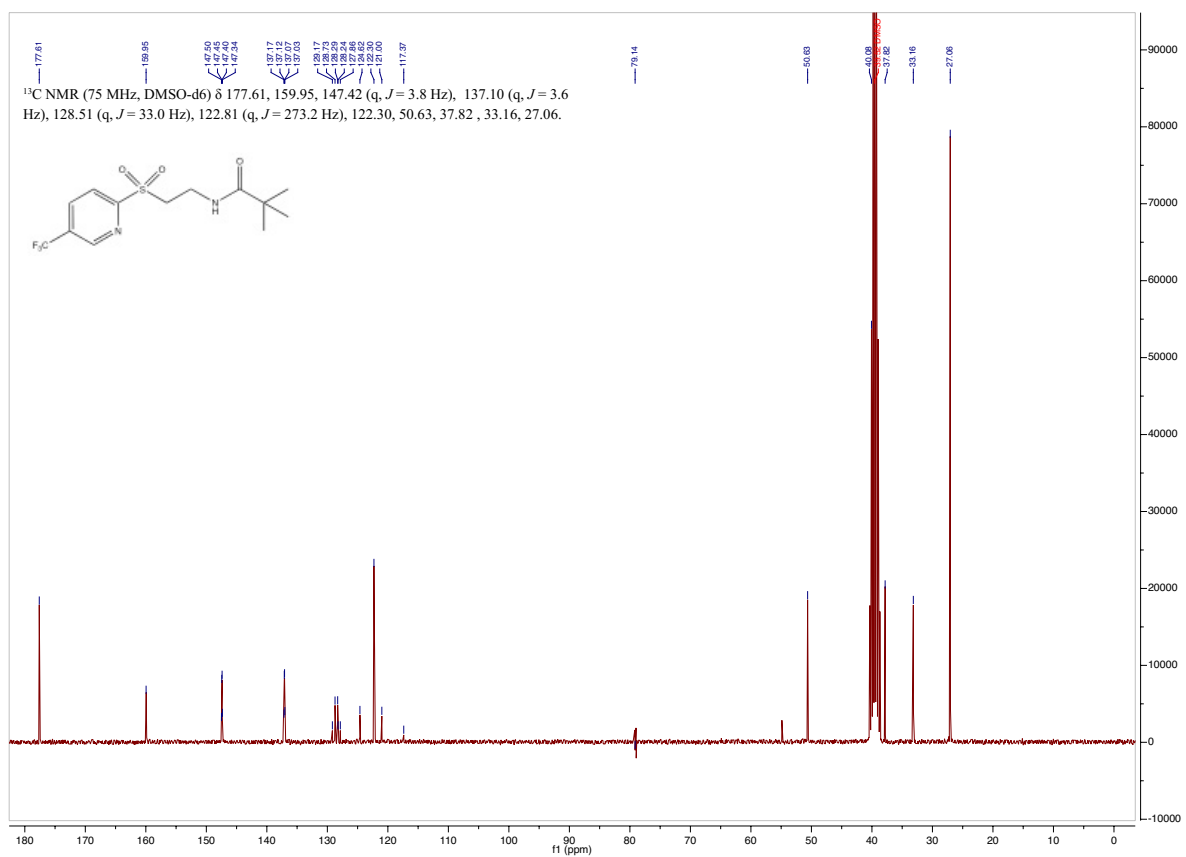
^1H , ^{13}C and DEPT135 spectra of compound 9



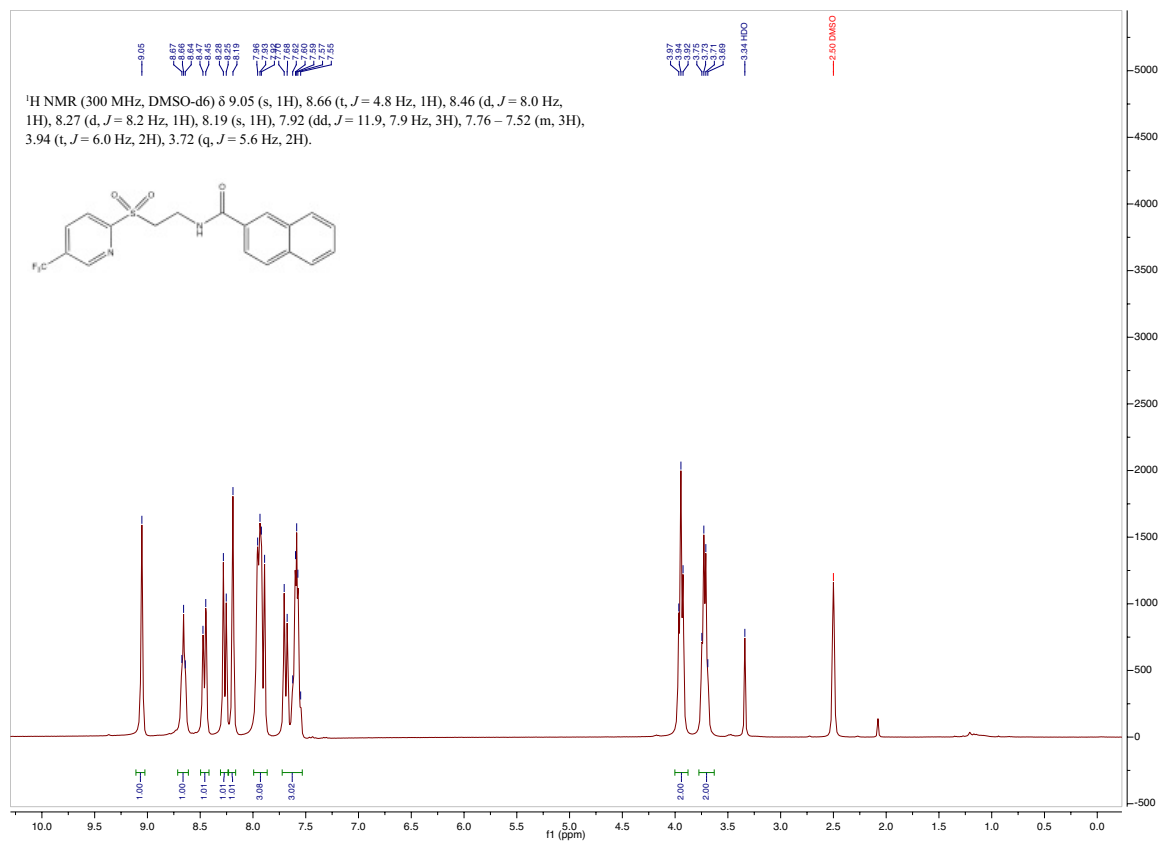


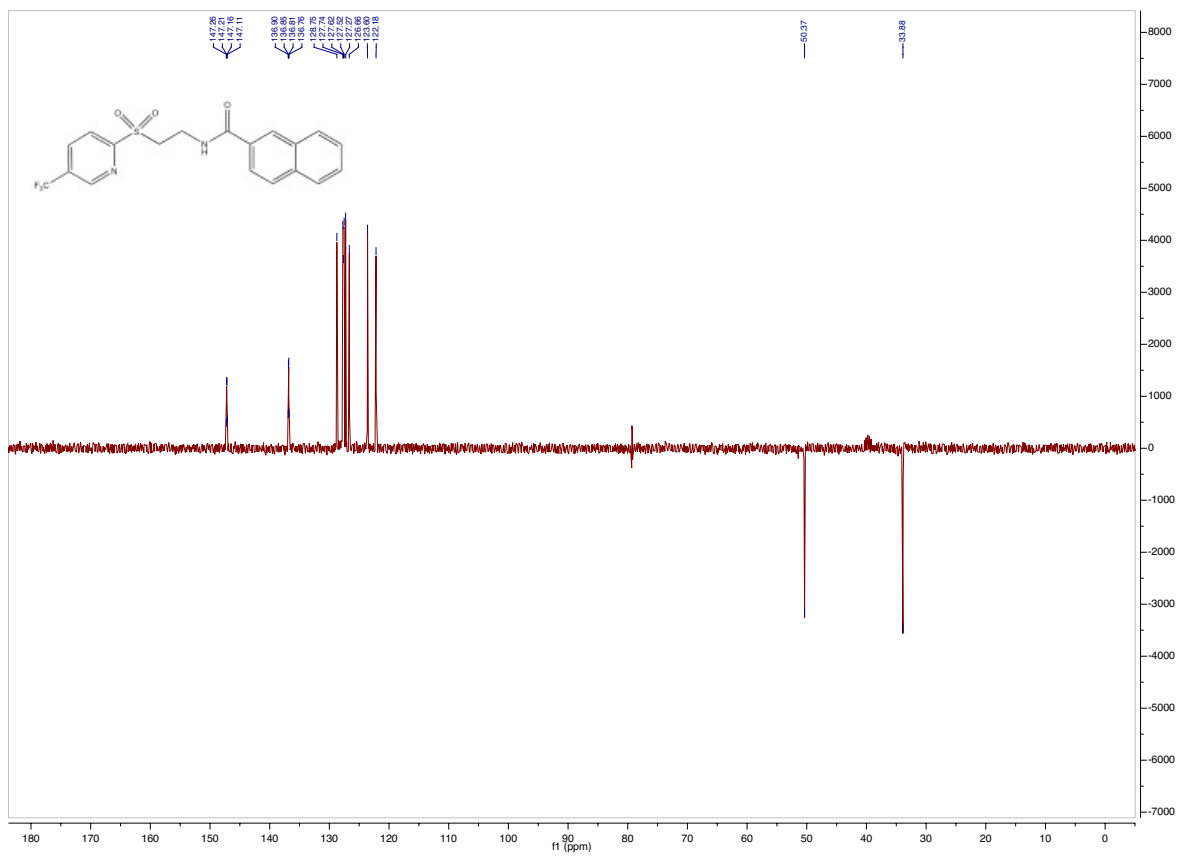
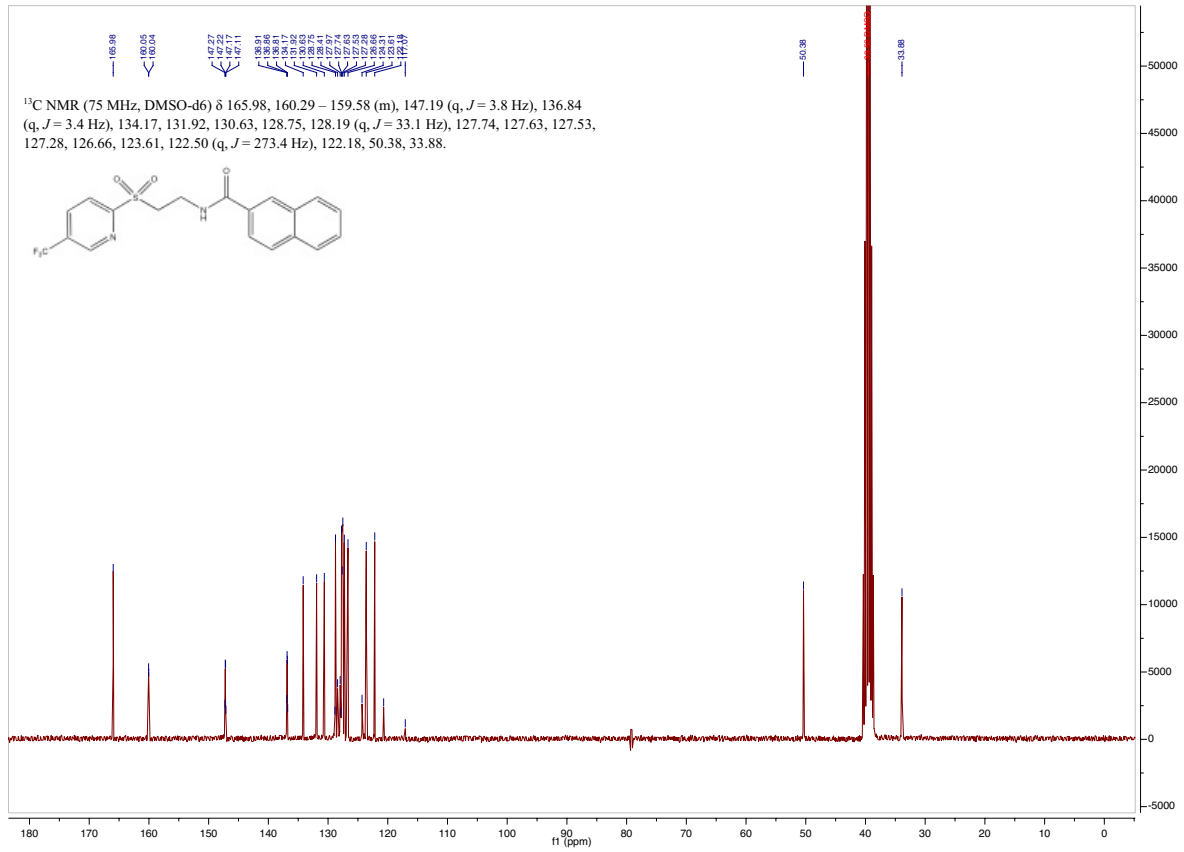
^1H , ^{13}C and DEPT135 spectra of compound 10



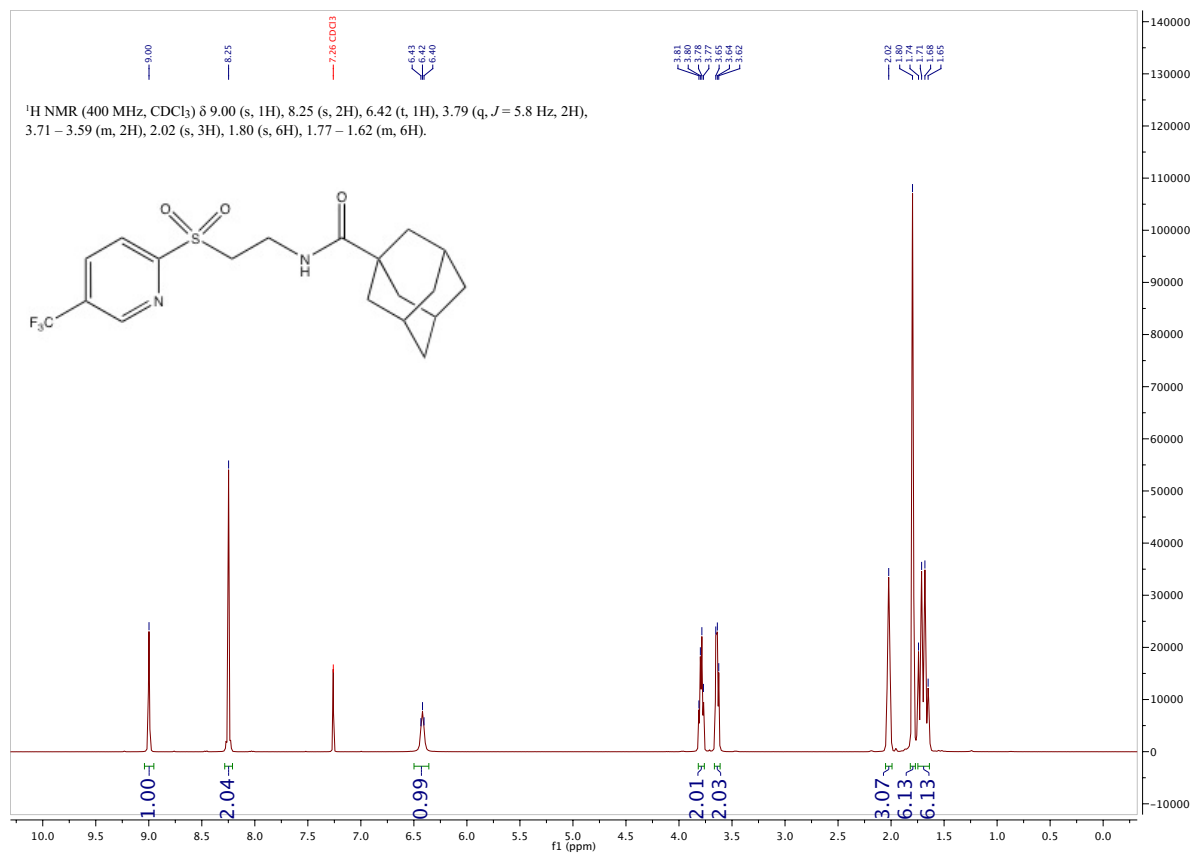


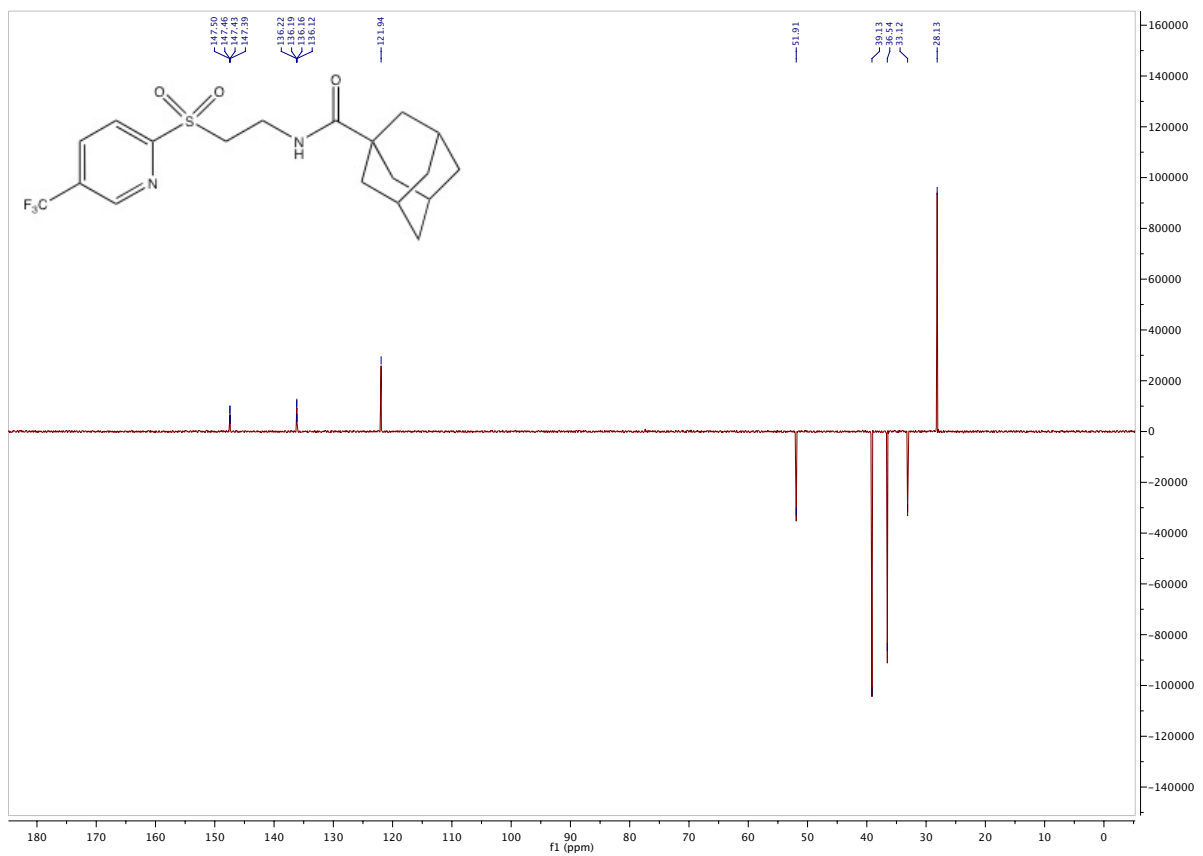
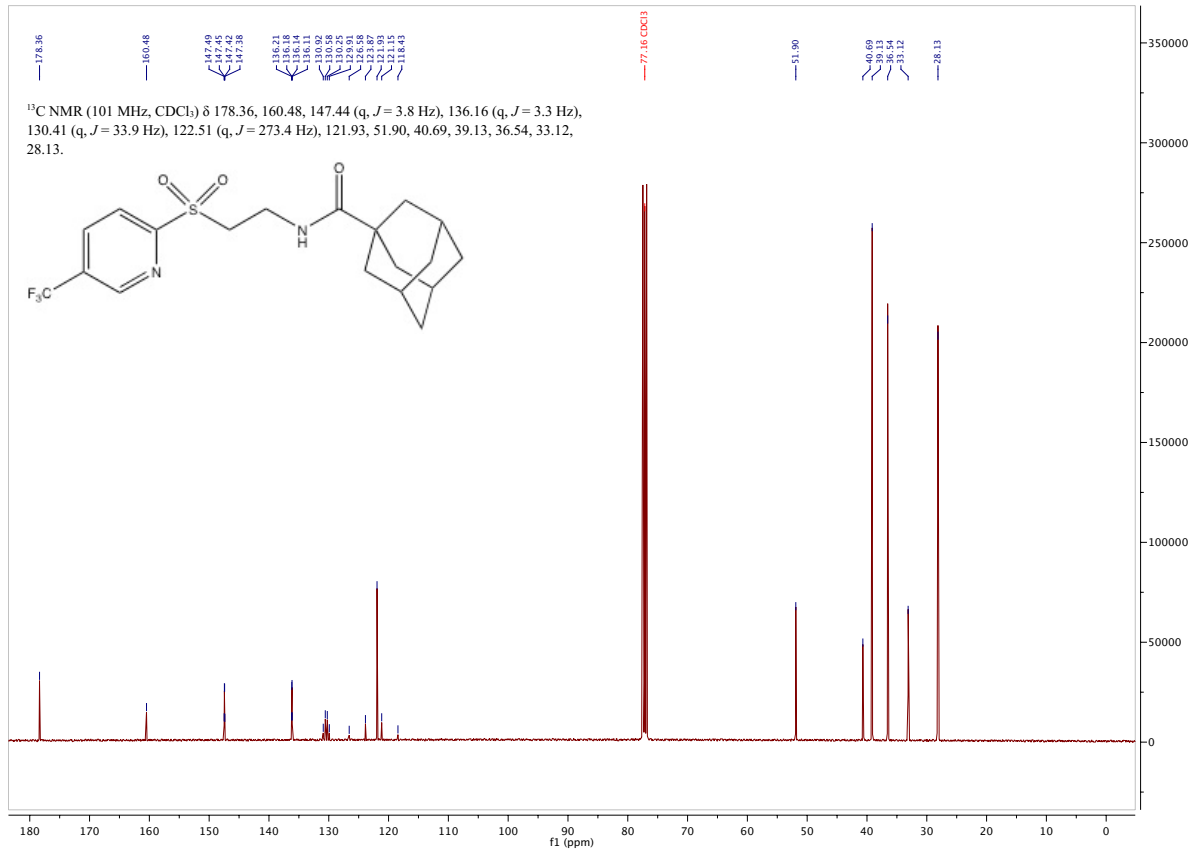
^1H , ^{13}C and DEPT135 spectra of compound 11





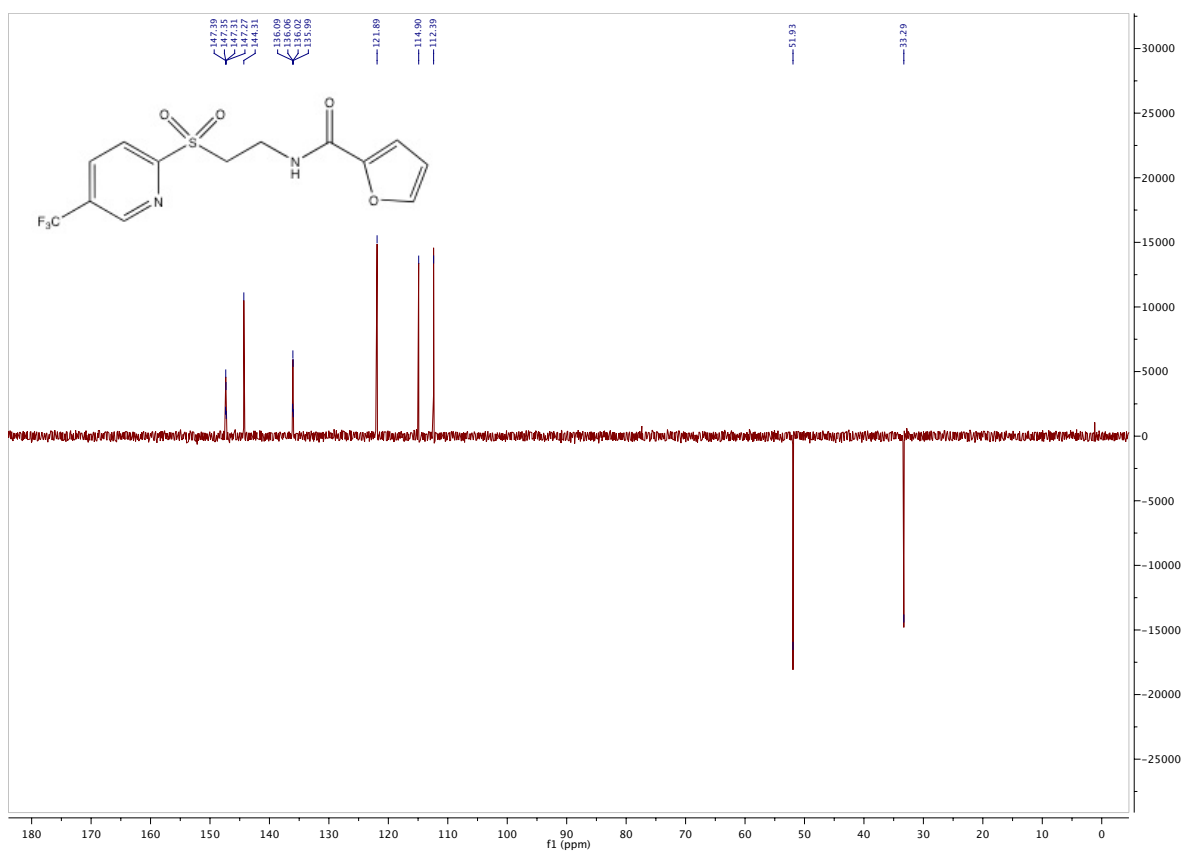
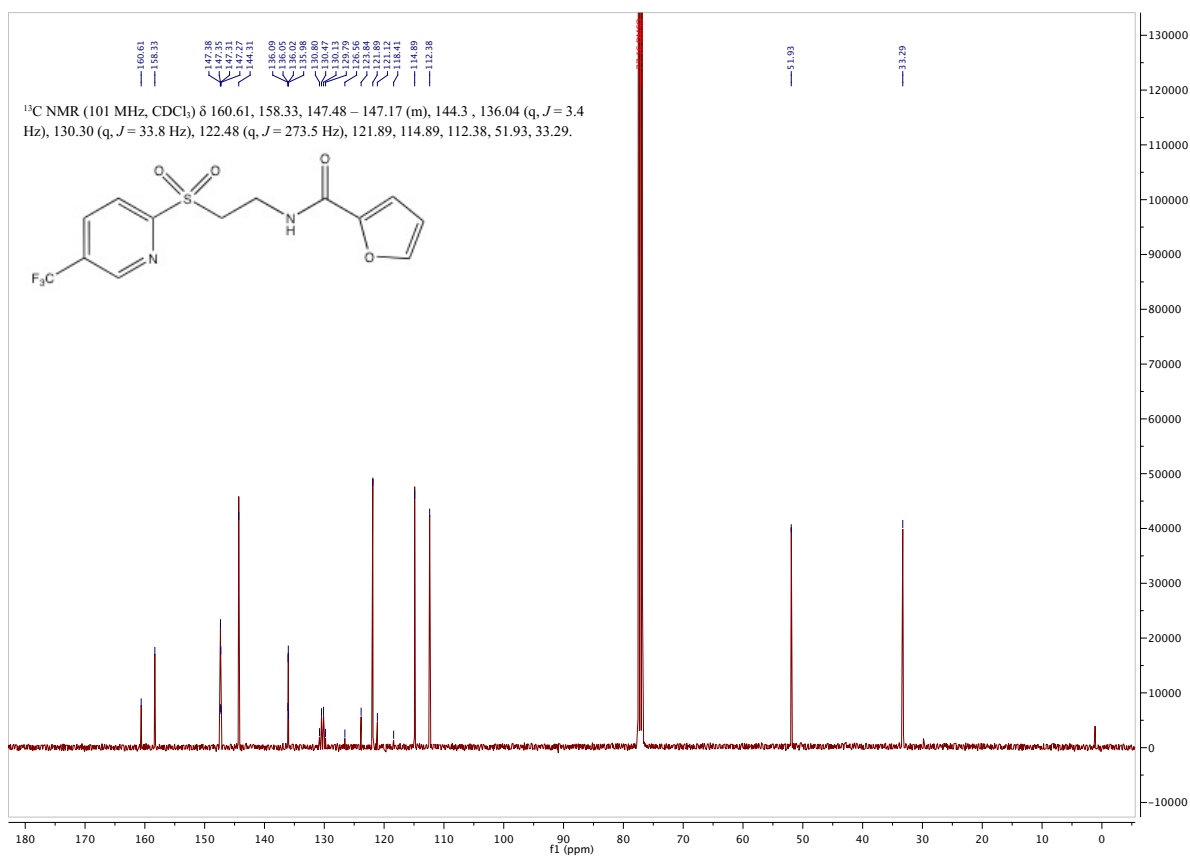
^1H , ^{13}C and DEPT135 spectra of compound 12



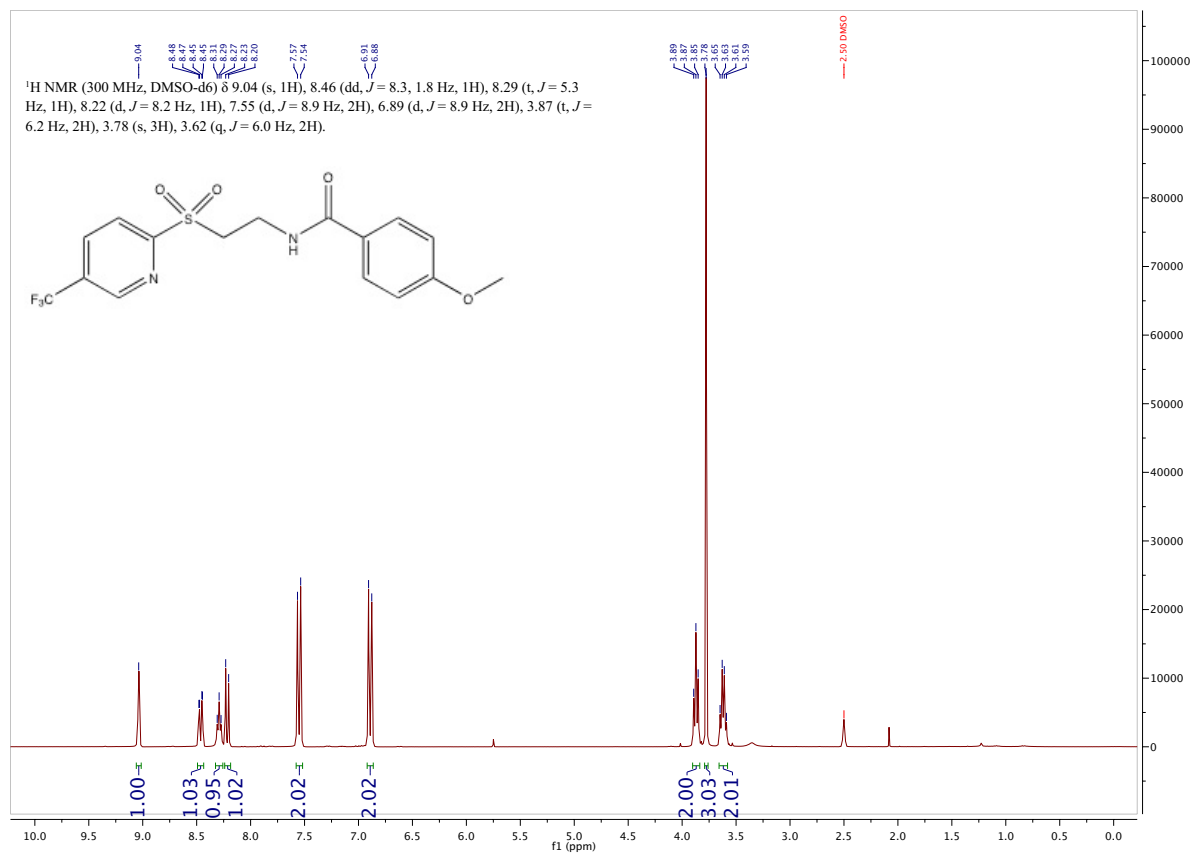


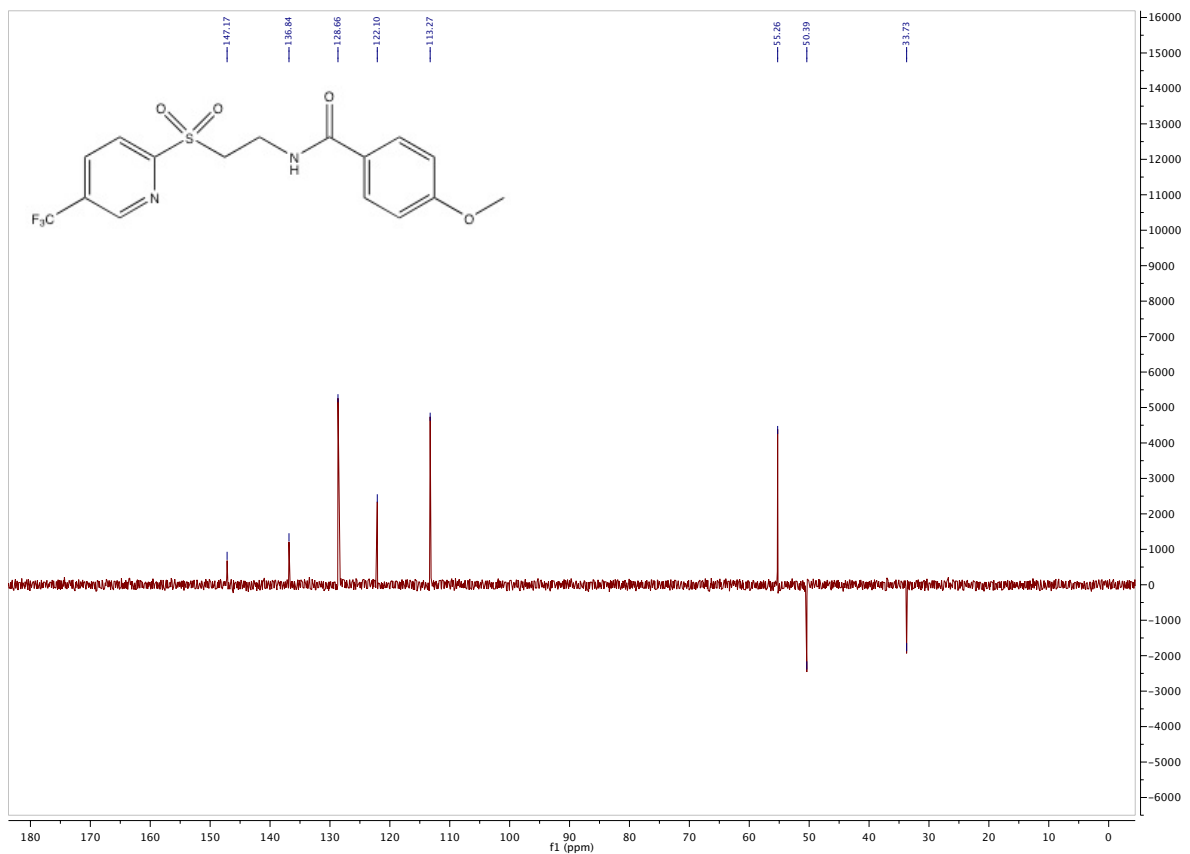
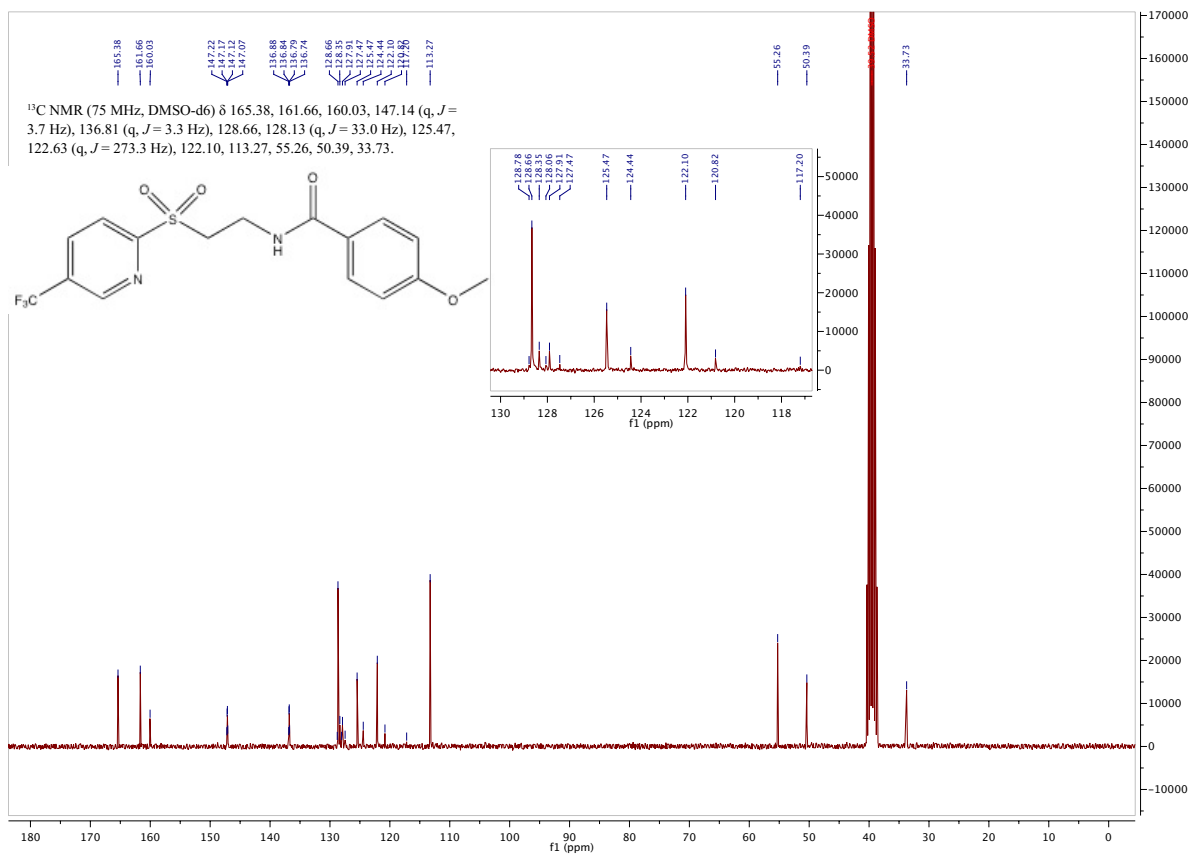
^1H , ^{13}C and DEPT135 spectra of compound 13



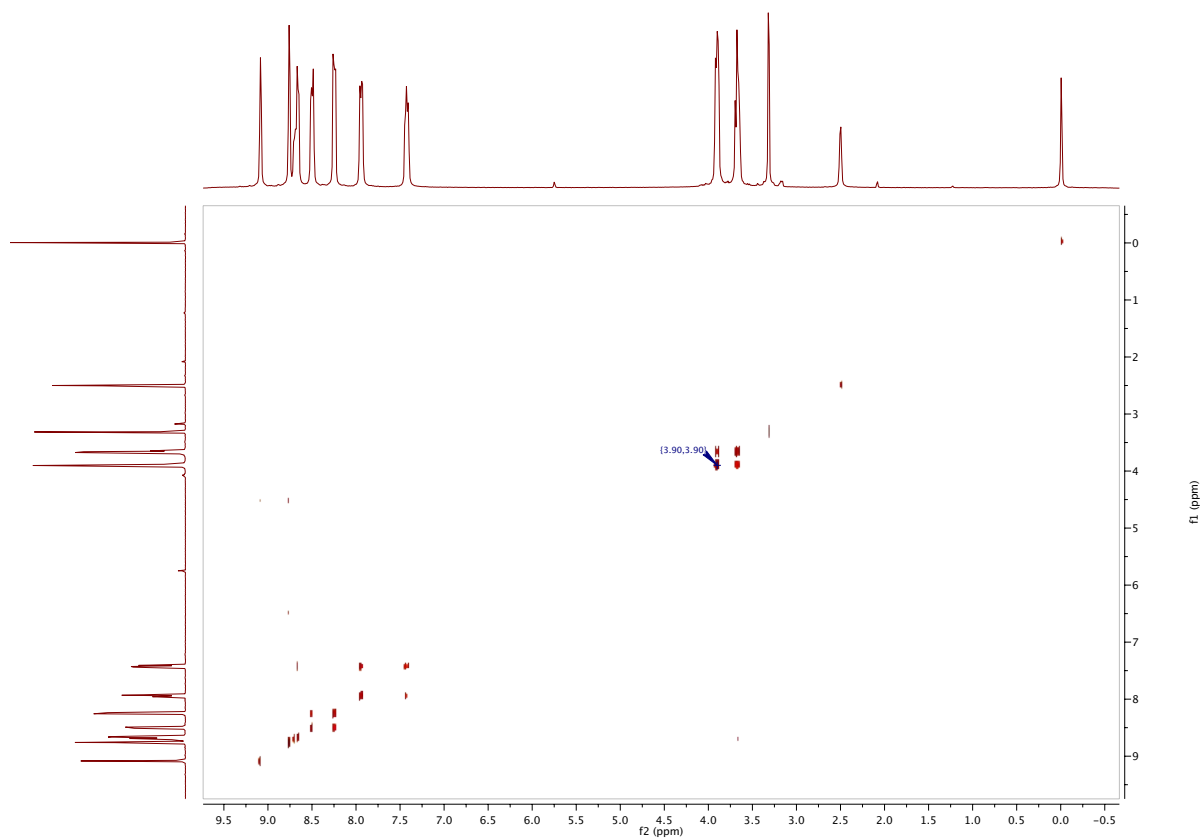
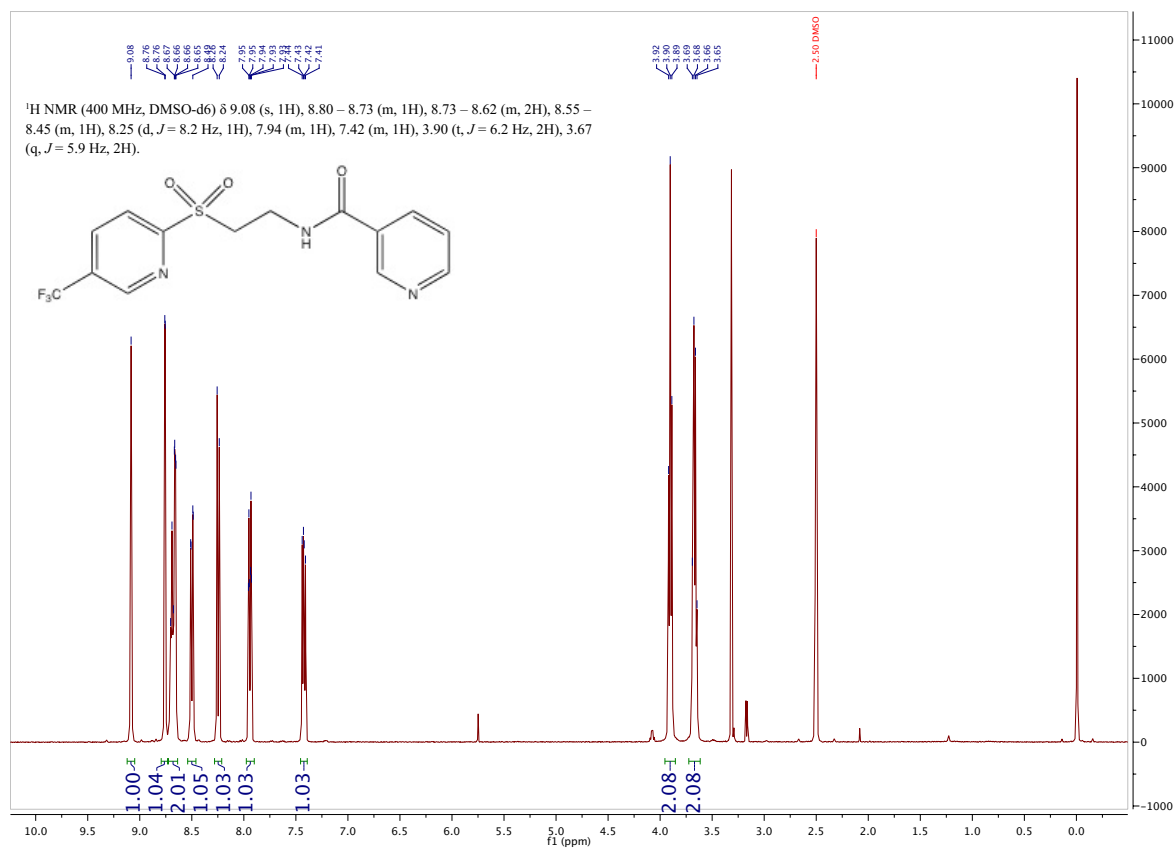


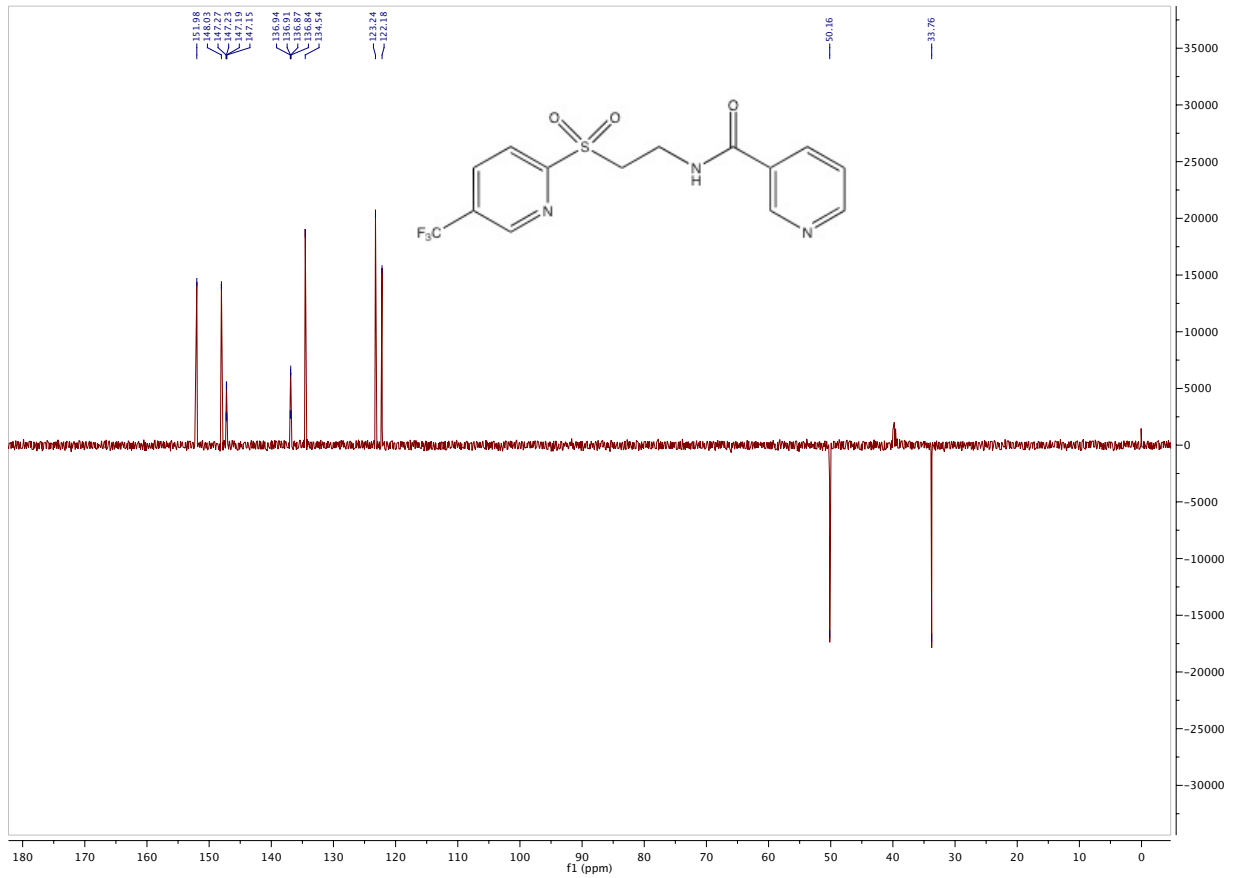
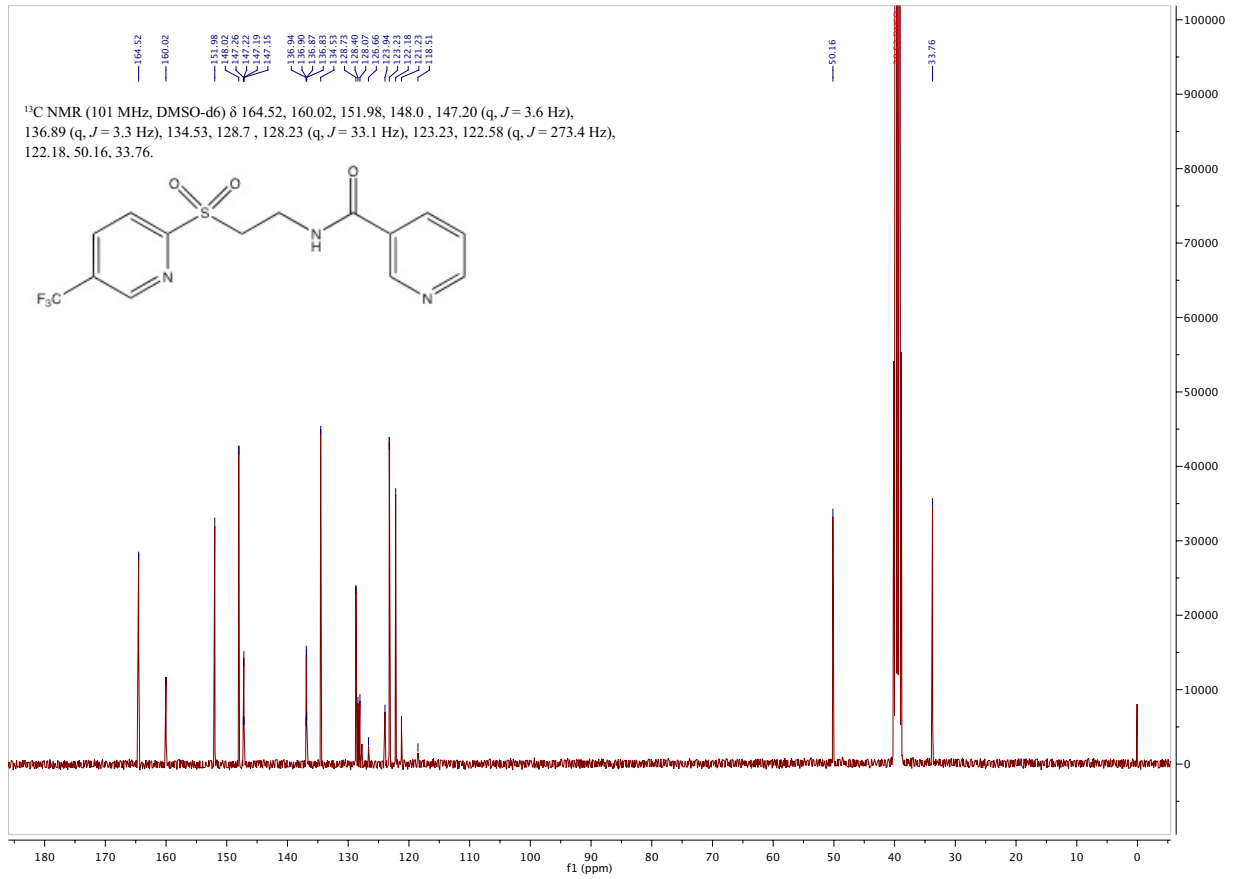
^1H , ^{13}C and DEPT135 spectra of compound 14





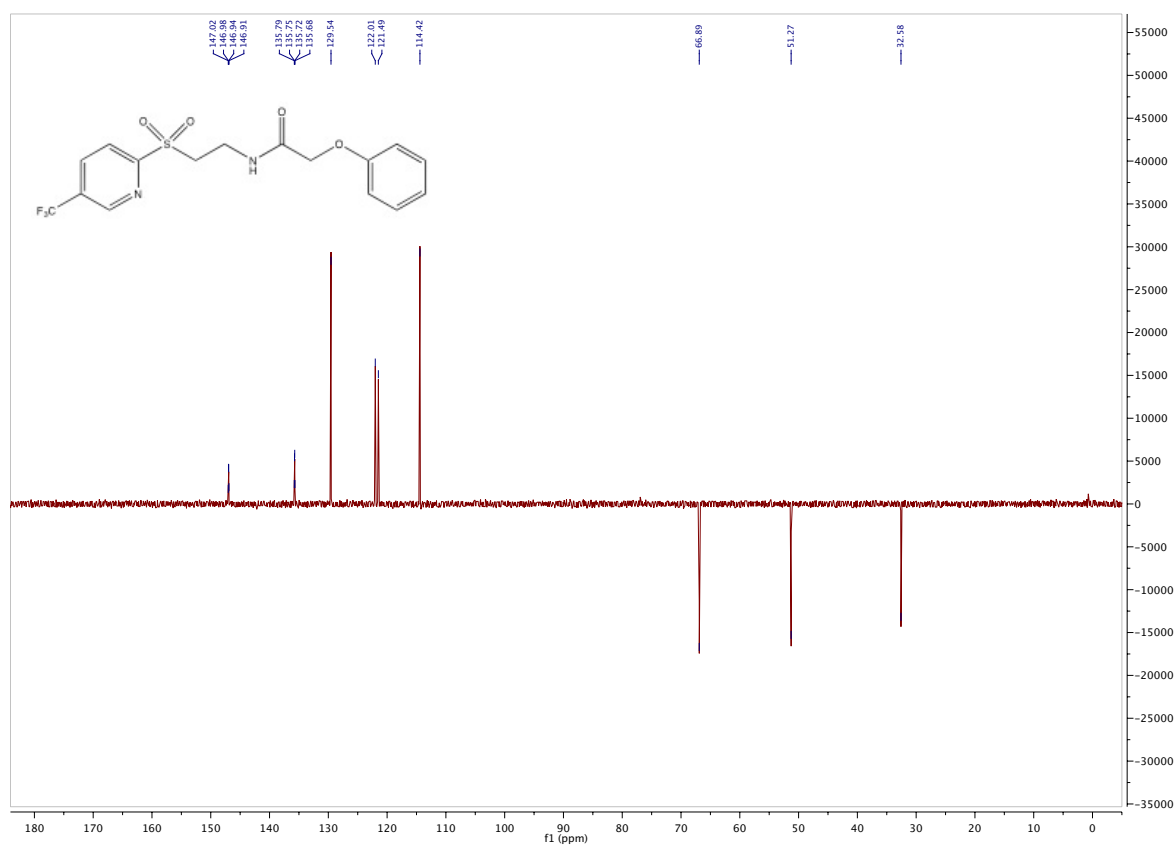
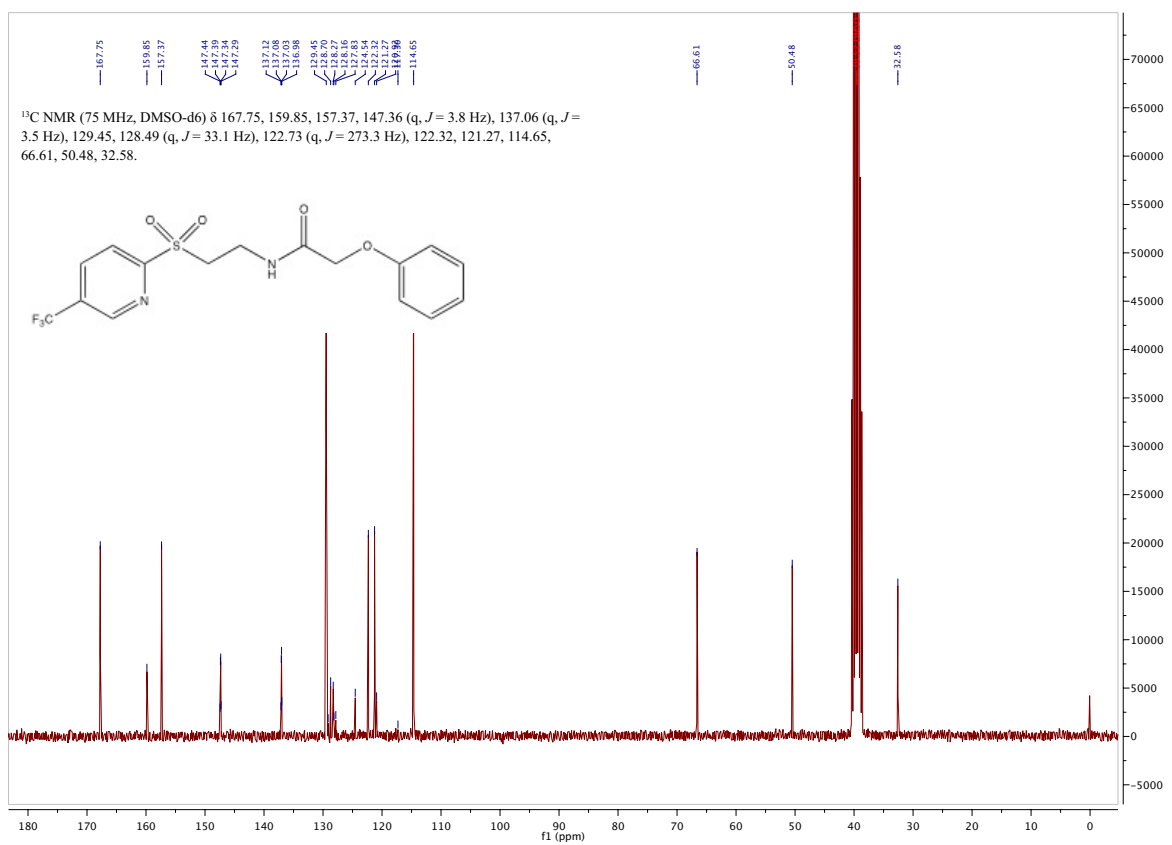
¹H, COSY45, ¹³C and DEPT135 NMR spectra of compound 15



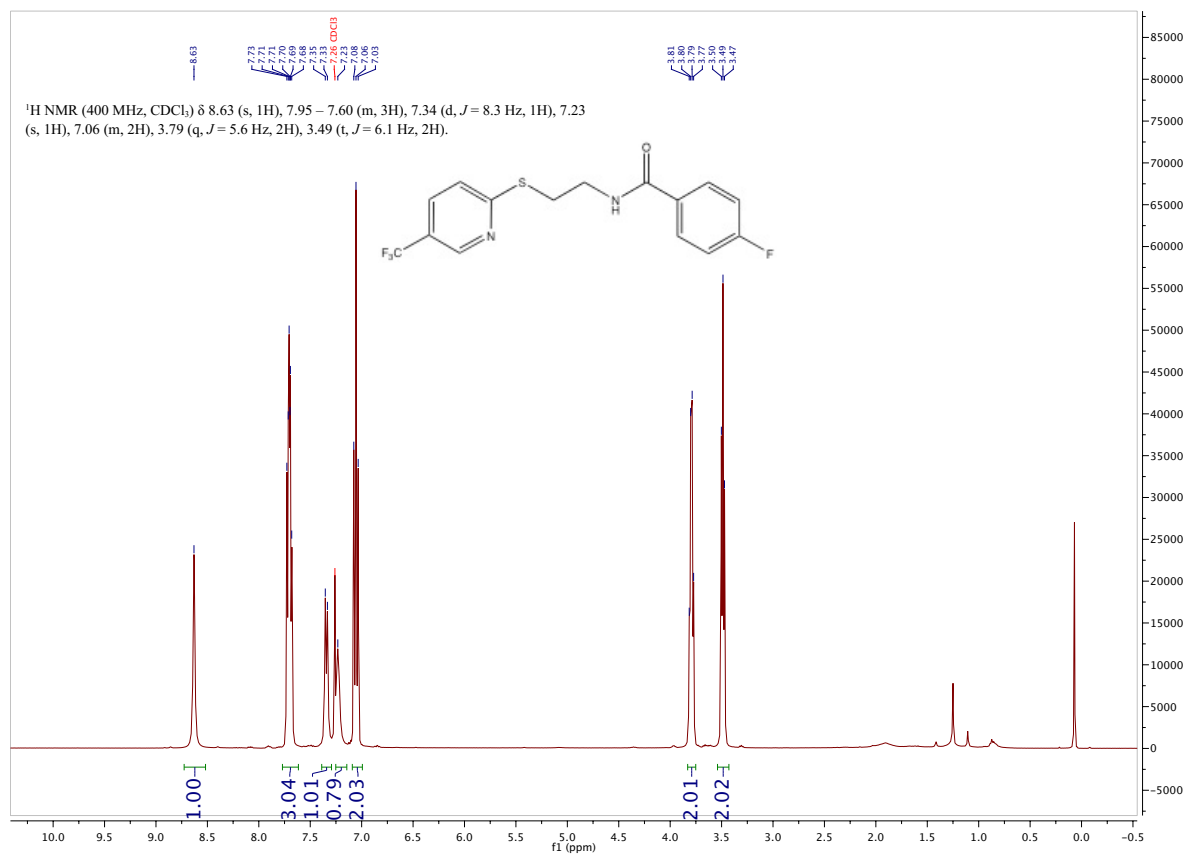


^1H , ^{13}C and DEPT135 spectra of 16

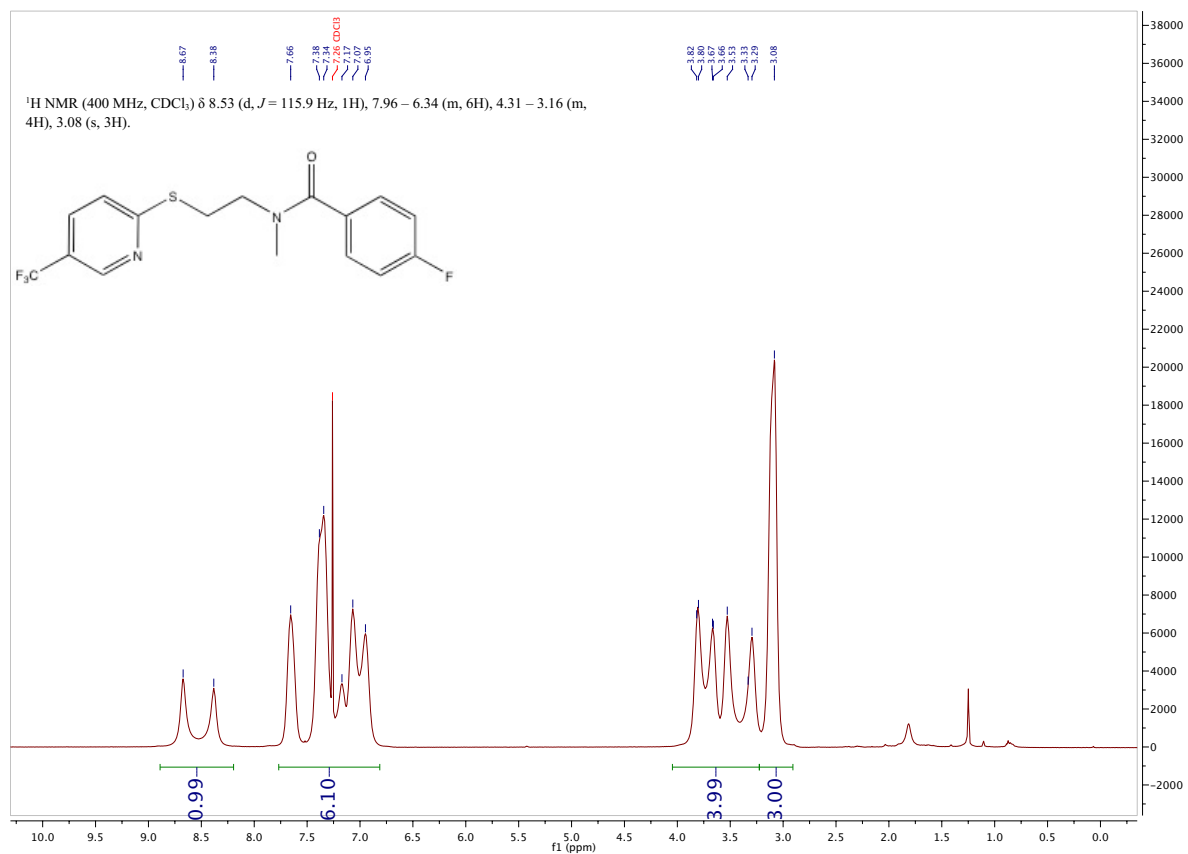




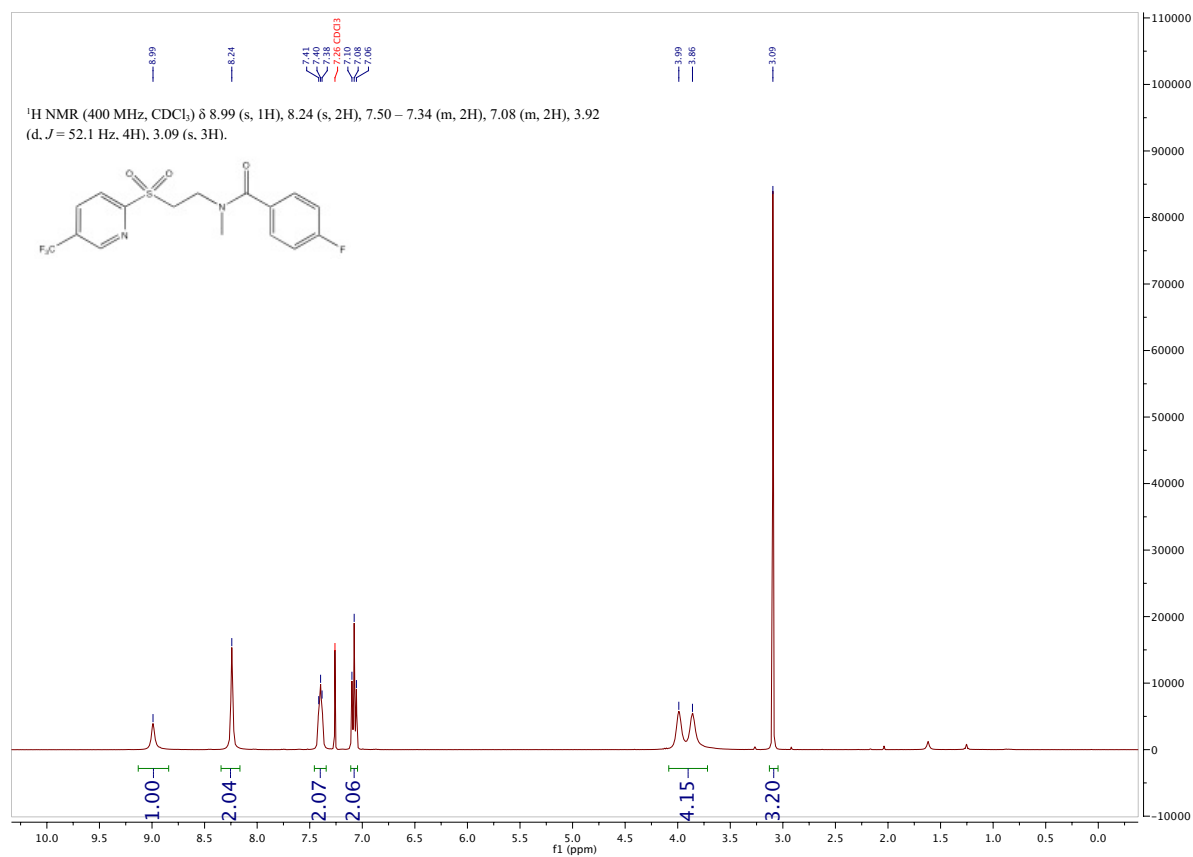
¹H-NMR spectrum of compound 48

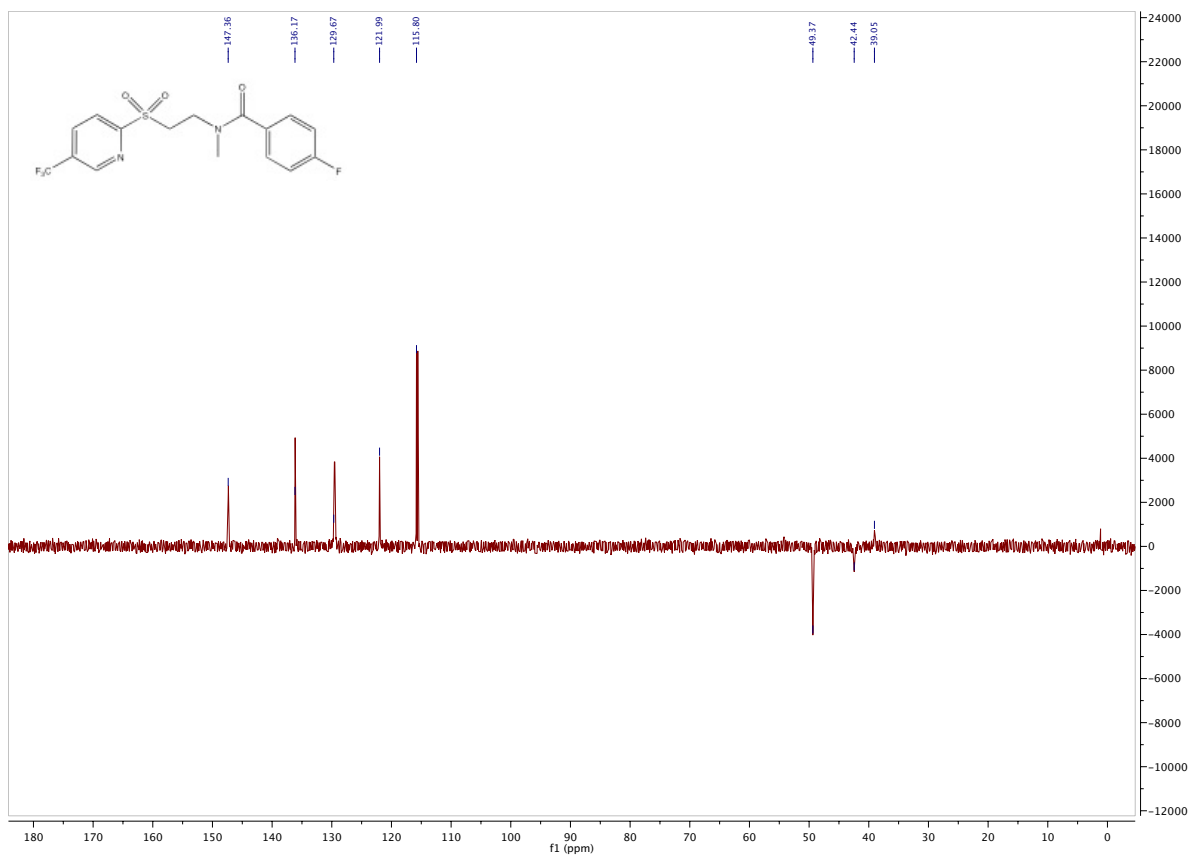
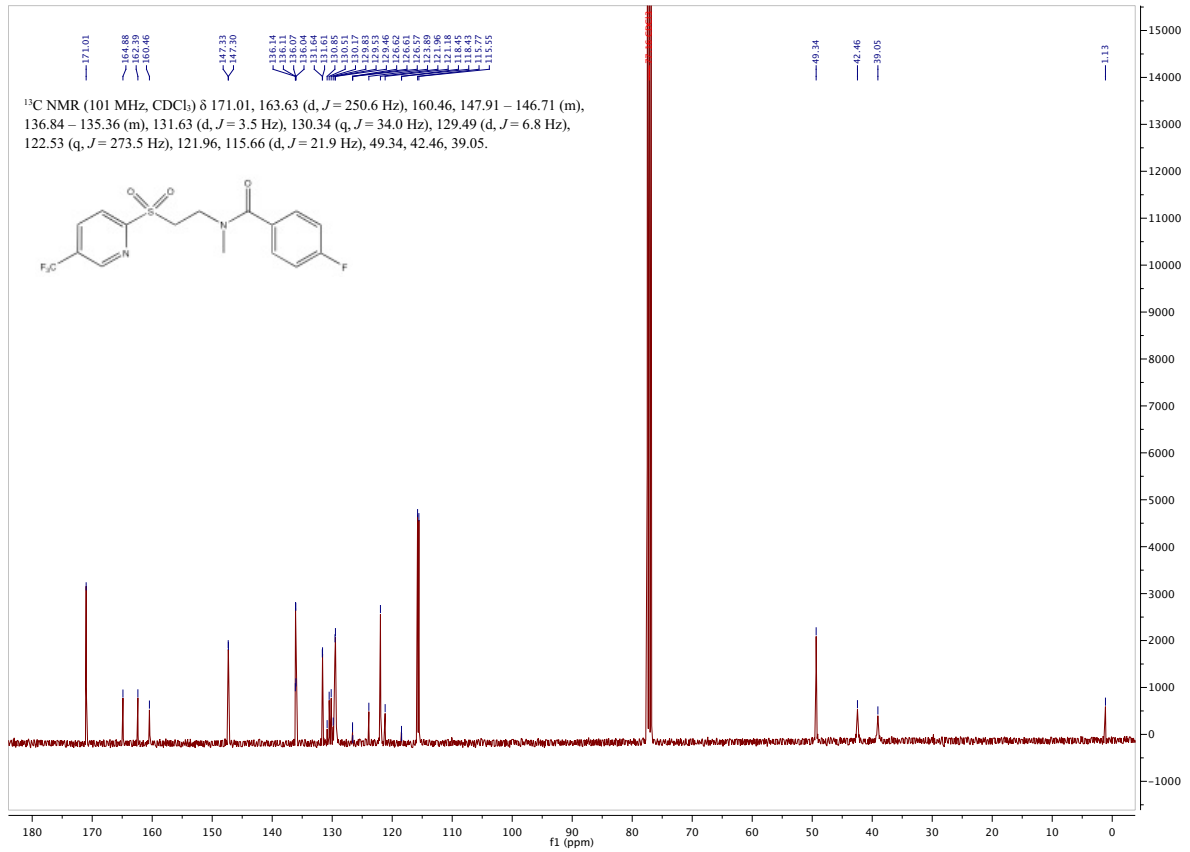


¹H-NMR spectrum of compound 49



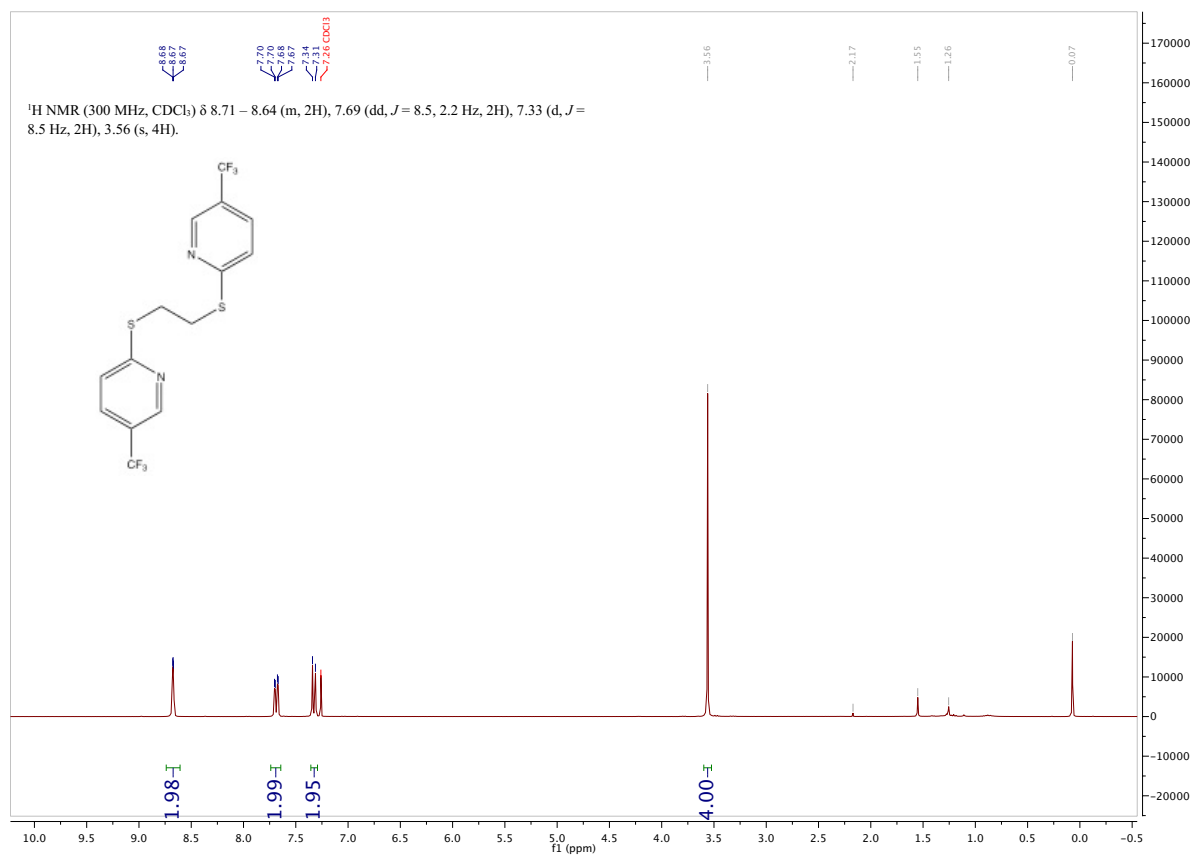
^1H , ^{13}C and DEPT135 spectra of compound 23

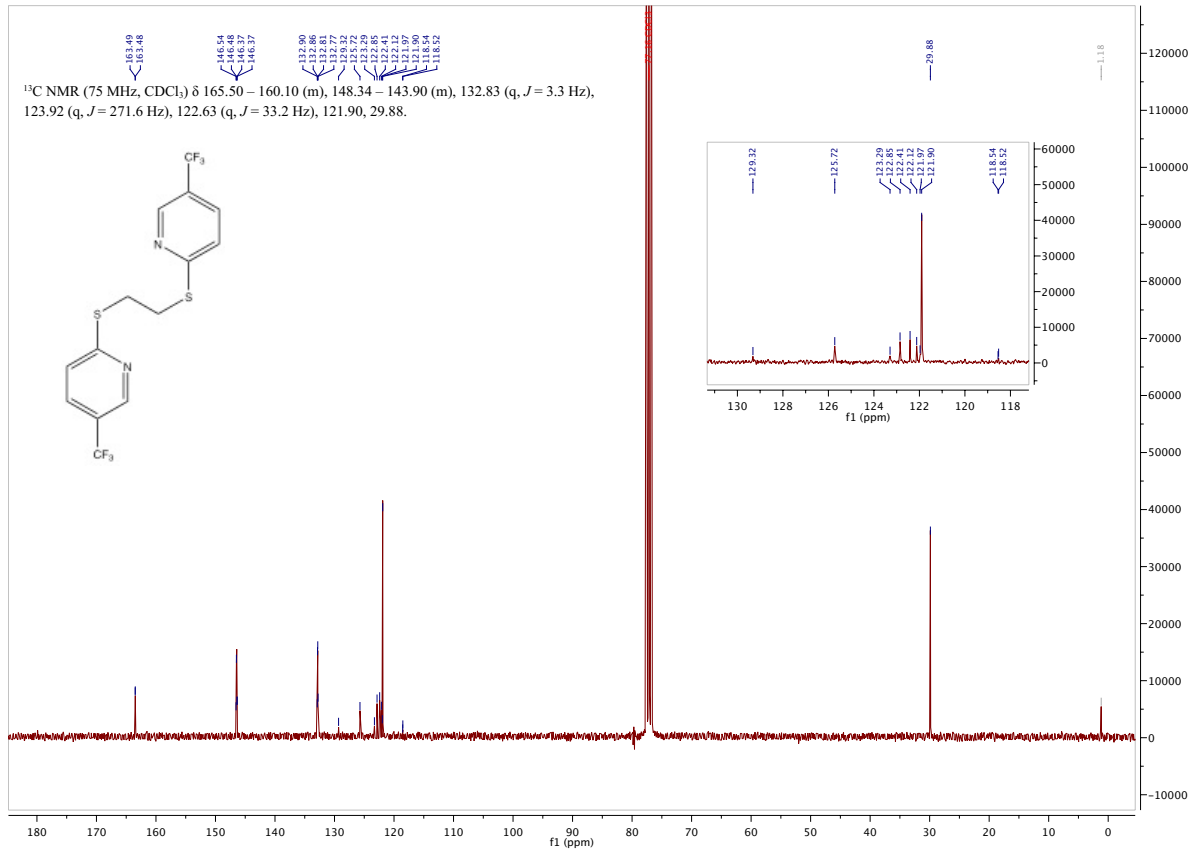




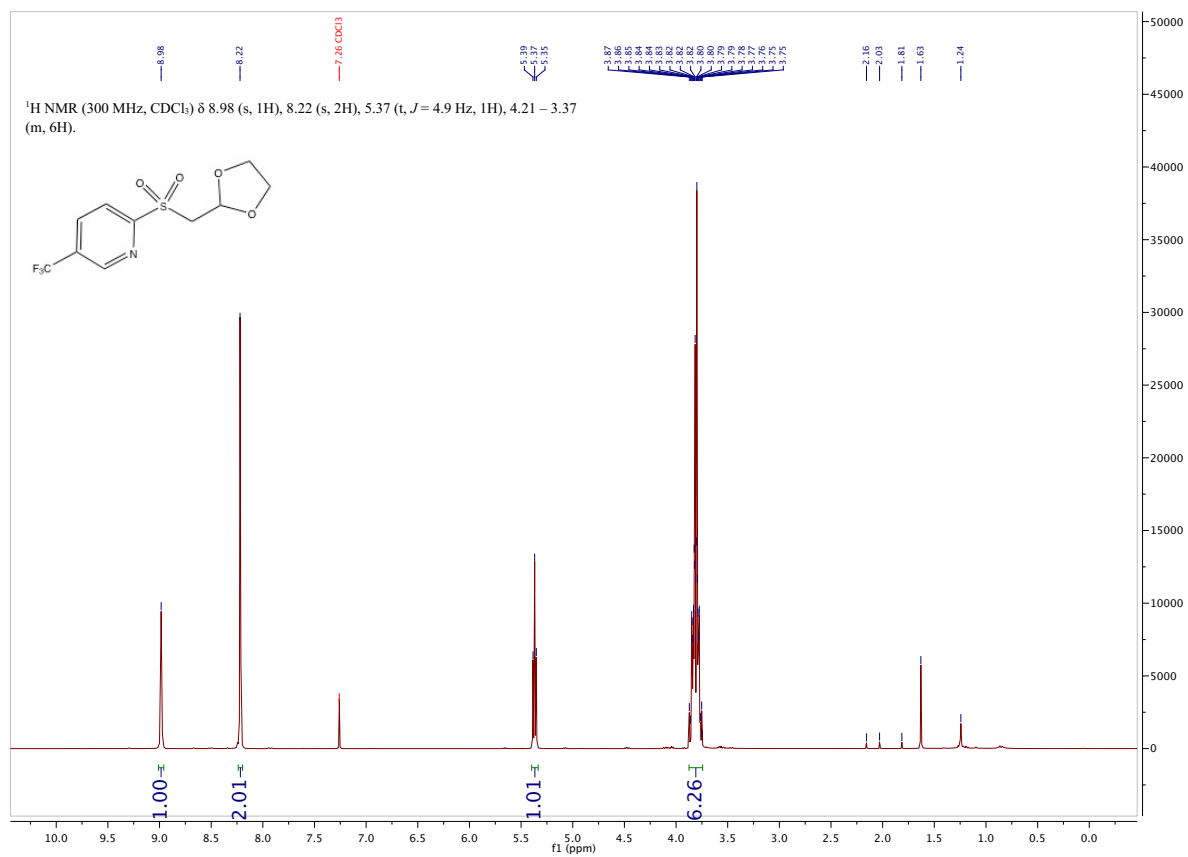
6.2 Spectra of intermediates from attempted approaches

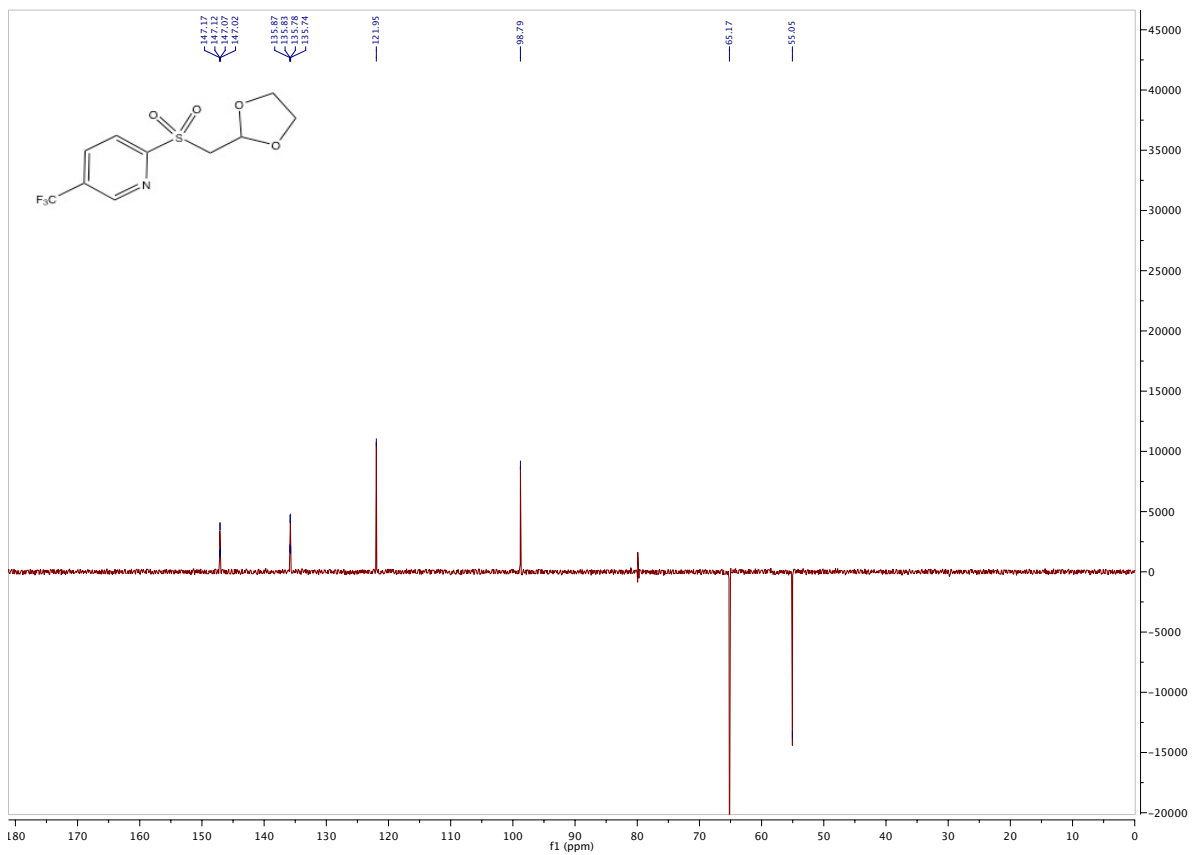
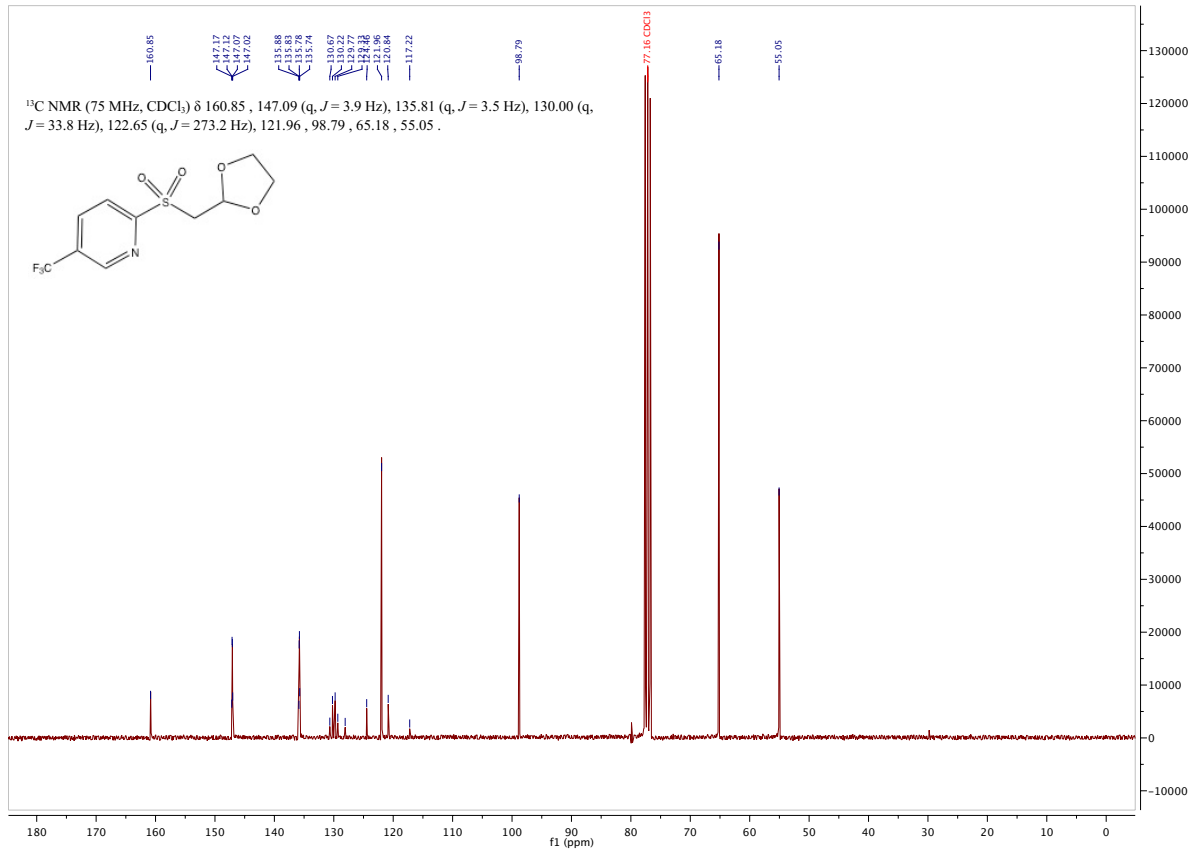
^1H and ^{13}C NMR spectra of compound 25



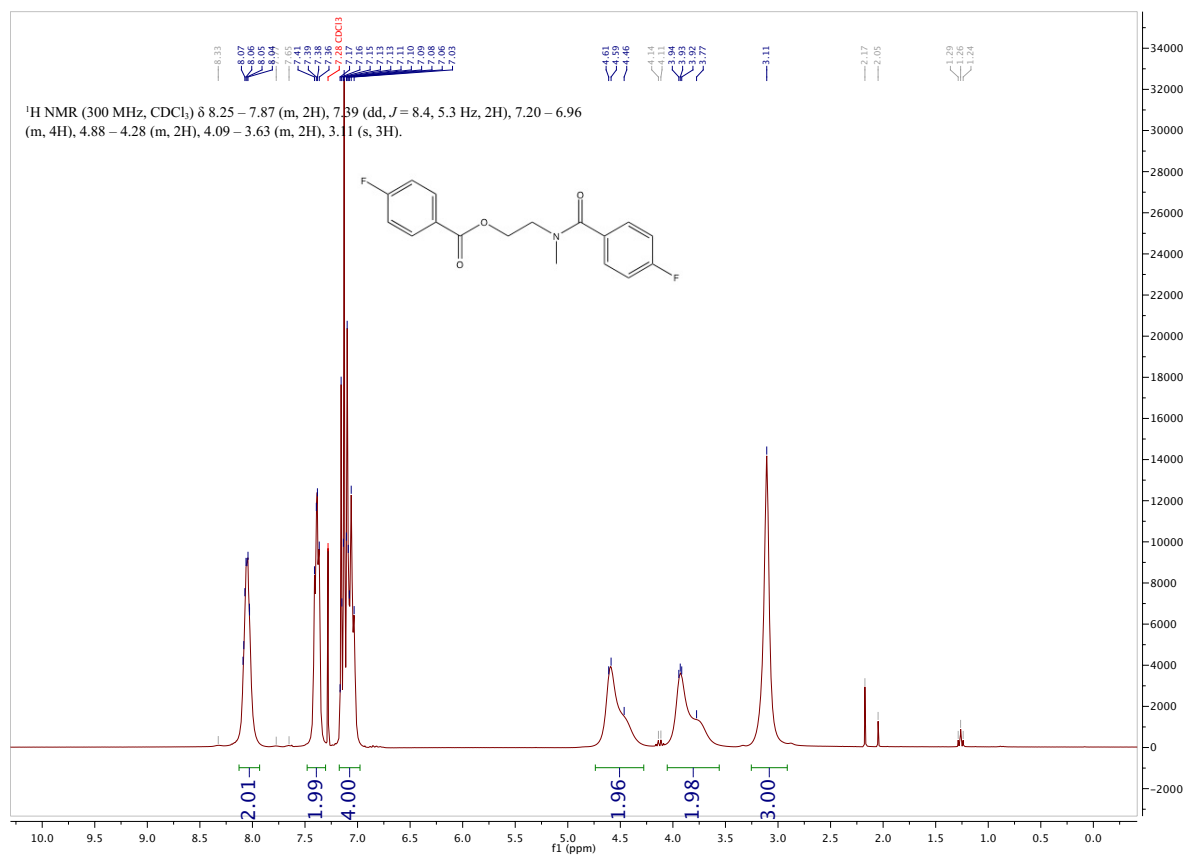


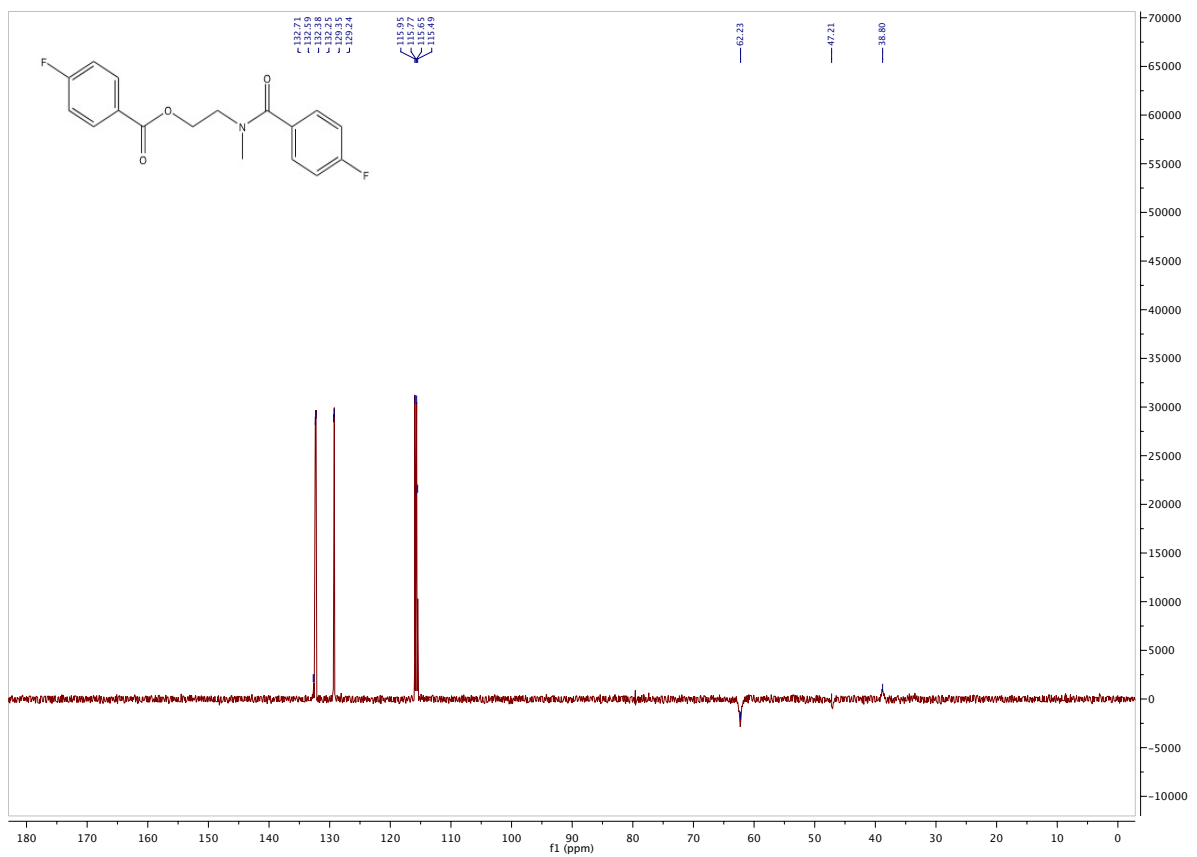
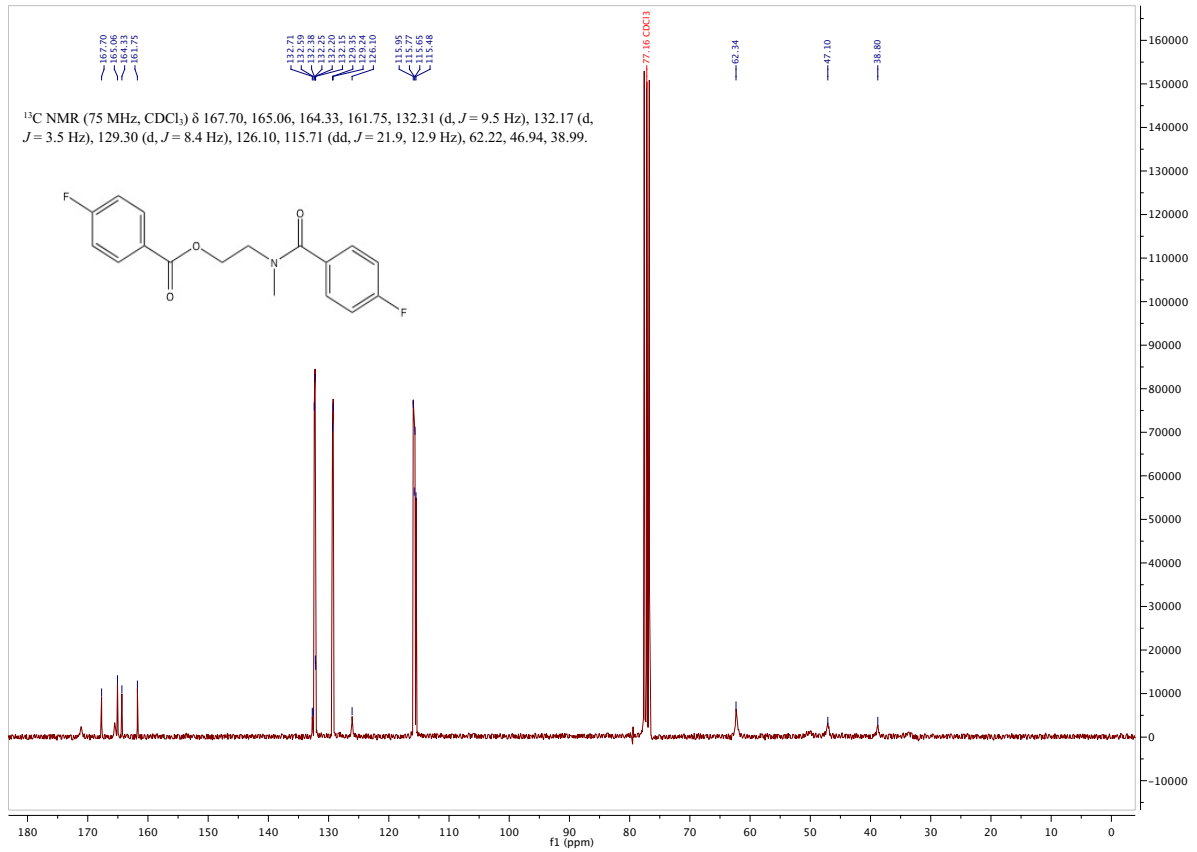
^1H , ^{13}C and DEPT135 NMR spectra of compound 30





^1H , ^{13}C and DEPT135 spectra of compound 42





¹H NMR spectrum of compound 43

